3-26-2015

The Fate of Malathion on Copper and Iron Piping within a Water Distribution System

Walter R. Lee

THE FATE OF MALATHION ON COPPER AND IRON PIPING WITHIN A WATER DISTRIBUTION SYSTEM

THESIS
MARCH 2015

Walter R. Lee Jr., Captain, USAF

AFIT-ENV-MS-15-M-164

DEPARTMENT OF THE AIR FORCE
AIR UNIVERSITY

AIR FORCE INSTITUTE OF TECHNOLOGY

Wright-Patterson Air Force Base, Ohio

THE FATE OF MALATHION ON TO COPPER AND IRON PIPING WITHIN A WATER DISTRIBUTION SYSTEM

THESIS

Presented to the Faculty

Department of Systems Engineering and Management

Graduate School of Engineering and Management

Air Force Institute of Technology

Air University

Air Education and Training Command

In Partial Fulfillment of the Requirements for the

Degree of Master of Science in Engineering Management

Walter R. Lee Jr., BS

Captain, USAF

March 2015

THE FATE OF MALATHION ON COPPER AND IRON PIPING WITHIN A WATER DISTRIBUTION SYSTEM

Walter R. Lee Jr., BS
Captain, USAF

Committee Membership:

Willie F. Harper, Jr., Ph.D., P.E.
Chairman

Gregory D. Hammond, Major, USAF, Ph.D., P.E.
Member

Justin D. Delorit, Captain, USAF, M.S., P.E.
Member

Abstract

Thermogravimetry, the study of mass loss as a function of temperature, has been used for oxidation, decomposition, and solid-state studies. This research used a thermogravimetric analyzer (TGA) coupled with Fourier transform infrared (FT-IR) spectroscopy in the study of copper and iron specimens exposed to malathion. Exposure to the malathion solution created a visible silver coating on copper and graphite-flake particles on iron specimens. Thermogravimetric mass loss curves revealed linear and nonlinear decomposition stages associated with mass loss reactions. Copper specimens exposed to malathion exhibited lower activation energy (E_a) values (2.28 to 4.40 kJ mol^{-1}) than for copper specimens exposed to deionized water (10.42 and 12.87 kJ mol^{-1}). Iron specimens exposed to malathion show lower E_a values (1.54 and 1.28 kJ mol^{-1}) than for iron specimens exposed to deionized water (3.30 and 6.40 kJ mol^{-1}). These results suggest association between malathion and lowered activation energies across all sample specimens. The FT-IR results indicate that specimens exposed to malathion may produce hydrogen sulfide. This research is the first to the author's knowledge to use TGA and FT-IR to test malathion adherence to metal surfaces. These results have application in water distribution piping analysis.

To my Jesus, Wife, and Family

Acknowledgements

I would like first and foremost to express gratitude to my Lord and Savior Jesus Christ for the faith, passion and energy to persevere to the end. My gratitude extends to the AFIT ENWM Fabrication and Model Shop for producing the many custom parts for the TGA and FT-IR. Additionally, I thank the EN lab technicians and the Chemist, Dr. Daniel Felker, for training, tools, parts, laboratory assistance, and data analysis assistance with both the TGA and FT-IR. Moreover, I thank the EN Lab students: Kandace Bailey for the hands-on laboratory training; CPT William D. Flemings Jr., and Captain Erik G. Rauglas for the laboratory assistance as well as for preparation of the malathion solution. I acknowledge and thank my EN Committee Members: Major Gregory Hammond and Captain Justin Delorit for providing critical feedback on my research ideas and methods. I also highly recognize and thank my ENV advisor: Dr. Willie F. Harper Jr., for his active guidance and support throughout the research. Furthermore, I acknowledge the sponsoring agency: the Environmental Protection Agency National Homeland Security Research Center for its guidance on procedures for research. The consolidated contributions of all parties furthered research and ensured successful completion of all requirements.

Walter R. Lee Jr.

Table of Contents **Page**

List of Figures

List of Tables

Glossary of Acronyms

AchE	Acetylcholinesterase
AFIT	Air Force Institute of Technology
DTG	Derivative of the Thermogravimetric
DTGS-KBr	Deuterated Tryglycine Sulfate–Potassium Bromide
E_a	Activation Energy
EDM	Electric Discharge Machine
EPA	Environmental Protection Agency
FT-IR	Fourier Transform Infrared
GC-MS	Gas Chromatograph Mass Spectrometer
kJ	kilo-Joule
MCT	Mercuric Cadmium Telluride
mg	milligram
mL	milli-Liter
mol	mole
NIOSH	National Institute of Occupational Safety and Health
ppm	parts per million
TGA	Thermogravimetric Analyzer/ Analysis

THE FATE OF MALATHION ON COPPER AND IRON PIPING

WITHIN A WATER DISTRIBUTION SYSTEM

I. Introduction

1.1 Background

Recently, America experienced catastrophic terrorist attacks within its boundaries. The infamous attacks of September 11th, 2001, which impelled America's involvement into the Global War on Terrorism, were the most significant. However a more recent story, *Assault on California Power Station Raises Alarm on Potential for Terrorism,* shows heightened concern. Smith (2014) explains the sniper attack associated with damaging the power distribution substation. She expresses the concern of the populace with the volunerability of high value infrastructure targets. The Chairman of the Federal Energy Regulatory Commission, John Wellinghoff, had this to say about the U.S. attack, "it was the most significant incident of domestic terrorism involving the grid that has ever occurred" (Smith, 2014). These recent attacks incite collective thought about the future of America's national security. If the enemy can penetrate and harm American national interests using primitive tactical means, what prevents it from choosing fewer direct means, possibly infecting water systems, to reach the same solution of mass catastrophe? Part of the preventive solution is a component of increased Environmental Protection Agency National Security responsibilities. Homeland Security Presidential Directive 7 explicitly provides information towards preventing and eliminating catastrophic terrorist attacks on critical infrastructure. One of the components includes protection of America's domestic water and waste water systems (U.S. Department of Homeland Security, 2012). Protecting the nation's 160,000 public sources from intentional and unintentional chemical contamination is integral to

homeland security and public health (Gallardo, et al., 2012; U.S. Environmental Protection Agency, 2014). The degradation of public health has the potential to result in social and economic harm to the American populace; therefore, all precautions must be taken to prevent it.

1.2 Problem Statement

In 2008 and 2012 a study and report explaining water contamination methods of analysis were completed. The National Institute of Standards and Testing (NIST) contracted ChemImage™ to perform a NIST contamination study detailing the use of ultraviolet illumination. Gallardo et al. (2012) show the characteristics of chemical residuals left on five piping materials with the use of mercuric chloride and strychnine. The piping material used was copper, polyvinyl chloride (PVC), brass, iron, and rubber. The analysis of the report revealed data towards understanding of the relationships between the mercuric chloride and strychnine contaminants. However, chemical and equipment sensitivity limitations precluded further understanding of the properties. Therefore, the EPA Homeland Security Research Program prepared a 2012 detailed report for NIST outlining five water contamination analysis methods. These methods include the bench scale test, dynamic fluid, and surface interface measurements, screening tests, water heater tests and full-scale dynamic tests. However, the results were inconclusive (Gallardo, et al., 2012). Furthermore, the two studies and reports did not yield promising methodological results towards chemical characterization and classification.

The need to close the research gap on definitive methods for chemical characterization and classification prompted the EPA to consider other possibilities. The EPA decided on pursing a more definitive way to study the chemical effects on water distribution piping materials. Thermogravimetry in conjunction with its coupling methods is a well-established method used in oxidation-degradation, decomposition, and solid-state studies (Dodd & Tonge,

1987). Thermogravimetry or the study of mass loss as a function of temperature has application in biological, polymers and plastics, explosive, inorganic compounds as well as metal and alloy research (Dodd & Tonge, 1987). There are numerous application studies that show thermogravimetry in conjunction with other instrumentation methods such as Fourier transform infrared spectroscopy or gas chromatography to be definitive methods for the decomposition and degradation exothermic reactions.

The investigative issue that the proceeding research will define and scientifically clarify is the reliability of thermogravimetry and its coupling methods as applied to the analysis of virgin piping material and malathion. The research will determine if there is evidence of the malathion solution adhering to the piping material. It will also determine whether the instrumentation is definitive in quantifying or qualifying the existence of the chemical on the surface of the copper and iron virgin piping material.

1.2.1 Research Justification.

The area of water contamination requires additional research, particularly in regard to the susceptibility of America's drinking water systems (U.S. Environmental Protection Agency, 2014). There is a national interest in understanding the effects of toxic chemicals on materials typical of water infrastructure technology. Additionally, this interest presents a need to devise new decontamination procedures and analysis methods consistent with the contaminate nature. Considerably, this research studying chemical adherence to metals is expected to be the first use of the coupling technique utilizing the thermogravimetric analyzer, the Fourier transform infrared spectrometer, and gas chromatograph. The research is anticipated to produce very promising results; successful research will provide a greater understanding of contaminate to piping material

adherence. The study may provide the blueprint and further insight into efforts relative to drinking water security as well as promote the broader national security goals.

1.3 Research Scope

The scope of this research is limited to experiments carried out with residue free virgin piping materials exposed to the malathion solution. Malathion solution has been used as a surrogate chemical resembling more potent organophosphorus chemicals (Boyd et al., 2006; Walker, 2009; Gervais, Luukinen, Buhl, & Stone, 2009). This research focuses only on the determination and analysis of activation energies using thermogravimetric mass loss profiles, as well as the determination of evolution gasses using Fourier transform infrared spectroscopy. The tasks associated with this research were performed using copper and iron piping materials. Chemical identification was performed using chemical libraries contained in the Fourier transform infrared spectrometer data bank. Data results are expected to be consistent with the adherence of malathion to virgin pipe materials.

1.3.1 Standards

The Public Health and Security and Bioterrorism Preparedness and Response Act of 2002 require all community sectors to perform water protection duties (EPA, 2012). Communities are required to implement periodic water vulnerability assessments, which must be validated by and environmental protection agency administrator. The Bioterrorism Preparedness Act also requires the environmental protection agency to perform strategy development for utility company consideration. The governmental statute promulgates the need for efficient methods to determine a chemical presence on water infrastructure materials as well as chemical decontamination procedures (EPA, 2012).

The Occupational Health Act of 1970 established the National Institute of Occupational Safety and Health (NIOSH) in conjunction with the Occupational Safety and Health Administration (CDC, 2013). Much like the Occupational Safety Health Administration, NIOSH is responsible for ensuring employee safety through knowledge-based research efforts. The NIOSH develops more than 9000 analytical material testing methods for hygiene analyzes applications (CDC, 2014). The NIOSH methods provide boundary for procedural testing of chemicals throughout the study and may allude to a greater understanding of research.

II. Literature Review

2.1 Malathion

Malathion, chemical formula $C_{10}H_{19}O_6PS_2$, is a clear and pungent odored organophosphate with many physical and chemical characteristics. According to the National Pesticide Information Center (NPIC) malathion has a water solubility of 145 milligrams per liter of water and a molecular weight of 330.56 moles (National Pesticide Information Center, undated). Malathion is known to persist in a water body for approximately 1.5 days in basic conditions [i.e. pH 8.16] and up to 17 days in low acidic conditions [i.e. pH 6.0] (Gervais, Luukinen, Buhl, & Stone, 2009). Malathion exhibits little persistence in soils because of animal and microorganism anaerobic metabolism (Walker, 2009). Malathion exhibits many characteristics that may reveal information about its ability to absorb to copper and iron sorbents resembling water infrastructure distribution networks.

2.1.1 Malathion Degradation Products

Malathion decomposes into by-products during exposure to differing external environments. Aqueous pH affects the degradation of the malathion solution (Bender, 1969). Table 1 identifies malathion byproducts and method of research found in the literature along with each corresponding NIST web book chemical reference. Malathion decomposes into more than one constituent of its composition. That decomposition is dependent upon the type of degradation method presented, as shown in Table 1. The degradation products may provide insight into the characterization of chemical constituents present in malathion off-gasses.

Table 1. Common Malathion Byproducts and Research

Malathion By-products [additional chemical names from NIST, 2011]	Chemical Equation (NIST, 2011)	Method of By-product	Researcher
Diethyl Succinate, [Succinic Acid]	$C_8H_{14}O_4$	GC-MS Photodegradation Study	Bender, 1969; Kralj, Franko, and Trebse, 2006
Dimethyl Phosphorodithiotic Acid	$C_9H_{21}O_2PS_3$	Hydrolysis Bioassay	Bender, 1969
Phosphorodithioic S-trimethyl Ester	$C_3H_9O_3PS_1$	GC-MS Photodegradation Study	Kralj, Franko, and Trebse, 2006
Phosphorothioic S-trimethyl Ester	$C_3H_9O_2PS_2$	GC-MS Photodegradation Study	Kralj, Franko, and Trebse, 2006
Diethyl Furamate, [2-Butenedioic acid]	$C_8H_{12}O_4$	Hydrolysis Bioassay	Bender, 1969
Diethyl Ester, [Butanedioic Acid, Malaoxon]	$C_{10}H_{19}O_7PS$	Biocatalytic Oxidation	Kralj, Franko, & Trebse, 2006; Lazarevic-Pasti et al., 2011

2.1.2 Malathion Toxicity and Bioaccumulation in Vertebrates and Invertebrates

Malathion is highly toxic to insects and weeds and less toxic to mammals (Moore, Yedjou, & Tchounwou, 2010); however, its toxic effects on mammals are under investigation. Malathion and other organophosphates have been in use since the mid-1950s resulting from the usage and testing of more chemically potent substances with similar properties [e.g. sarin, and VX] during the World War II era (Boyd, et al., 2006; Walker, 2009; Gervais, Luukinen, Buhl, & Stone, 2009). Malathion is also a nervous system inhibitor: according to a National Pesticide Information Center 13 week rodent study, researchers found low and high doses of malathion attached to the acetylcholinesterase (AchE) enzyme preventing nervous system response in the rodents (Gervais, Luukinen, Buhl, & Stone, 2009). Moore et al. (2010) discovered from exposing human liver tissue to malathion that increased dosages of malathion promulgated cytotoxicity and liver DNA

damage. Lasram et al. (2014) discovered decreased insulin response and induced hyperglycemia in a study using 10-week old Winstar rats subjected to 200 mg kg^{-1} of malathion. Cellular oxidative stress from malathion may cause diseases and damage in mammalian cells.

Malathion exhibits biological accumulative properties in organic tissue. Research has captured the nature of this issue within the aquatic environment. Henson-Ramsey et al. (2008) exposed a group of salamanders to contaminate environmental and food conditions of 50 µg cm^{-2} to 100 µg cm^{-2} and 200 µg cm^{-2} of soil and worms, respectively. The results were conclusive; there were no indications of malathion bioaccumulation toxicity present (Henson-Ramsey H. , et al., 2008). During a biological accumulation study by Ashauer et al. (2012), malathion was discovered in aquatic invertebrates at the cellular level. Malathion bioaccumulation in earthworms (Henson-Ramsey H. , et al., 2007) and amphibians (Van Meter, et al., 2014) presented comparative results. Malathion biologically accumulates in aquatic environments; these studies from previous literature present characteristics about its composition and persistence.

2.1.3 Absorption and Partitioning Coefficients

This research includes two sorbents [i.e. absorptive or adsorptive surfaces]: copper and iron. Depending on the use of the product, commercial piping systems are made up of differing metals and compounds: cast, ductile, and galvanized irons and steel. Understanding how the different material properties of various metals and compounds affect the adherence of malathion may contribute to the significance of data produced as well as the relevance of the research.

Research shows absorption isotherm experiments may be essential to understanding a solution's liquid-solid phase partitioning. Magnusson et al. (2013) demonstrate the use of liquid chromatography coupled with mass spectrometry for solvent removal and pesticide

concentration checks. Magnusson et al. (2013) suggest the ratio of solid concentration to dissolved concentration may be used to determine partitioning coefficients [i.e. coefficient of attachment between two elements in the same phase].

2.1.4 Infrared Spectroscopy Characteristics of Malathion

Infrared spectroscopy of malathion reveals chemical bond and band characteristics. Bourquin (1977) indicate in his malathion degradation study that double sulfur to phosphorous bands exist near 655 cm^{-1} wave numbers. He identified stretching asymmetrical carbon-hydrogen and sulfur-hydrogen vibrations [e.g. 2960 cm^{-1} to 1450 cm^{-1}] (Bourquin, 1977). Stuart (1996) provides infrared spectroscopy identification. According to Stuart's methods, phosphorus-oxygen-methyl bonds and phosphorus-sulfur bonds exist in the 2960 cm^{-1} to 1170 cm^{-1} and 750 cm^{-1} to 580 cm^{-1} infrared range, respectively (Stuart, 1996). These numbers are consistent with Bourquin's (1977) study. Quintás, Garriques and de la Guardia (2004) in their Fourier transformation spectrometry study indentify carbon-oxygen bands relative to malathion near 1737 cm^{-1}. The National Institute of Standards and Technology (2011) webbook displays selective infrared data for malathion. The NIST webbook in conjunction with literature may aid in further identification of gas evolution between malathion and metal adherence.

2.2 Thermogravimetric Analyzer

Research shows that the thermogravimetric analyzer (TGA) instrument may be used to study thermal stability or mass loss in materials (Groenewoud & de Jong, 1996; Boyd, et al., 2006). Thermal stability describes a materials ability to resist change at high temperatures (Wang, et al., 2014). Sample mass loss between the metal and the malathion solution is anticipated to reduce; however, there is a possibility for the mass to reduce or remain constant. Additionally, the degradation of reactive products may persist during increasing temperature rates. Studying how

and when these reactive products are removed or degraded may be useful in studying malathion adherence. Coupling the TGA with other instruments may reveal and qualify initial information related to the fate of malathion in drinking water systems; however, some limitations may exist.

2.2.1 Thermogravimetry

Isothermal or non-isothermal thermogravimetry can be used to study the chemical mass of a sample of interest. According to Boyd et al (2006), this is accomplished over a specified temperature or time gradient. However, each method shows advantages and disadvantages. Table 2 below provides a literature review of advantages and disadvantages of each technique. The Table shows a comparison of the two techniques used in TGA.

Table 2. Advantages and Disadvantages of Isothermal and Non-Isothermal Techniques

Type	Advantages	Disadvantages
Isothermal	Constant temperature, and pressure (Kok & Okandan, 1995)	Low accuracy (Jaber & Probert, 2000; Niu, Han, Lu, & Sun, 2010)
	Improved sensitivity (Arii & Masudo, 1999)	
Non Isothermal	Prevents simultaneous reactions by maintaining equilibrium across all stages (Arii & Masudo, 1999)	Inconsistent volatilization; polymer fragments volatilize at later rates (Rychly, et al., 2011)
	Provides dynamic heating rates across experimentation (Rychly, et al., 2011)	

2.2.2 System Purging and Heating Rates

Many authors show the need for a TGA system purge and calibration through the use of prescribed standards. Background reactions may interfere with elucidation of chemical degradation mechanisms (Arii & Masudo, 1999). Boyd et al. (2006) purged the TGA system using nitrogen supplied for 20 minutes at a max temperature of 773 Kelvin prior to experimentation to prevent background build-up and unwarranted contaminants in the sample

analysis. Due to the high probability of air infiltration, vacuum precursory methods should be performed prior to experimentation. Importantly, purge gas leakage should be prevented because heating and purge gas rates may be uncertain (Groenewoud & de Jong, 1996).

Heating rates of chemical decomposition depend on the goals of the study, previous studies show a variety of heating rates used. Kok and Okandan (1995) used a constant temperature rate of two degrees Kelvin in their study of crude oils. Authors Niu, Han, and Sun (2010) use heating rates of 5.0, 7.5, 10.0 and 15.0 Kelvin per minute in their study of calcium oxide. Lai et al. (2012) varied temperature rates [e.g. 283 K, 293 K, and 313 K] in their differing atmospheric municipal waste study indicating that residual mass is positively affected by heating rate.

2.2.3 TGA Coupling Methods

The TGA method coupled with gas chromatography (GC) mass spectrometry (MS) and or Fourier transform infrared (FT-IR) spectroscopy analytical instruments, or used as the primary method, has a many modes of application. Groenewoud and De Jong (1996) qualify in their TGA coupling technique research that the TGA coupled with the FT-IR and MS is a very suitable method that is applicable to quantitative analysis of volatile compounds. Similarly, Arrii and Masuda (1999) used thermogravimetry coupled with mass spectrometry (TG-MS) method to identify thermolysis and evolution of off-gasses from copper acetate hexahydrate. Boyd et al. (2006) used the TGA method to develop vapor standards for chemical warfare surrogate agents such as malathion. Their study identified TG-MS use in complex reaction studies. The TGA coupled with the FT-IR mass spectrometer was also used by Tudorachi and Chirac (2011) to determine the thermal integrity and degradation routes of polymers. Jiao et al. (2014) used the TG and FT-IR coupling technique proving carbon dioxide formation and carbonyl esters based on the spectral features of interest. This study validated extruded polystyrene multi-stage reactions

(Jiao & Sun, 2014). The coupling technique is well-established analysis method and may prove useful in the study of chemical to metal adherence.

2.3 Kinetic Analysis

2.3.1 Arrhenius Equation and Activation Energies

Arrhenius' equation, when applied as the first reaction order of mass loss, may reveal information on the chemical reaction properties of the malathion solution. Studying thermogravimetric curves may provide the insight into the behavior of the malathion, piping material constituents.

Subsequently following first-order mass loss, the decomposition rate can be modeled using reaction kinetics or Arrhenius' equation. The Arrhenius reaction model, $k = Ae(-Ea/RT)$ as applied to sample mass loss depends on three constituents: rate constant, sample weight and temperature (Kok & Okandan, 1995). Starink (2003) indicated comparisons between two well-known activation energy methods: the rate isoconversion based on the Friedman model and the p(y) isoconversion model based on temperature approximations. He indicated that p(y) isoconversion modeling with the use of Arrhenius' equation yields higher accuracy than models based on the Friedman model. Niu et al. (2010) use the Arrhenius' equation with the Vyazovkin method and Avrami theory within their reaction model and activation energy calculations. They revealed two important concepts with respect to the calcium-based sorbents: rapid decomposition may equate to variation in reaction orders, and activation energy decreases with increasing temperature (Niu, Han, Lu, & Sun, 2010). Much literature suggests Arrhenius modeling may provide insight into first-order kinetic analysis.

Defining kinetic parameters contributes to well-defined kinetic analysis. Vlaev et al. (2008) in their non-isothermal calicum oxlate study expressed the significance of predeterming

kinetic factors using thermogravimetric data. They determined calcium oxalate dehydration relied on the kinetic type (Vlaev, Nedelchev, Gyurova, & Zagorcheva, 2008). Jackic, Vrandecic and Klaric (2013) determined thermogravimetric kinetic analysis using activation energy, the pre-exponential factor and the equation of a line [i.e. kinetic triplet] may be used to estimate interrelationships with process rate, conversion, and temperature. Pazur (2014) discovered in his polyisobutylene study that a high association may exist between activation energies of byproducts. He verified this through the results shown for the proximity of the carbonyl, hydroxyl, and beta lactone by-products (Pazur, 2014).

2.3.2 Disadvantages with Arrhenius-Based Kinetic Modeling

Undoubtedly, there are disadvantages to Arrhenius-based kinetic modeling. Starink (2003) indicates approximation concerns with the temperature integral in his isoconversion method comparison study. He reported loss of consistent approximation for values of 'y' greater than 60 or less than 15. Similarly, Chen and Lui (2010), in their non-isothermal calcium carbonate solid state study, regard the temperature integral as undefined. Vyazovkin (2002) illustrates the solution to the temperature integral lies in the use of numerical iterative methods, which allow for interval variation. The aforementioned give insights into the temperature integral approximations. The insights demonstrate the need for careful experimental control and analysis.

2.3.3 Thermogravimetric Curves

The thermogravimetric (TG) and derivative of the TG (DTG) curves are indicative of a sample's kinetics and provide insights into the kinetic behavior of the sample analyte. The TG and DTG curves may prove useful in characterizing an analyte's kinetics (Kok & Okandan, 1995). Jaber and Probert (2000) show activation energy increases with positive increases in temperature heating rate. These increases are seen through thermogravimetric curve analysis. Additionally, the peaks on the DTG curve shift as a result of heat transfer variance, low particle exposure at

increased heating rates and decomposition (Jaber & Probert, 2000). In relation to Jaber's and Probert's study, Park and Kim (2006) discover from their DTG curve analysis that the reduction of internal analyte temperature decreases with direct increases in temperature.

2.4 Transition Metal Redox and Effects on Activation Energies

Metals exhibit chemical properties when exposed to oxidative products; these products may affect the value of associative activation energies. Graham (1972) indicated in his corrosion study that iron shows linear to parabolic rate change between 673 K and 773 K. He illustrated that low activation energies [e.g. 33 kJ mol^{-1} to 50 kJ mol^{-1}] are a product of oxidation (Graham, 1972). Zhu, Mimura, and Isshiki (2002) show similar inferences in their material oxidation study. They show copper exhibits characteristics of parabolic functions near the temperature range of 623 K to 1073 K. Activation energies are virtually the same for oxide and water absorption. Grosvenor et al. (2005) prove this in their iron surface study; they discovered E_a values of 28 ± 3 kJ mol^{-1} and 32 ± 6 kJ mol^{-1}, respectively. Grosvenor et al. (2005) also note lower activation energies among logarithmic kinetics than that of parabolic kinetics. The results suggest there may be some calculation error between the two methods. Wang, Tao, and Bu (2006) in their dissociation study of water, found the activation energies for virgin copper surfaces [e.g. 73.3 kJ mol^{-1}] to be nearly twice that of oxygen preabsorbed surfaces [e.g. 135.1 kJ mol^{-1}]. These activation energies align with 111 kJ mol^{-1} and 40 kJ mol^{-1} values contained in Zhu's, Mimura's, and Isshiki's, (2002) copper oxidation study. Oxidation lowers activation energies in transition metals; therefore, it is prudent to consider the factor in determining activation energies of chemical to metal reactions.

III. Research Objectives

The primary goal of this research is to determine if thermogravimetry combined with the Fourier transform infrared spectroscopy technique is a definitive method for classification of chemical adherence to water infrastructure piping material for the purpose of providing a greater understanding of contaminate to piping material adherence properties.

(1) The first objective is to determine the effect of malathion exposure on standard activation energy required for malathion to begin volatilizing from copper and iron piping.

(2) The second objective is to determine the volatile chemical effect of malathion on the elemental composition of copper and iron piping gas evolution during thermogravimetric analysis

The research is the first use of thermogravimetry and Fourier transform infrared spectroscopy techniques used in material and chemical studies. Successful research will provide a greater understanding of contaminate to piping material adherence. The research is also expected to provide further insight into efforts relative to drinking water security and further national security interests.

IV. Methodology

4.1 Introduction

This chapter will define the experimentation materials, equipment, methods and procedures applied in classifying and characterizing malathion adherence to copper and iron piping. Laboratory equipment and operating procedures are explained in theory within the contents of the chapter with additional details contained in appendices. Laboratory preparation, sample preparation, thermogravimetric analysis, Fourier transform infrared spectroscopy, as well as gas and liquid chromatography are explained as related to the water research study.

4.2 Laboratory Preparation

4.2.1 Reorganization and Circuitry

In the initial phases prior to experimentation, the Physics Laboratory was reorganized and to accommodate the thermogravimetry and infrared spectroscopy methods of analysis. During the renovation, the research required development of additional circuitry to support the instrumentation coupling method. The idea centered on allowing only a proportionate amount of gas transport from the thermogravimetric analyzer (TGA) to either the Fourier transform infrared (FT-IR) spectrometer or the gas chromatograph mass spectrometer (GC-MS). The off-gasses are restricted to prevent unequal flow of sample concentration between instruments. Circuitry was developed and placed using a workability framework to support maximizing the capability to implement daily sample runs across the three instruments. Reconstruction also included programming the available Microsoft© Windows 95 operating system. Additionally, eight new electrical receptacles with relays were placed to provide power to the solenoid valves. Each relay was spliced within each of the eight receptacles to a diagnostics digital to analog box and grounded

on a wire bus bar using 16 gauge wire. Figures 1 and 2 show the laboratory reconstruction and circuitry installs, respectively.

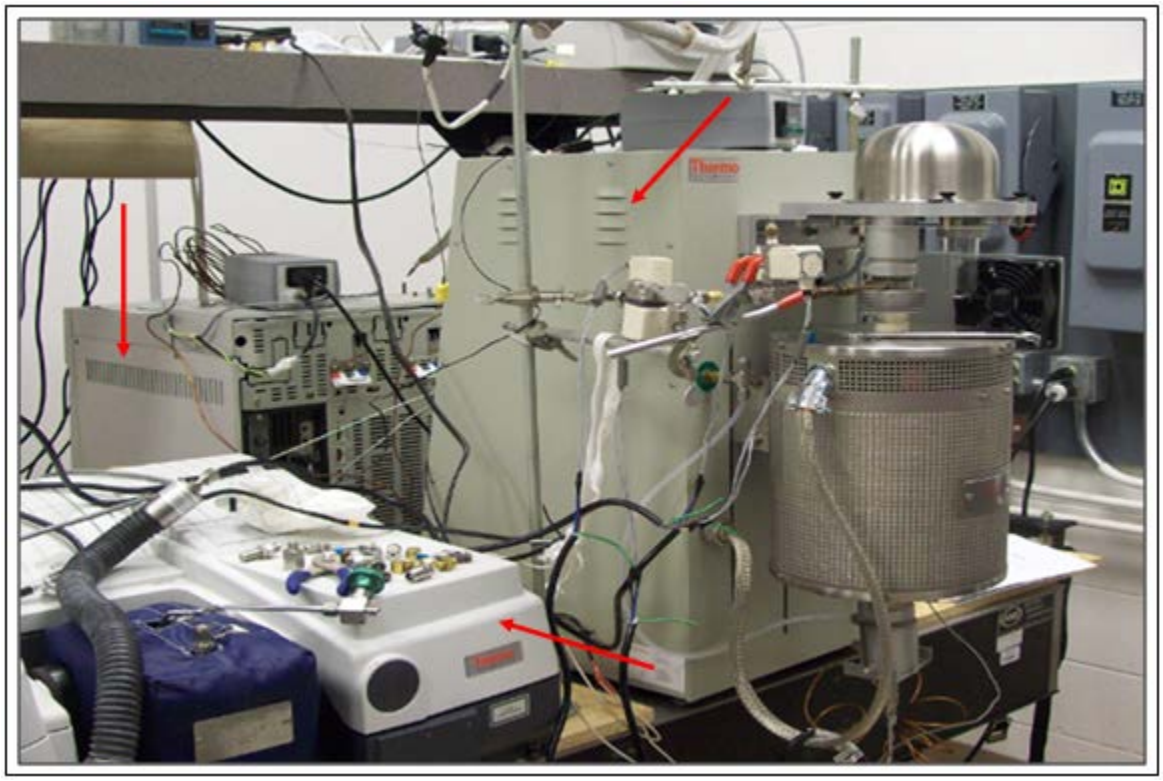

Figure 1. Laboratory Prior to Reconstruction Showing TGA/FT-IR and GC-MS

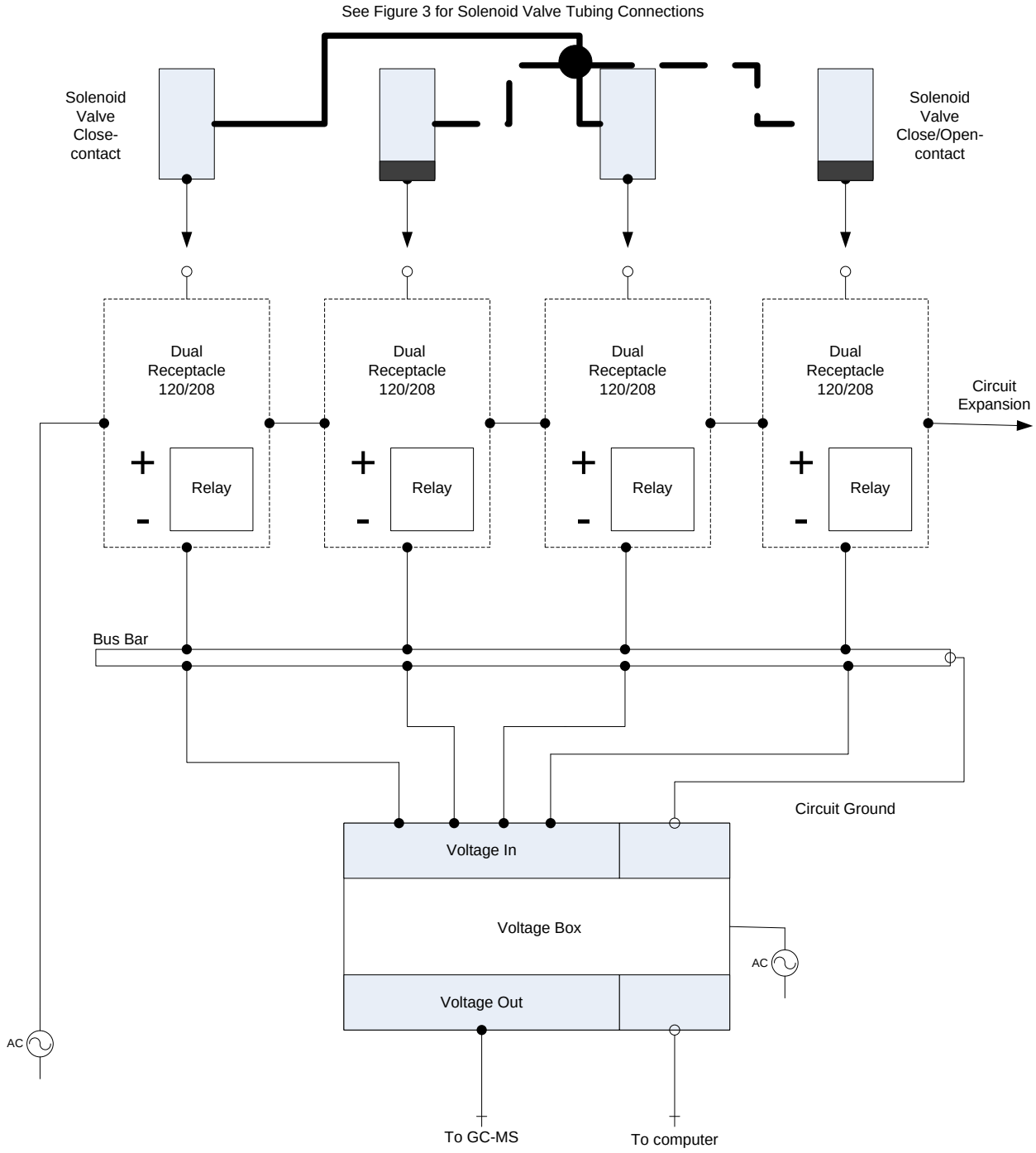

Figure 2. Expansive Circuitry and Diagnostics for the TGA/FT-IR/GC-MS

4.2.2 Gas Line and Valving

In addition to the circuitry, contact-closed and contact-opened solenoid valves were installed in succession for the instrumentation coupling methods. The valves open and close proportionate to the amount of sample gas emitted from the TGA to the FT-IR or from the TGA to the GC-MS. This procedure allows for single instrumentation analysis in a multifunctional system and prevents sample gas carry over between instruments. These valves were purchased and connected to three-prong computer cords through soldering (Figure 3). The connections are necessary for electronic switching and power of the solenoids contained in the valve.

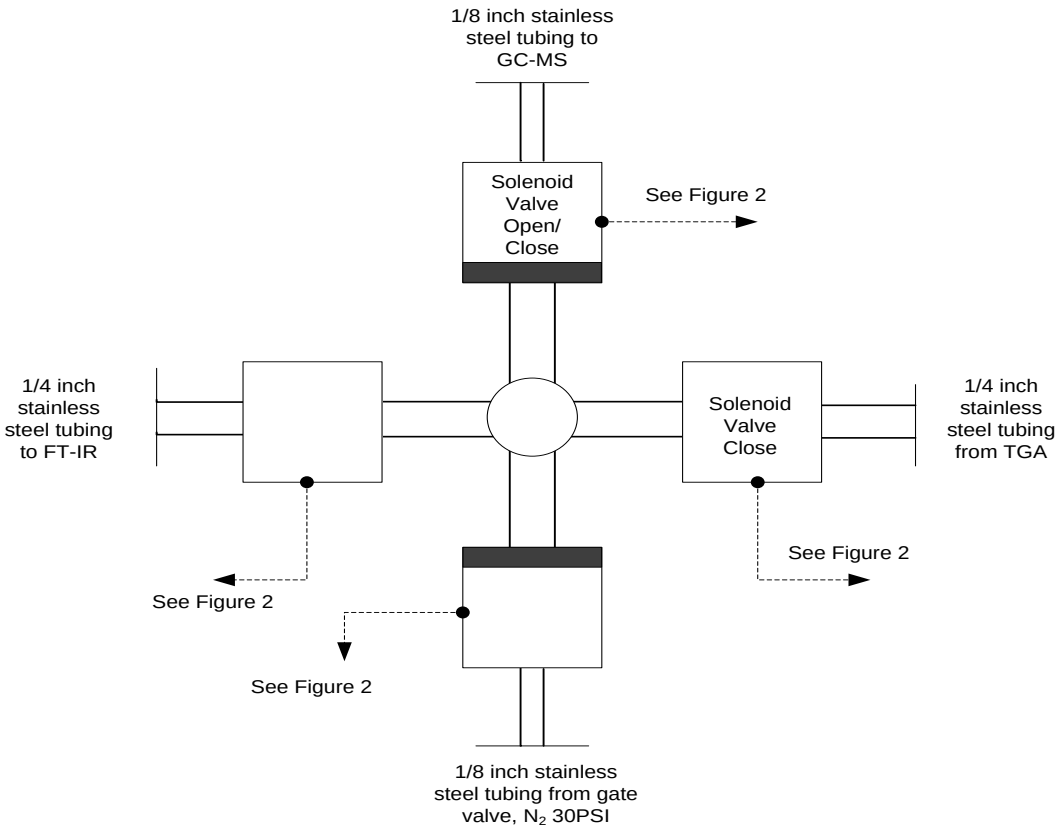

Figure 3. Solenoid Valve Connections and Tubing

4.3 Material Overview

4.3.1 Coupon Sample Preparation

Sample preparation required two items: coupons provided by the sponsoring corporation, the Environmental Protection Agency (EPA), and a solution of malathion in water provided by the Air Force Institute of Technology (AFIT). The EPA provided samples were in the form of cylindrical disks [i.e. coupons] approximately one-half inch in diameter and one-eighth inch in depth. These sample coupons were 99.99% copper and cast iron, no impurities, each weighing approximately three to four grams each.

4.3.2 Coupon Size Reduction

The AFIT Fabrication and Modeling shop machinist reduced the coupon size due to the need to accommodate analysis techniques used in this research. The coupons were severed into quarters operating an electrical discharge machine (EDM) (diagram shown in Figure 4). The EDM uses electrical conductivity to severe metallic samples (New Jersey Precision Technologies, Inc, 2015). Each coupon was submerged in a dielectric fluid [i.e. water] prior to the EDM sending an electrically charged brass wire over the sample. The wire disintegrated the sample's particles until the sample was fully decapitated. Following size reduction, each coupon quarter was sanded using Norton™ T414-400-50-C Blue-Bak waterproof paper to remove excess filings and contaminates from the severing process. Figure 5 shows the reduced coupons and abrasive paper used.

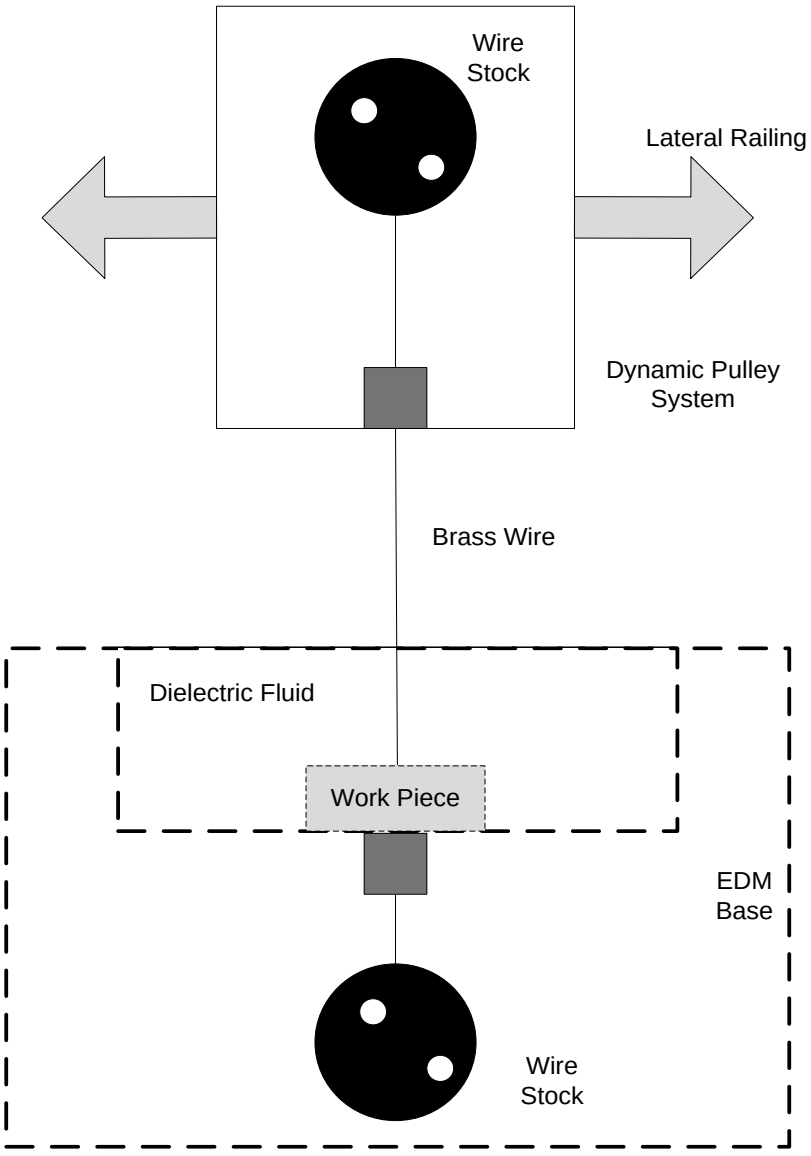

Figure 4. Electric Discharge Machine

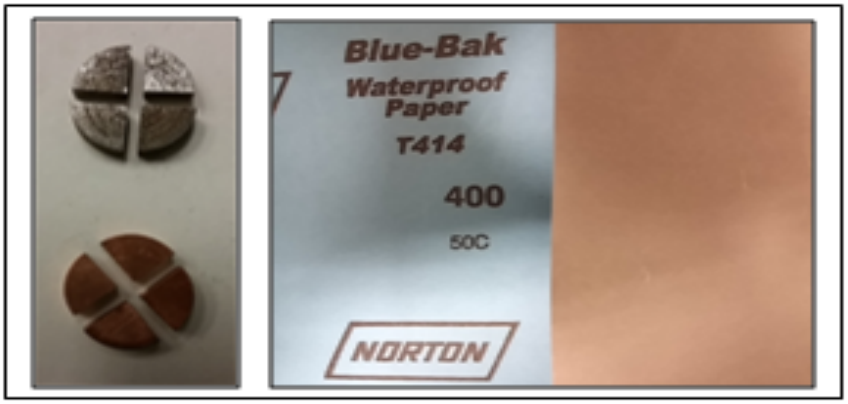

Figure 5. Sample Coupons (left) and Abrasive Paper (right)

4.3.3 Malathion in Water

The AFIT environmental laboratory technician provided a one-hundred parts per million (ppm) solution of Malathion in water. Malathion is a reasonably toxic solution thus National Institute of Occupational Safety and Health (NIOSH) methods were used in developing standard concentrations to prevent hazardous exposure. Careful measures were taken including sterile pipetting to ensure accurate dilution of the solution in deionized water. The NIOSH standards were used in regards to all hazardous chemical labeling and disposal. The solution of malathion was mixed at low agitation for 24 to 36 hours. After preparation, the solution was placed in the refrigerator and kept at a controlled temperature of 278 K until experimentation. Prior to storage and each use, the pH of each solution was checked to ensure the liquid was not too acidic. The pH was tested as an experimentation precaution to ensure the deionized water did not acquire any positive ions from the surrounding air, consequently, changing the chemical composition of the solution. Figure 6 shows the malathion solution, encasement and flask used to for preparation.

Figure 6. 95% by Volume Malathion Solution and Volumetric Flask

4.4 Equipment Overview

The thermogravimetric analyzer (TGA) measures mass loss as a function of time and temperature (Dodd & Tonge, 1987). The AFIT physics laboratory stores the Thermo Fisher Thermax© 400 TGA, a Nicolet^{TM} 8700 Fourier Transform Infrared (FT-IR) Spectrometer and a Hewitt Packard HP®6890 Gas Chromatograph Mass Spectrometer (GC-MS). The TGA was used to produce thermogravimetric curves for analyzing the mass change of the piping coupon immersed in the malathion solution. Additionally, a FT-IR spectrometer was employed to study the TGA gas evolution and provide verification and validation of the TGA procedure. Moreover, the GC-MS was prepared for expansion and along with the TGA and FT-IR connection apparatus; however, it was not used for this procedure.

4.4.1 Thermogravimetric Analyzer

The Thermax© 400 TGA is comprised of four main components: balance, furnace, a programmer, and recorder (ThermoFisher, 2008). These components enable the study of mass loss as a function of time and temperature. The Thermax© 400 TGA uses a two-sided balance with one side used for sample loading and the other used for weight tarring. Both sides use platinum wires and crucibles for sample and mass storage. Dodd and Tonge (1987) explain TGA, its instrument components, and materials. Platinum has specific uses in the TGA because it is heat resistance and is nonreactive with other metals; it is the preferred choice of material. The furnace is the most critical component of the TGA comprised of coiled windings, a sample container, a thermocouple, and a liner. The coiled windings and liner are direct components of the furnace. The platinum sample container provides the mechanism for sample loading. A thermocouple made of two metal alloy wires is housed within the furnace (Dodd & Tonge, 1987). These alloy wires are capable of withstanding temperatures above 1773 Kelvin (ThermoFisher, 2008). The thermocouple acts like a pseudo temperature sensor sending information to the reaction gas valve signaling it to open and close. Dodd and Tonge (1987) express that this mechanism is based on the heat given from the furnace. The temperature sensor, on the other hand, is directly connected to the programmer and sends electric signals to it controlling furnace temperature (Dodd & Tonge, 1987). Moreover, the recorder from the Thermax© 400 TGA receives inputs from the thermocouple and temperature sensor then provides real-time diagnostics information on sample weight, furnace temperature, and TGA run time to an integrated computer system (ThermoFisher, 2008). Figure 7 depicts a schematic showing instrumentation and equipment components of the TGA instrumentation contained in the AFIT physics laboratory.

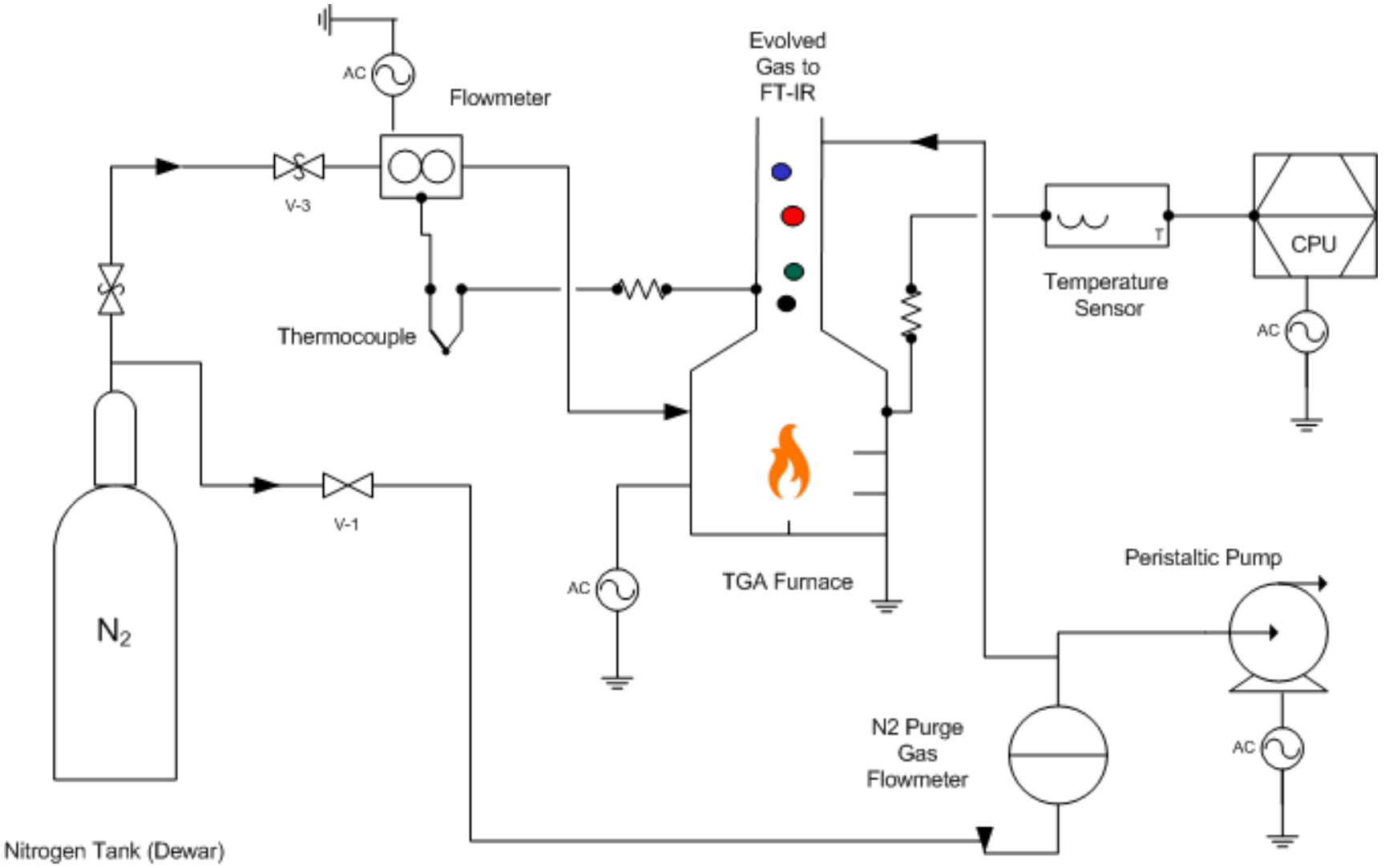

Figure 7. Schematic of TGA Displaying Gas Transfer, Diagnostics, and Electrical Equipment Located in the AFIT Physics Laboratory

4.4.2 TGA Coupled with Fourier Transform Infrared Spectrometer

Directly aside the TGA is a Nicolet™ 8700 Fourier transform infrared (FT-IR) spectrometer. Stuart (1996) explains the FT-IR components and their integration of analysis. The instrument is comprised of five key components: mirrors, an infrared radiation source, a Michelson interferometer, a sample compartment, and a detector. These components enable the study of TGA gas emissions as a function of time and enable understanding of the sample decomposition. The principal technique depends on the detection of molecule absorbance of infrared radiation; the absorbance of radiation is proportionate to increases in molecule vibration (Stuart, 1996; ThermoFisher, undated).

The Nicolet™ 8700 FT-IR employs five mirrors, two [i.e. stationary and mobile] housed within the Michelson interferometer (Stuart, 1996; ThermoFisher, undated). The mirrors redirect concentrated light from the laser. After the sample is introduced into the sample compartment, the laser sends light over the infrared radiation emitting source. The laser acts as both a light energy generator and an internal instrument calibrator continuously calibrating the FT-IR (ThermoFisher, undated). Stuart (1996) describes the interferometer and beam splitting process. Light energy transmits to the interferometer where it is directed by a beam splitter and encoded prior to refracting 50 percent of the light to a follow-on mirror and the remaining 50 percent back to the source. The sample compartment houses the sample the light energy passes through, therefore absorbing a percentage of light. The remaining portion travels to one final mirror and then to the mercury cadmium telluride (MCT) detector (Stuart, 1996). Based on peak intensity, the MCT detector transforms the beam into computer signals (ThermoFisher, undated). Figure 8 depicts the FT-IR instrumentation process.

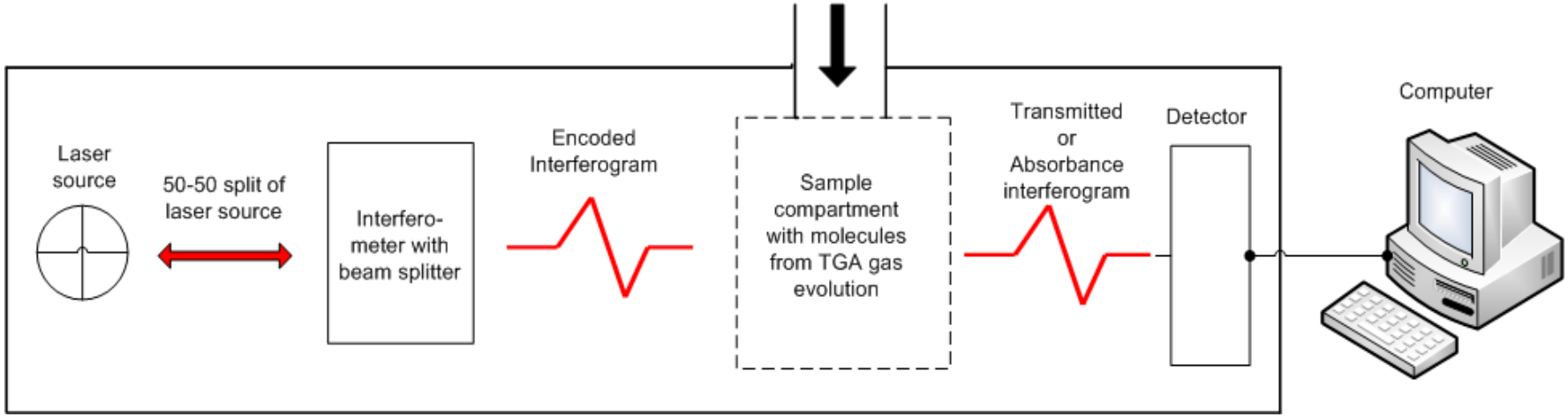

Figure 8. FT-IR System of Operations

4.5 Experimentation

4.5.1 Experiment Synopsis

The experiment consisted of initiating test runs and calibrating the equipment using calcium oxalate. Following the equipment calibration and testing, the metal coupons subjected to deionized water and malathion solution were examined. The procedure provided a baseline to compare experimentation data to. The general outcome determined if there was a change in the actual experimentation data as compared to the water baseline. The experiment was performed using each coupon type, copper and iron, subjected to deionized water then malathion, in sets of three with three repetitions each for 24-hour periods.

4.5.2 TGA and FT-IR Calibration and Testing Using Calcium Oxalate

Calcium oxalate was required for instrumentation calibration. Approximately 50 milligrams (mg) of calcium oxalate was carefully placed using a spatula onto weighing paper. The compound was weighed using an analytical balance prior to transportation to the TGA platinum crucible. The nitrogen purge and reaction gas was initiated and allowed to fill the FT-IR gas cell for approximately 15 minutes prior to experiment start. The preprogrammed calcium oxalate experiment located in the TGA Thermax© program was used to perform initial experimentation set-up. The program included a heating rate of 20 K min^{-1} for two hours. After experimentation set-up, the calcium oxalate program commenced analyzing the calcium compound. The *Results and Discussion* section of this research contains the analysis.

4.5.3 TGA and FT-IR Sample Preparation

Prior to analyzing the severed iron and copper coupons for experimentation, coupons were prepared 24 hours in advance. Preparation included recording general data and environmental conditions: date, weight, temperature, pressure, relative humidity, pH, and incubation and desiccation periods. The weight, temperature, pressure, and relative humidity were recorded. The study required the use of a Mettler Toledo© pH meter and probe. The pH meter was calibrated using the pH 4.0 and pH 7.0 buffer solutions prior to testing and recording pH of the deionized water and malathion solutions, respectively. The procedure was repeated for each experiment.

In conjunction to recording environmental conditions and pH, the copper and iron coupons were incubated then desiccated prior to TG analysis. The coupons were submerged into a glass vial of 10 milliliters (mL) of deionized water or 10 mL of 100 parts per million (ppm) malathion solution. Experimentation required keeping solution under controlled conditions [i.e. 298 K] for a 24-hour period using a hot water bath instrument. Due to the fact that the internal components of the water bath erroneously vibrated, an encasement of glass beakers was used preventing lateral movement of glass vials containing the solution and coupon of choice. After the 24-hour incubation period, the coupon samples were removed from the glass vial, placed on a plastic sample holder, and allowed to dry in the desiccator for a four-hour period. Meanwhile, the pH of the liquid solution was retested. The research required repetition of the method for each experiment prior to TGA and FT-IR analysis. Figure 8 shows the experiment procedure. Refer to Appendix A for sample preparation and for the detailed experimentation procedure.

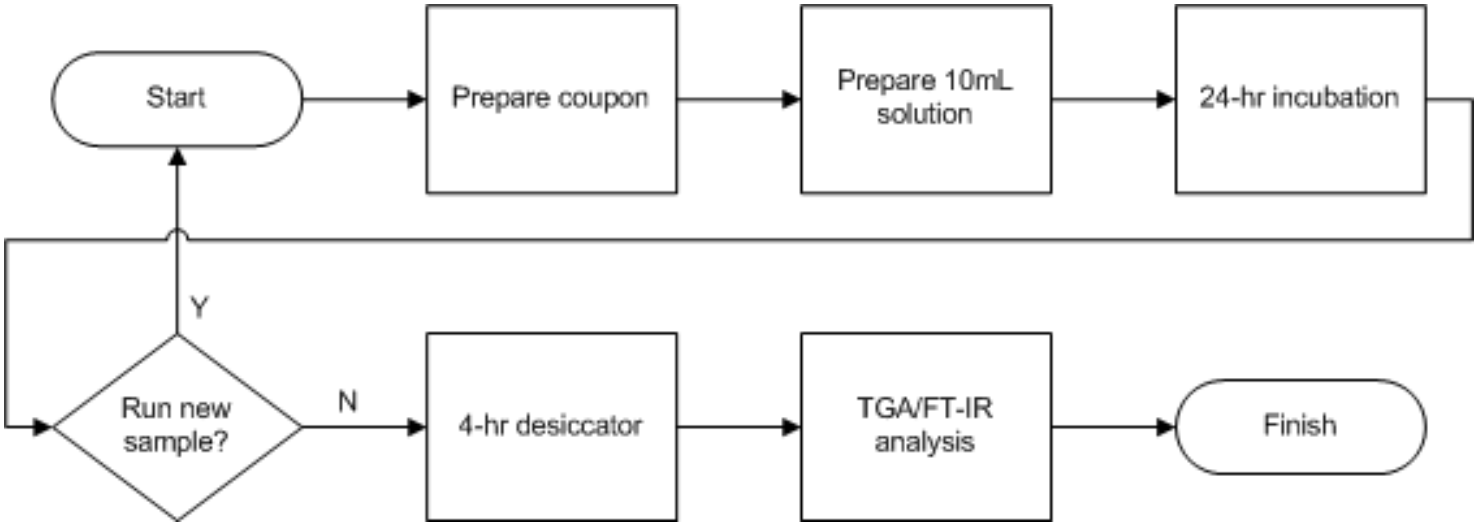

Figure 9. The Coupon Sampling and TGA/ FT-IR Analysis Experimentation Procedure

4.5.4 TGA and FT-IR Operation

Experimentation was a four part process inclusive of a multifaceted arena of preliminary and final checks. Appendix B shows the detailed TGA and FT-IR experiment sequence of operations from beginning to finish. The appendix outlines the intricacies of the experimentation preparation and process employing and process flow framework.

4.5.4.1 Initial Checks

Prior to start, the thermocouple and temperature sensor were checked ensuring they were securely connected to and wrapped around the 1/4 inch tubing connecting to the FT-IR insulated line. Additionally, the thermostat was checked for room temperature conditions, approximately, 295.1 K. The system was restarted if the thermocouple was either separated or not properly wrapped in insulated material.

Thermogravimetric analysis precluded additional initial checks prior to sample loading. Initial checks included checking the nitrogen Dura-Cyl® tank [i.e. Dewar] for at least 25% remaining gas, and ensuring there were no vacuum leaks throughout the TGA and FT-IR coupled system. Negative checks were rectified by replacement or fixation. After initial checks, the TGA and the acquisitions program were manually started. The TGA instrument screen was visually observed for digital weight and temperature, if the weight was not shown or if an error message appeared, the system was electronically initialized using the TGA program and the digital screen checked again. Proper TGA weight display illustrated initial check completion.

4.5.4.2 Sample Loading

Sample loading hinged on digital weight verification being correct and the quality of the physical state of the platinum wire adjoined to the balance fulcrum and platinum crucible. A metal sample was carefully loaded into the platinum crucible using nonreactive and nonmagnetic

plastic teasers. The crucible stabilized and the platinum wire attached to the balance fulcrum and TGA crucible was checked for severe bends. If the wire showed any major signs of torsion or bends, the sample and wire were carefully removed from the TGA baffle and straightened. The straightening process included carefully attaching a paper clamp to the one end, as a stabilizing weight, and the other end to a metallic stand as a means to hold the wire during the heating process. During the heating process, the wire was subjected to the blue flame emitting from the Bunsen burner until completely straightened. Afterwards, the wire was carefully reattached to the balance fulcrum, lowered down through the baffle, and reattached to the platinum crucible prior to reloading a sample.

The digital weight required one final check before raising the furnace housing. After sample loading, the weight was checked on both the instrument panel and the computer screen for additional error messages. Sixty seconds succeeding weight checking, the furnace housing was carefully hand-guided into the TGA porcelain baffle. The sample was in-place after a few manual turns of the mechanical locking mechanism.

4.5.4.3 Final Checks

The research required one final vacuuming recheck before initializing the FT-IR. This included checking all hoses and the peristaltic pump for leaks and degradation. Any damages were replaced and the experiment restarted. Once the checks were complete, a TGA computer file was opened and saved using the material type, sample number, and solution name [e.g. Cu(1)_Mala]. The FT-IR was started and the experiment set up commenced. During the experiment set-up, the bench test was initialized for the right auxiliary experiment module (AEM) and the interferometer checked for an interferogram consistent to proper detector alignment. If the bench test failed, the computer was restarted and the test was performed again. Immediately

following, the mercury cadmium telluride detector (MCT) was checked for cooling, if hot, liquid nitrogen was carefully applied to the encasement until the detector cooled. After multiple runs, the MCT detector became inoperable; later experiments used a deuterated trglycine sulfate potassium bromide (DTGS-KBr) detector, which decreased sensitivity of analysis. Analysis results using both detectors are contained in the *Results and Discussion* section and appendices of this research.

4.5.4.4 Data Collection

Sample background and vectors were collected following the experiment set-up. The procedure lasted approximately 30 minutes. Afterwards, an FT-IR data file was opened, saved using the date system [e.g. 3_26_15] and then initiated upon starting the TGA. The entire experiment lasted approximately 450 minutes. Immediately following experimentation, the nitrogen gas Dura-Cyl®, the peristaltic pump, and the FT-IR purge gas were all manually and electronically turned off.

4.6 Analysis Methods

4.6.1 TGA and FT-IR Program Method Creation and Use

4.6.1.1 Calcium Oxalate Preprogrammed Settings

The Thermax© Acquisitions program included premade experiments. The calcium oxalate preprogrammed experiment was used for calcium oxalate data generation. A single heating rate over two temperature changes was used: 278 K min^{-1} from 295.1 K to 773 K.

4.6.1.2 Malathion in Water Program Settings

A method for malathion was developed using the Thermax© Acquisitions program prior to analyzing the sample coupons immersed in malathion. The method development for this research stemmed from TGA method concerns with improper heating rates. Dodd and Tonge (1987) state

this as a principal concern associated with dense samples. Understanding this, the temperature program included a low heating rate of 275 K min^{-1} and an overall max temperature of 773 K. Additionally, the method was applied to three temperature changes: 0 to 295.1 K, 295.1 K to 473 K, and 473 K to 773 K.

4.6.1.3 FT-IR Program Settings

The OMNIC™ program enabled Fourier transform infrared data generation. The program was experimentally set-up to run using a gas cell specifically manufactured for the ThermoFisher Thermax© 400. Early on, transmittance and absorbance data were observed using the MCT detector at 4 cm^{-1} wave numbers. Later tests used a DTGS-KBr detector at 16 cm^{-1} wave numbers.

4.6.2 Thermogravimetric Mass Loss Profiles

The Thermax© Analyst program allowed for observation and analysis of thermogravimetric data thus producing thermogravimetric analysis (TGA) and derivative of thermogravimetric analysis (DTGA) curves. The TGA curves depicted mass loss over time and temperature. The derivative of the weight with respect time was taken over the TGA curve producing DTGA curves showing inflection points along the x-axis.

4.6.3 Arrhenius Plots Depicting Activation Energies

Data manipulation of thermogravimetric analysis (TGA) comma splice files using Microsoft© Excel produced TGA mass loss profiles and Arrhenius plots showing activation energies. The graphs were created using the first derivation of the mass loss function, temperature integral, and Arrhenius's equation substitution. This reaction model is a well-defined method used in previous TGA first order kinetic research (Jaber & Probert, 2000;

Park & Kim, 2006; Vlaev, Nedelchev, Gyurova, & Zagorcheva, 2008; Lai, Ma, Tang, & Lin, 2012; Jakic, Vrandecic, & Klaric, 2013).

Equation 1 shows the mass loss differential equation; Equation 2, the temperature integral i.e. heating rate]; and Equation 3, Arrhenius' equation:

$$dX/dt = k(1 - X) \quad (1)$$

$$dT/dt = h \quad (2)$$

$$k = Ae(-Ea/RT) \quad (3)$$

Where *k* is *rate constant*; *X* is *fractional difference of initial to final mass divided by the initial mass* per unit of time; *A* is the *pre-exponential factor*, E_a is the *Activation energy* (kJ), *R* is the *Ideal gas constant* (J mol^{-1} K), and *T* is the *temperature* (K).

Therefore, the first derivation of equation 1 and 2 with substitution of equation 3, as well as, integral calculus applied to the compilation of the three equations produces a function similar to the algebraic function for the equation of a line, y = mx + b, as defined by Equation 4:

$$ln\,[-ln(1 - X)] = (-Ea/RT) + lnB \quad (4)$$

Where, *B* is a *constant* [i.e. not used in this research]. Appendix C details the integration steps producing Equation 4. The integration steps are based on previous kinetic studies cited by others (Coats & Redfern, 1964; Dollimore & Lerdkanchanaporn, 1998). Activation energy graphs were created by plotting the natural log of the mass loss, y-axis, to the inverse temperature, x-axis. The slope of the line, m [i.e. E_a/R], is the activation energy. The energies were compared to literature to determine potential chemical bond characteristics. Data are contained in the *Results and Discussion* section of this research.

4.6.4 TGA Mass Loss Profiles and FT-IR Absorbance Spectra

Analysis included comparing FT-IR absorbance spectral features of interest with respect to the DTG mass loss inflection points. The TG curve was smoothed seven times using 25 point smoothing for TG peak clarity. Analysis procedures also included taking the derivation of the TGA curve for each sample during four to five inflection time intervals between points of interest across the TG curve. These points were then compared to FT-IR spectral features within the time intervals corresponding to the DTG curve used. Each FT-IR feature spectrum was smoothed and analyzed at wave number intervals corresponding to the chemicals of interest contained in the OMNIC^{TM} FT-IR spectral libraries. Tables listing associative chemical compounds for the analyzed spectrum comprised the output.

V. Results and Discussion

5.1 Visual Properties of Coupons

5.1.1 Copper Coupons Before and After Thermogravimetry

Each copper coupon was subjected to both a 10 mL of solution of deionized water or malathion for 24-hour periods prior to thermogravimetry. Copper exhibited physical changes after thermogravimetry, particularly when exposed to malathion. Figure 10 shows the before (left) and after (right) changes. There appeared to be a lustrous silver metallic coating on all copper samples exposed to malathion and thermogravimetry. The presence of this lustrous coating suggests possible physical adsorption between the copper and malathion.

Figure 10. Copper Coupons Before and After Thermogravimetry

Physical adsorption involves electrostatic attraction between two opposing charged compounds, such as between a metal and a chemical (Schweitzer, 1987). The adsorption may be dependent on the constituents within malathion and reactions taking place at extreme temperatures above 373 K. Malathion is composed of elements carbon, hydrogen, oxygen, phosphorus and

sulfur. Understanding this, it may be that the extreme temperatures changed the elemental composition of the malathion producing a salt film in the form of a sulfide. The proposed reaction is shown in Equation 5. Traces of this salt or sulfide may have physically bonded to the copper.

$$H(g) + S(s) \longrightarrow H_2S(g) \quad (5)$$

Where *H*, *hydrogen gas*; reacts with *S*, *sulfur*; to form the *hydrogen sulfide*

There were a few instances after thermogravimetry where the copper exhibited blue-green spots on the exterior of the coupon. In these cases, the atmospheric conditions of the experiment changed. However, these conditions may have changed prior to and during thermogravimetric analysis. The TGA uses an inert gas [i.e. nitrogen] to prevent the interactive effect as a result of oxygen changing atmospheric conditions (Dodd & Tonge, 1987). The inclusion of air in the system in conjunction with the aqueous electrolyte [i.e. malathion in water], may be attributed to the atmospheric corrosive protective coating as shown in Equation 6. Reactions between nitrogen, oxygen and possibly sulfur commenced resulting from air infiltration of the TGA. The resulting combustion product may have been a form of oxide such as carbon, nitrogen, or even sulfur oxide as shown in Equations 7 and 8. The formation of surface oxides may be a reason copper exhibited blue-green spotting on its surface; these blue-green spots are indicative of copper exposure to air (Schweitzer, 1987).

$$Cu(s) + O_2(g) + H_2O \longrightarrow CuO(s) + H_2O \quad (6)$$

Where *Cu*, *copper*; reacts with *O*, *oxygen*; to form the corrosive protective coat that advances in the presence of water (Schweitzer, 1987).

$$N_2(g) + O_2(g) \longrightarrow NO(g) \quad (7)$$

$$C(s) + O_2(g) \longrightarrow CO_2(g) \quad (8)$$

Where *N*, *nitrogen*; reacts with *O*, *oxygen*; to form *nitrous oxide*. Similarly, *C*, *carbon* reacts with two molecules of oxygen forming *carbon dioxide*.

5.1.2 Iron Coupons Before and After Thermogravimetry

Iron, after exposure to malathion, exhibits graphite-corrosion. The corrosion results from the cast iron graphite flakes interacting with each other over the aqueous electrolyte [i.e. malathion in water] (Schweitzer, 1987). Equation 9 (Whitten, Davis, & Peck, 2000) shows two possible chemical reactions affecting the iron sample between the two mediums: air and water. Within 24 hours of incubation, each metal sample exhibited similar characteristics. The physical results were no different from using TGA. Figure 11 shows the before [i.e. left] and after [i.e. right] pictures of an iron sample exposed to malathion and TGA.

$$2Fe(s) + 3O_2(g) + H_2O(aq) \longrightarrow 2FeO(OH)(s) \quad (9)$$

Where *Fe*, *iron*; reacts with *O*, *oxygen*; and H_2O, water; to form a constituent of *iron oxide*

Figure 11. Iron Coupons Before and After Thermogravimetry

5.2 Activation Energies

5.2.1 TGA Analysis of Calcium Oxalate

Figure 12 shows the TGA mass loss profile for calcium oxalate. Over the course of the experiment, the mass fraction decreased from 1.0 to approximately 0.70 after 35 minutes. The mass loss profile shows two distinct, linear thermal decomposition stages: the first, beginning at approximately 450 K and ending at approximately 520 K and the second, having occurred at approximately 800 K. The transition from 100% mass to first thermal decomposition stage reduced the mass fraction by 10% to 0.90. The proceeding stage reduced the mass fraction 17% to approximately 0.75. The steep peak at approximately 25 minutes indicates the second decomposition stage occurred at a faster rate than the first. According to Vlaev et al. (2008) thermal oxidation of calcium oxalate involves three primary reactions: first, dehydration at temperatures less than 573 K; second, the formation of calcium carbonate, and third, the formation of calcium oxide. The presence of these reactions can be assessed by determining the activation energies associated with the decomposition stages; see Figure 12. The Arrhenius plot depicted in Figure 13 shows the first order reactions as a function of mass loss and inverse temperature. The

activation energies associated with the first and second thermal decomposition stages are 7.3 kJ mol^{-1} and 15.0 kJ mol^{-1}, respectively. The E_a relative to the overall reaction is 6.05 kJ mol-1. These activation energies are significantly lower than the published E_a values for dehydration between 46 kJ mol^{-1} to 143 kJ mol^{-1}, calcium oxalate formation between 96 to 392 kJ mol^{-1}, and calcium oxalate formation between 110 kJ mol^{-1} to 231 kJ mol^{-1} (Vlaev, Nedelchev, Gyurova, & Zagorcheva, 2008). Therefore, the activation energy determination cannot be used to characterize the thermal decomposition reactions shown in Figure 12. However, the observed E_a values shown in Figure 13 are in the same range of those used to describe the evaporation mechanism from powders [e.g. 10 kJ mol^{-1} to 25 kJ mol^{-1}] (Prado & Vyazovkin, 2011). Dehydration reactions may be responsible for thermal decomposition stages shown in Figure 12.

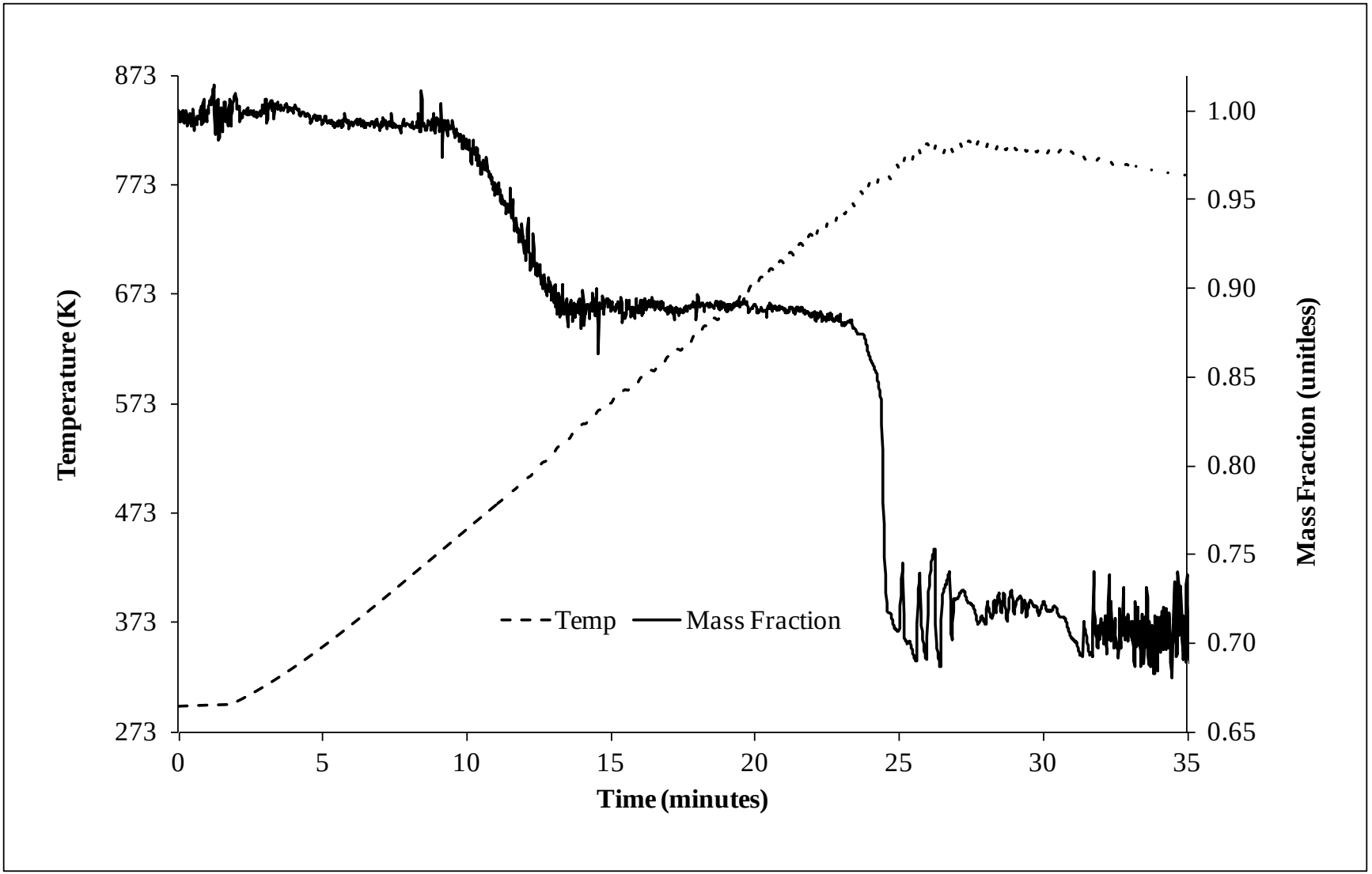

Figure 12. Calcium Oxalate TGA Mass Loss Profile, Displays Multi-Stage Mass Loss versus Time and Temperature

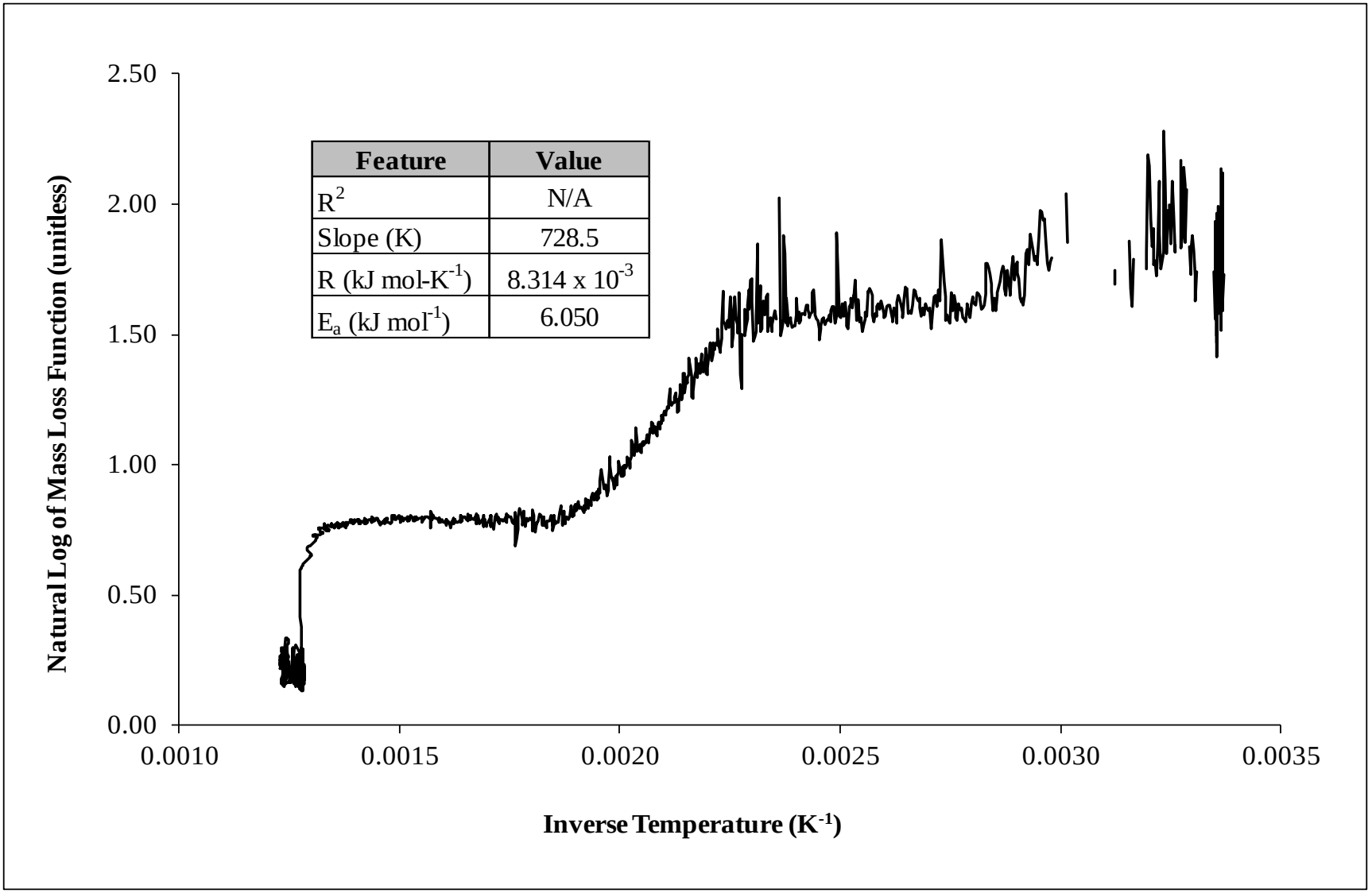

Figure 13. Calcium Oxalate Arrhenius Plot, The Graphed Line Suggests the Mass Loss is Consistent with Multi-stage Reactions.

5.2.2 TGA Analysis of Copper Specimens Exposed to Deionized Water

Deionized water provided a baseline for malathion absorption testing. Figure 14 and Figure 15 show generated thermogravimetric profiles and Arrhenius plots for the deionized water experiment with copper. The mass fraction increases 0.0002 during the first 60 minutes of the experiment to an approximate magnitude of 1.0002. This strongly suggests air intrusion into the TGA system. The mass loss profile shows linear decrease during the 67 to 230 minute time interval, which ends at a maximum temperature of 700 K. A second decomposition stage is seen between 230 and 250 minutes. The mass fraction is reduced by 0.0001 in this stage. The third stage shows negligible decomposition and is seen at times greater than 250 minutes and temperatures exceeding 750 K. The final mass fraction observed at 773 K was 0.9999, indicating thermal stability of the copper specimen. Appendix D shows additional TGA profiles for copper specimens exposed to deionized water. The Arrhenius plot in Figure 15 shows a single linear region followed by a non-linear, parabolic profile. The 0.7667 coefficient of determination describes the linearity. The non-linear profile suggests the presence of multiple mass loss mechanisms in-line with oxidation mechanisms as indicated in Zhu, Mimura, and Isshiki's (2002) pure copper study. The linear region is associated with an E_a of The 12.87 kJ mol^{-1}, which is in the expected interval for the evaporation mechanisms of water and powders, as described in Prado and Vyazovkin's (2011) work. Activation energies for copper may be found in between 40 kJ mol^{-1} to 111 kJ mol^{-1} as described by Zhu et al. (2002). Therefore, the E_a may not be consistent with the fact that the copper specimen was exposed to deionized water, but does allude to the possibility of oxidation mechanisms having a catalytic effect on the surface reaction. Additional Arrhenius plots for copper are contained in Appendix E.

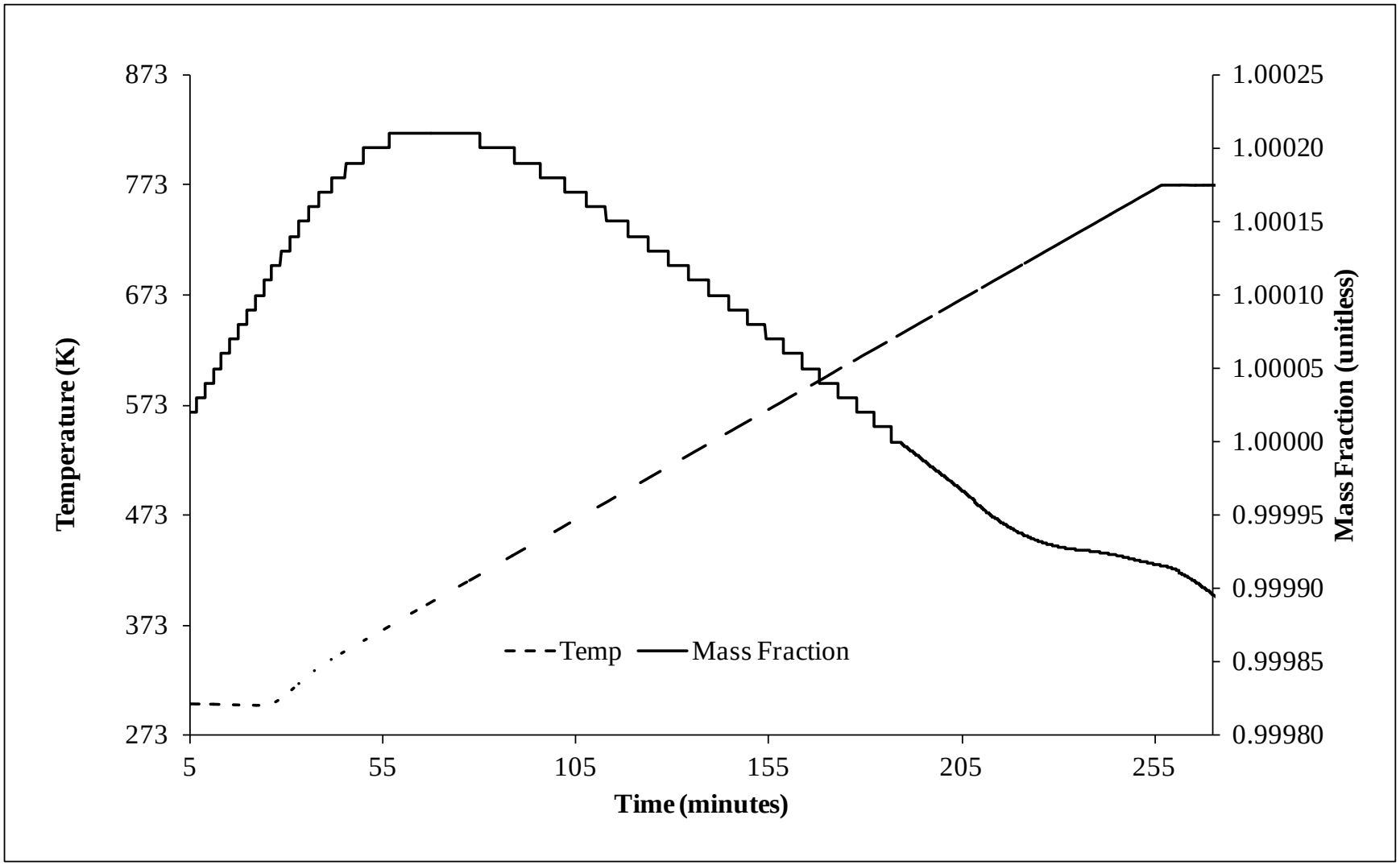

Figure 14. Copper Exposed to Deionized Water TGA Mass Loss Profile, Displays Mass Gain and Loss versus Temperature and Time

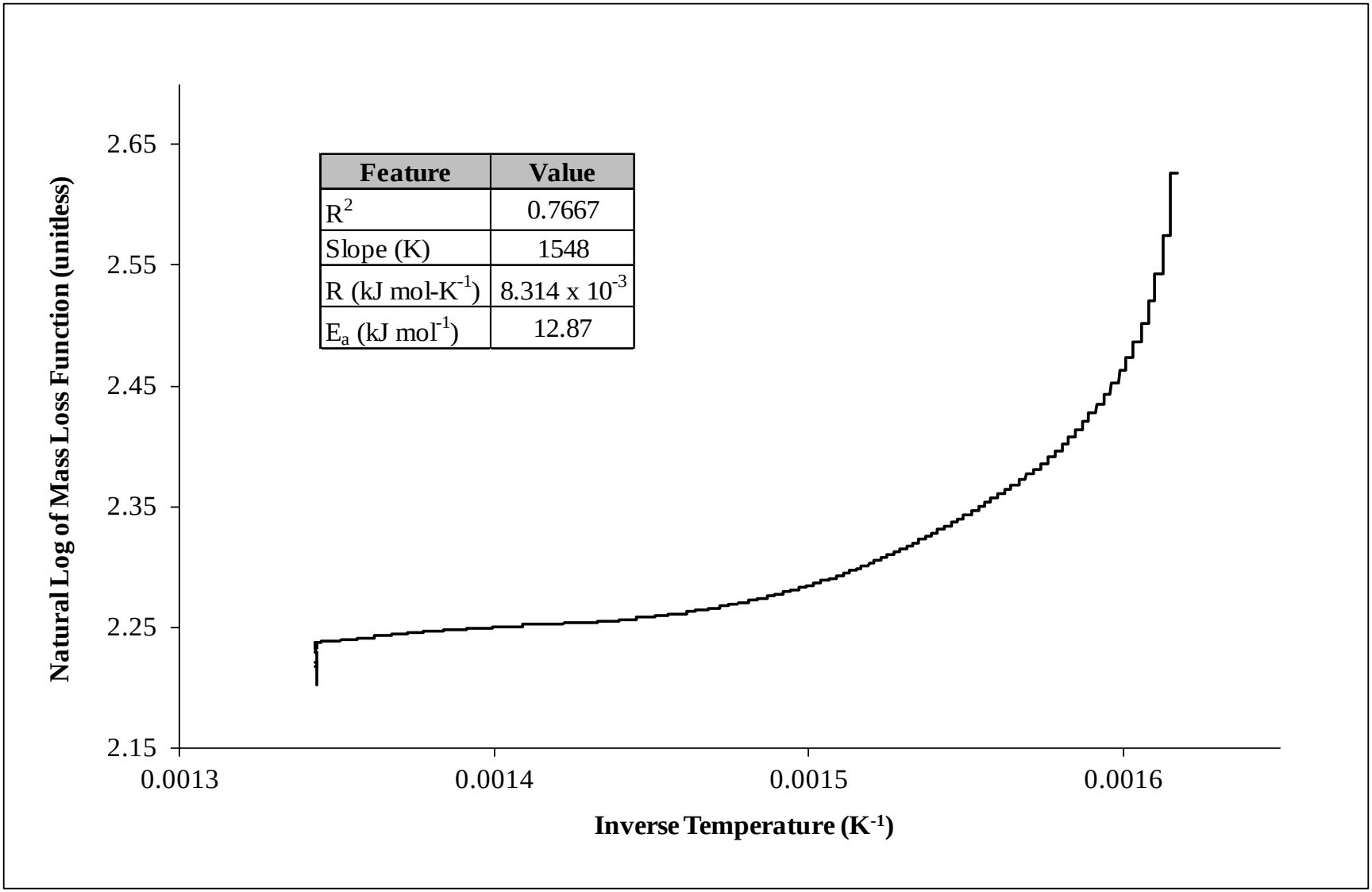

Figure 15. Copper Exposed to Deionized Water Arrhenius Plot, Curved Line Indicates Mass Loss is Inconsistent with First-Order

5.2.3 TGA Analysis of Copper Specimens Exposed to Malathion

Figure 16 shows the TGA mass loss profile inclusive of the heating rate and maximum temperature. Mass loss decreased approximately 0.0001 every 100 K. The linearity of the mass loss profile suggests the presence of a single rate-controlling reaction. There are, however, several small nonlinear segments present through the mass loss profile. The reason for these features is not clear; it may be attributed to oxidation in the presence of water and or absorbed oxygen as expressed by Wang, Tao, and Bu (2006) in their study of water dissociation on transition metals. An approximate 9.6×10^{-4} final mass fraction observed at 773 K indicates thermal stability of the copper specimen. The Arrhenius plot in Figure 17 shows a straight line consistent with the presence of a single state first-order reaction. The 0.9794 coefficient of determination complements this fact. The corresponding slope and E_a are 274.3 K and 2.28 kJ mol^{-1} respectively. This E_a value was unexpected, because it is lower than the previously observed value for copper specimens exposed only to deionized water (from Figure 15). The low E_a value in Figure 17 is consistent with the dissociation of weak chemical bonds. It is possible to observe low E_a values with metal catalysis in thermal decomposition reactions (Whitten, Davis, & Peck, 2000). It might be that the copper is exhibiting contact catalytic properties between the surface of the copper specimen and the malathion solution. This finding suggests copper pipes exposed to malathion may thermally degrade more easily than those that have only been exposed to deionized water. Appendix E show additional Arrhenius plots of copper exposed to malathion; observations of these plots show low activation energies across the experiments. These plots provide more evidence supporting the association with low activation energies and copper.

5.2.3.1 Additional Observations of Copper Specimens Exposed to Malathion

Appendix D shows additional raw data TGA mass loss profiles for copper exposed to malathion after thermogravimetry. These profiles show a greater variance in mass loss throughout the course of experiments performed using malathion. These data reveal interesting characteristics about the potential reactions and their effects during thermogravimetric analysis. For instance, Figure D2 shows a case where the TGA profile for copper exhibited qualities of mass gain and loss. According to Schweitzer (1987), copper, when exposed to some medium [i.e. air or water] produces a blue-green protective coating against oxidation. It is highly possible that exposure to air during abrasive cleaning of the sample, as well as its exposure to the aqueous solution of malathion produced this coating. This is important because physical absorption might have resulted from TG analysis of the copper sample.

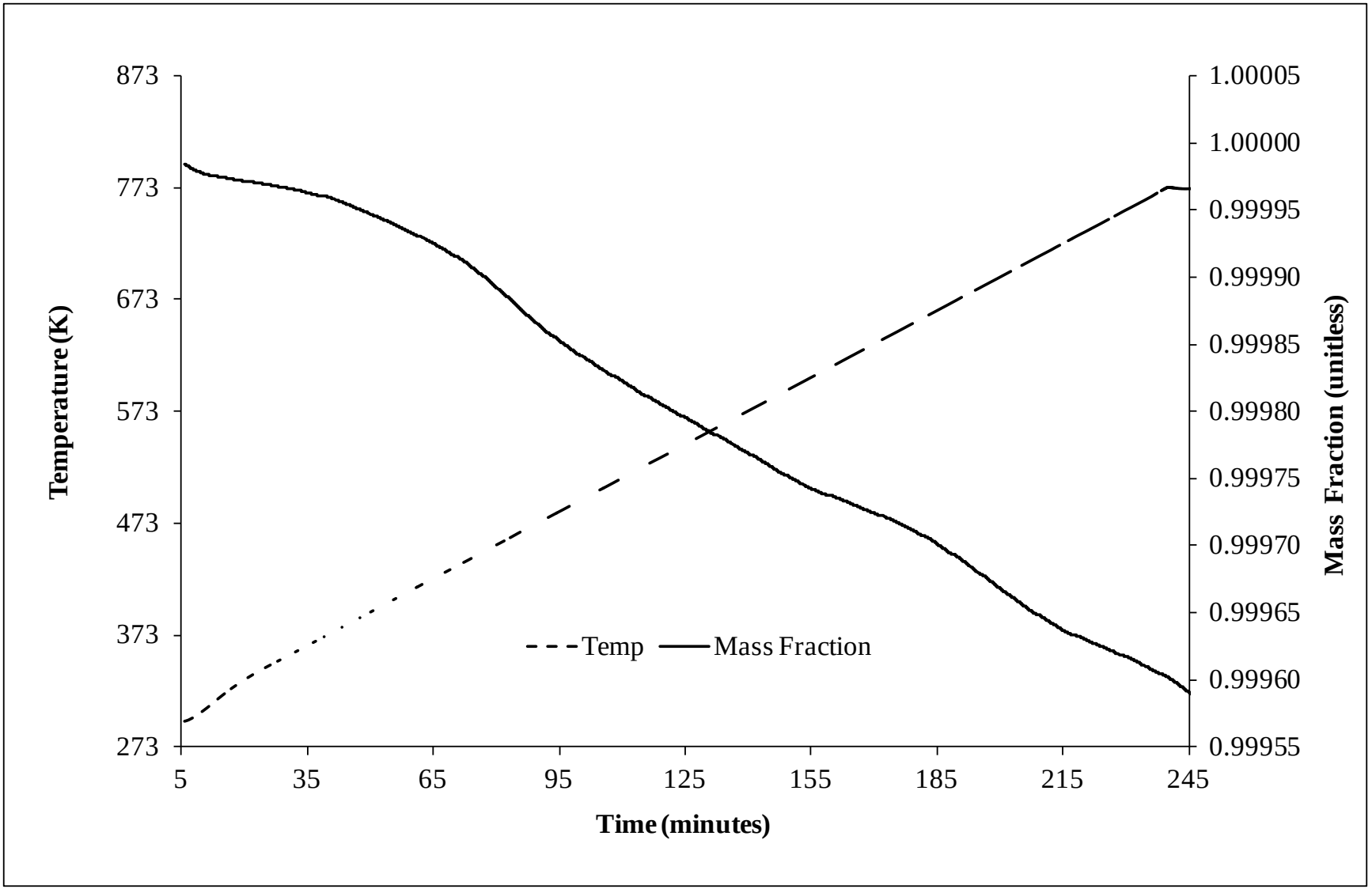

Figure 16. Copper Exposed to Malathion in Water TGA Mass Loss Profile, Displays Mass Loss versus Temperature and Time

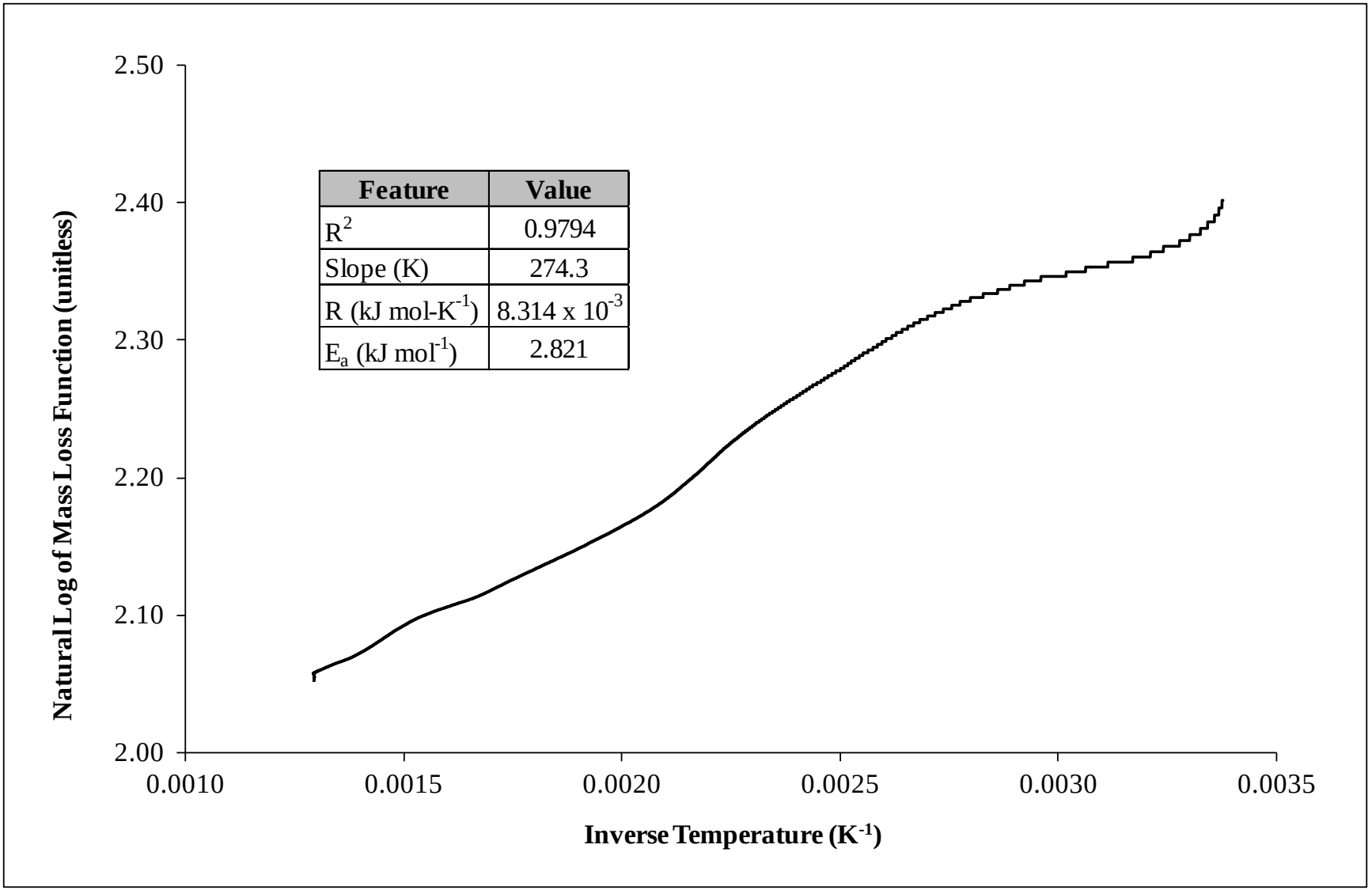

Figure 17. Copper Exposed to Malathion in Water Arrhenius Plot, Straight Line Suggests Mass Loss is First-Order

5.2.4 TGA Analysis of Iron Specimens Exposed to Deionized Water

Figures 18 and 19 show the TGA mass loss profile and Arrhenius plot, respectively. The mass loss profile displays no apparent increases in mass, partly, due to successful TGA system purge using nitrogen gas. The TGA mass loss profile does, however, show three distinct linear decomposition stages corresponding to the mass loss profile's inflection points. The profile shows the inflection point separating the first and second decomposition stage, which occurred at 50 minutes. An approximate temperature of 370 K corresponds to that time. Mass decreased by 0.0005 every 100 K further displaying linear mass loss as function of temperature. The total mass fraction decreased 0.0025 to an approximate mass fraction of 0.9975. This is observed near 773 K indicating thermal stability of the iron specimen. Appendix D shows additional TGA mass loss profiles for iron. The Arrhenius plot in Figure 19 shows a linear plot suggesting mass loss consistent with first-order reaction. The coefficient of determination of 0.9425 confirms this fact. The slope is 394.15 K at 3.27 kJ mol^{-1}. This E_a value is lower than the range expected for the evaporation of water on iron surfaces [e.g. 28 kJ mol^{-1} to 32 kJ mol^{-1}] as described in Grosvenor, Kobe, and Mclntyre's (2005) publication. This result suggests that the evaporation of water may proceed with lowering activation energies than were previously published. These lowered activation energies may be mechanistically possible in the presence of a thermal catalyst. Appendix E contains additional Arrhenius plots for iron.

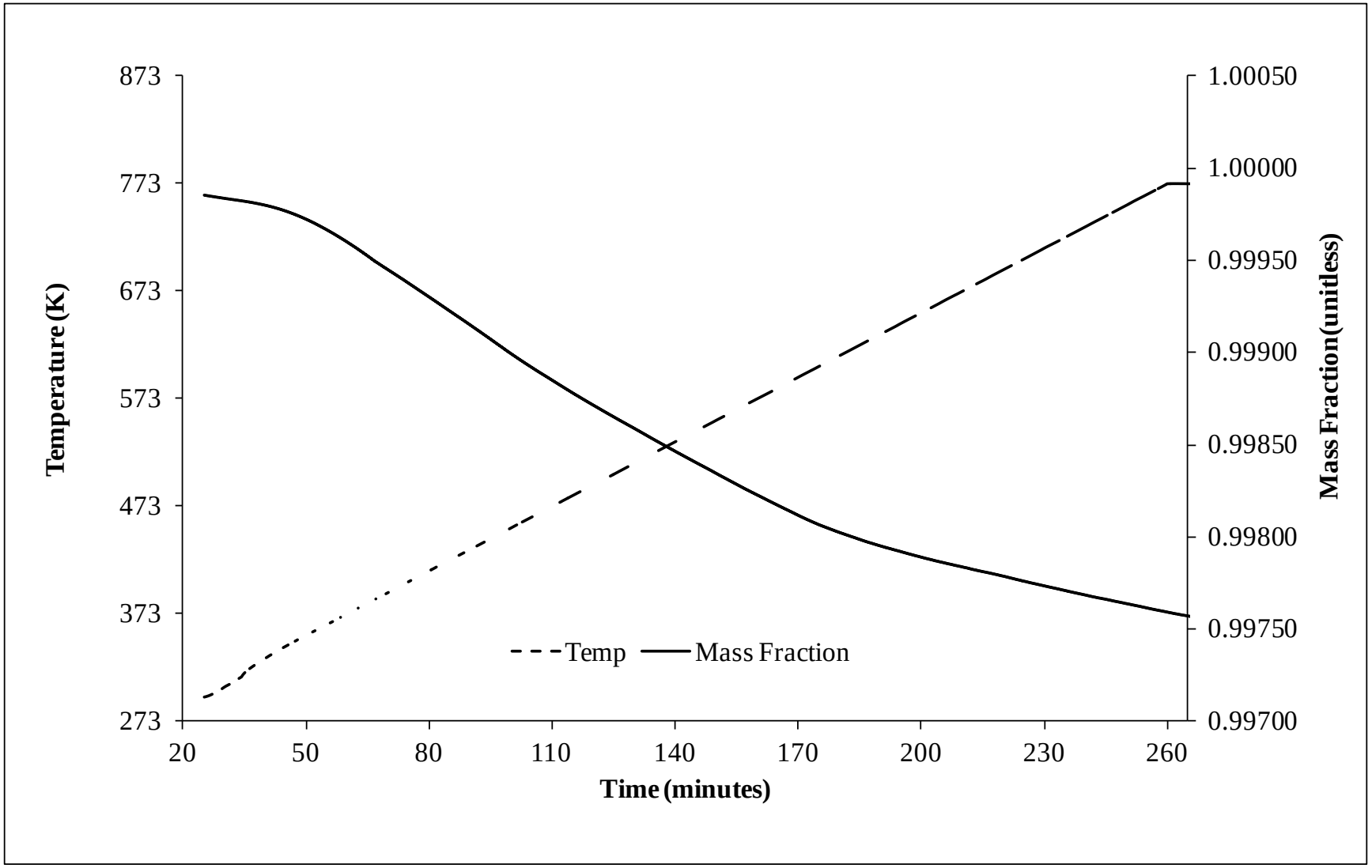

Figure 18. Iron Exposed to Deionized Water TGA Mass Loss Profile, Displays Mass Loss versus Temperature and Time

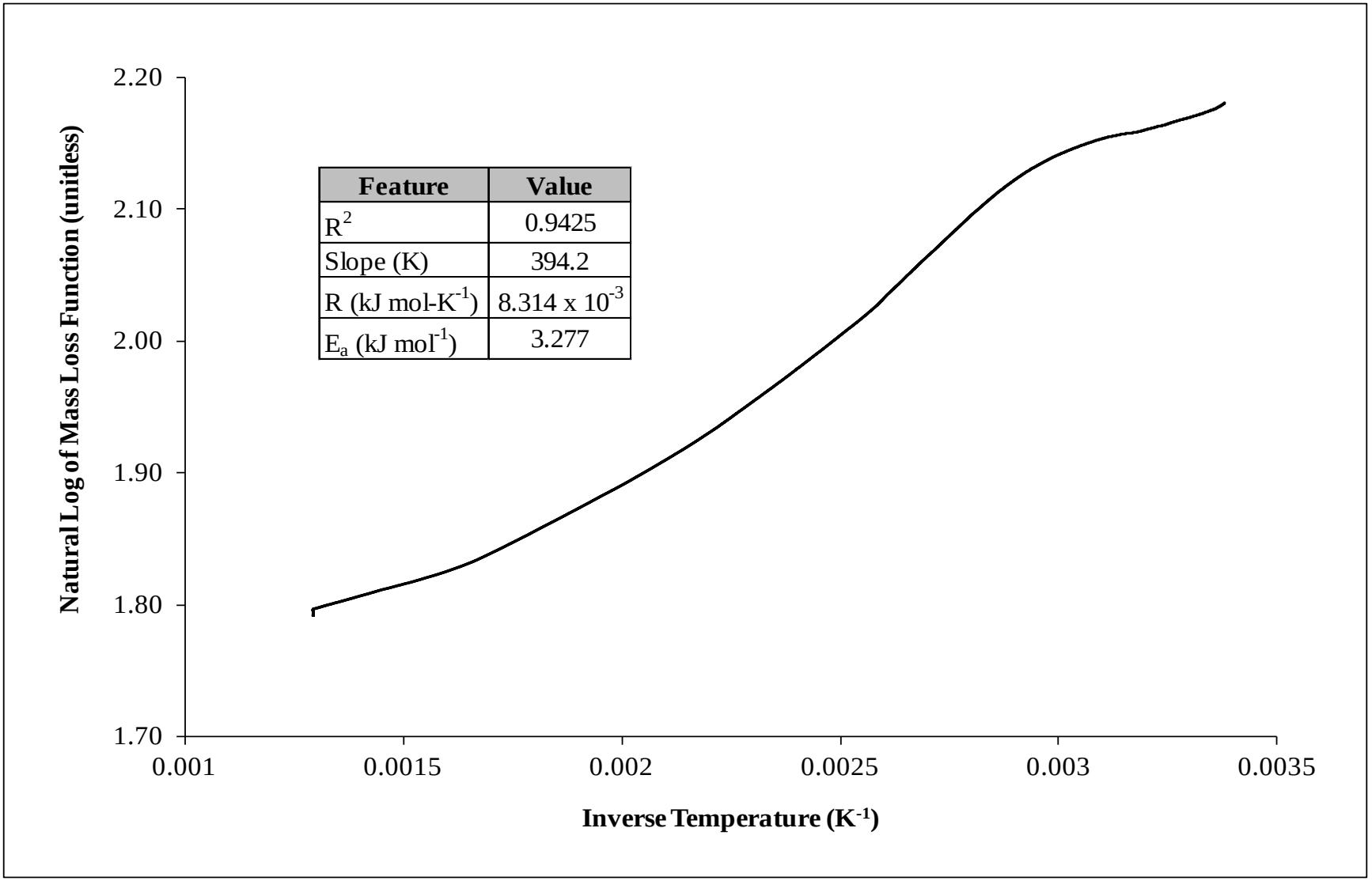

Figure 19. Iron Exposed to Deionized Water Arrhenius Plot, Straight Line Suggests That Mass Loss is First-Order

5.2.5 TGA Analysis of Iron Specimens Exposed to Malathion

Figures 20 and 21 show the TGA mass loss profile and Arrhenius plot for iron, respectively. The TGA profile mass loss curve was initially erratic showing both mass gain and loss providing non useful data. Therefore, the first 180 minutes exhibiting as mass gain of 0.0002 were removed. The erratic display indicated the presence of oxygen [i.e. air intrusion] accounting for the observed variability. Because of the variation, these data required a thermogravimetric technique called curve smoothing (see *Gas Evolution and Characterization)* at twenty-five point heavy smoothing. Linear thermal decomposition stages appear present in the last 75 minutes between 185 and 230 minutes and 230 and 250 minutes. The final mass fraction is observed at 773 K is 0.998. The initial point of the plateau and the change in slope indicates that the iron specimen is reaching thermally stability. The Arrhenius plot was nonlinear as determined by observation and the 0.4298 coefficient of determination. The nonlinear plot is an indication that more than one rate-controlling reaction occurred during the course of the experiment. This indication also illustrates that the plot is inconsistent with first-order mass loss. The slope is small, displaying 184.59 K as compared to previous data. Activation energy of 1.54 kJ mol^{-1} corresponds to this slope and is less than the E_a value observed for specimens exposed only to deionized water. This suggests the observed value may be possible if the malathion is exhibiting catalytic properties on the surface of the iron. Appendix D and E contain additional mass loss profiles and Arrhenius plots for iron, respectively.

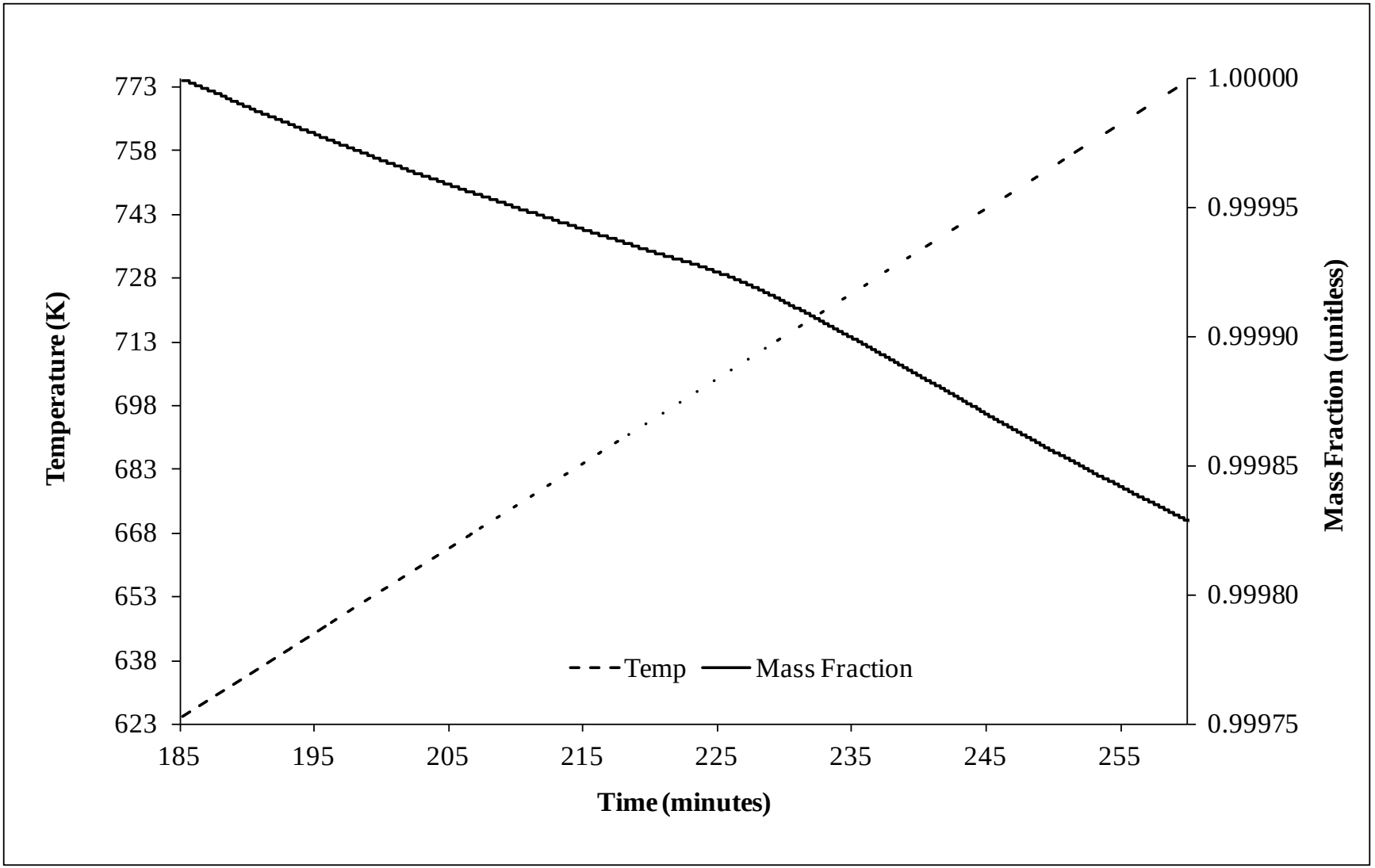

Figure 20. Iron Exposed to Malathion TGA Mass Loss Profile, Displays Mass Loss versus Temperature and Time

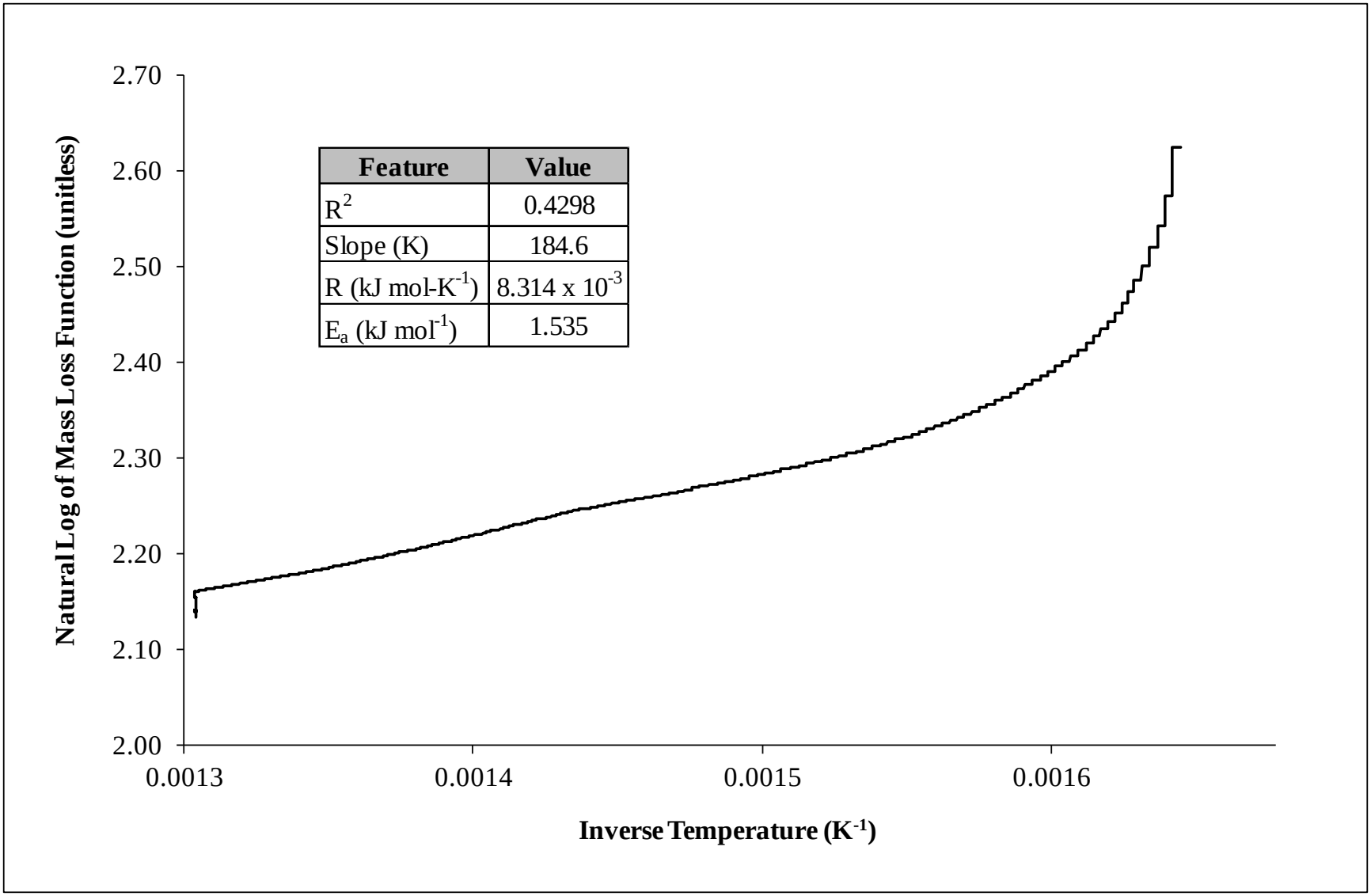

Figure 21. Iron Exposed to Malathion Arrhenius Plot, Curved Line Shows Mass Loss is Inconsistent with First-Order

5.2.6 The Effect of Malathion on Activation Energy

Table 3, organized by decreasing total temperature range activation energies [i.e. column 8], summarizes the slope, activation energy (E_a), and reaction start temperatures for the research generated Arrhenius plots. The activation energies taken at four temperature ranges correspond to displayed times. The following temperatures categorize the activation energies: 296 K to 398 K, 399 K to 523 K, 524 K to 648 K, and 649 K to 773 K. The table illustrates activation energies over the entire experimentation period. Notice the energies are significantly different across the four temperature intervals versus the total experimentation period. Copper and iron exposed to both malathion and water recognize these differences [e.g. Cu sample no. 2 & 3; Fe sample no. 1 & 3]. These results are relative to previous analyses corresponding to parabolic and linear reaction rates (Zhu, Mimura, & Isshiki, 2002; Grosvenor, Kobe, & Mclntyre, 2005). The actual reaction start temperature shows the initial temperature where the reaction type commenced. Higher activation energies correspond with higher reaction start temperatures for both metals; these data align with Jaber and Probert's (2000) study. This is an indication that temperature is associated with higher activation energies. All specimen and solution types illustrate erratic activation energies. Exposure to malathion outlines overall lower E_a values for both the copper and iron specimens. Notably, the E_a values for iron specimens were lower than that of the copper specimens. The same is true of the E_a for copper and iron exposed to water. The copper value appears twice that of iron exposed to water. Multi-stage [i.e. parabolic] reactions were observed for samples that were exposed to malathion and deionized water; however, the type of catalyst involved may include either the metal or the hydroxyl groups present in water. This evaluation should be clarified in future research efforts.

Table 3. Activation Energies for Copper and Iron

Temp Interval (K)			**296 - 398**	**399 - 523**	**524 - 648**	**649 - 773**		**0 - 773**	
Time Interval (minutes)			**0 - 72**	**73 - 134**	**735 - 197**	**198 - 270**		**0 - 270**	
Sample Type	**Sample No.**	**Solution Type**	**Activation Energy, E_a (kJ mol^{-1})**					**E_a (kJ mol^{-1})**	**Actual Reaction Start Temp (K)**
Copper	2	Water	0.000	0.000	54.89	6.576		12.87	638.0
	2	Malathion	0.448	9.946	15.12	0.000		10.88	309.5
	3	Malathion	0.000	0.000	53.83	2.073		6.867	538.5
	3	Malathion	4.878	29.24	0.000	0.000		6.443	295.0
	1	Malathion	21.64	1.820	1.135	1.570		2.821	295.0
	1	Malathion	4.638	0.990	0.821	1.108		2.512	295.0
	1	Malathion	2.78	2.412	1.730	1.570		2.371	310.0
Iron	3	Water	0.000	33.831	5.219	2.575		6.406	512.0
	3	Water	5.806	1.837	1.252	0.763		3.277	294.0
	3	Malathion	---	---	---	6.626		1.535	295.0
	1	Malathion	2.289	3.089	0.420	2.439		1.285	297.0

5.3 Gas Evolution and Characterization

5.3.1 FT-IR Results for Copper Specimens

Table 4 and 5 show the time intervals for both deionized water and malathion inflection intervals [e.g. TGA Point]. The time intervals show a distribution of coverage across the time of experimentation. For deionized water experiments, two inflection points [e.g. Time (a) and Time (b)] were chosen for each TGA point interval. The times taken between the inflection points demonstrate the sensitivity and workability of the FT-IR detector. Times (a) and (b) displayed in Tables 4 and 5 also express available data at the corresponding TGA point. Times not shown indicate the inconclusive FT-IR data at the corresponding TGA point. Figure 22 illustrates a derivative thermogravimetric (DTG) curve for copper exposed to malathion. The DTG curve shows inflection at the approximate 2, 100, and 200 minute time intervals. These inflection points indicate changes in the curve during experimentation. The use of FT-IR smoothing techniques removed data variance for clarity of expression of features of interest. Figures 23 through 26 show the FT-IR spectra for specific areas of interest corresponding to NIST data and literature for malathion features of interest after data smoothing. (Note: each of these figures shows one point in time corresponding to the temperature at that point. Data were only considered at that one point, because it was discovered from analysis that all other points contained throughout the experiment either were similar or inconclusive.) Figure 23, a spectrum taken at 0.168 minutes [e.g. 2500 cm^{-1} to 3100 cm^{-1}], does not show features consistent with the phosphorus-oxygen-methyl stretching bands normally found between 1380 cm^{-1} to 1640 cm^{-1} wave numbers within infrared spectra corresponding to malathion as shown in Burquins (1977) study or in NIST (2011) infrared data. These data are consistent throughout all temperature ranges. Figure 24, a spectrum taken at 0.1, between wave numbers 1950 cm^{-1} and 2550 cm^{-1},

shows little absorbance. Similarly, between 1650 cm^{-1} and 1050 cm^{-1} wave numbers, no prominent features exist resembling malathion absorption. In contrast, the 1100 cm^{-1} to 500 cm^{-1} band in Figure 25 shows what may appear to be sulfide bands, which is promising considering malathion is comprised of two sulfur molecules as seen in its molecular formula. Figure 26 further clarifies the inoperability of the FT-IR mercuric cadmium telluride (MCT) detector. These characteristics are indicated by the erratic display between the 900 cm^{-1} and 400 cm^{-1}. The corresponding data is inconsistent with features found in wave number bands described by Stuart (1996). These data suggest there may be little absorption of malathion on the copper coupon. Further experiments and analyses are required to determine the amount absorbed to the metal coupons. Appendix F provides additional spectra corresponding to the sample and solution type.

Table 4. TGA Inflection Points Coordinating with FT-IR Spectra for Copper Exposed to Deionized Water

TGA Point	Temp Interval (Kelvin)	Time Interval (minutes)	Time (a)	Time (b)
1	295.0 - 313.5	1.900 - 33.10	8.224	24.17
2	313.5 - 471.4	33.10 - 88.55	40.78	71.83
3	471.3 - 616.7	88.87 - 181.5	-	-
4	616.7 - 773.0	181.2 - 270.7	-	-

Table 5. TGA Inflection Points Coordinating with FT-IR Spectra for Copper Exposed to Malathion

TGA Point	Temp Interval (Kelvin)	Time Interval (minutes)	Time (a)	Time (b)
1	296.9 - 297.4	3.900 - 41.57	12.42	39.77
2	297.4 - 378.9	41.57 - 106.7	42.62	98.79
3	378.9 - 471.5	106.7 - 147.9	108.8	145.0
4	471.5 - 597.8	147.9 - 211.1	-	-
5	597.8 - 747.8	211.1 - 286.1	-	-

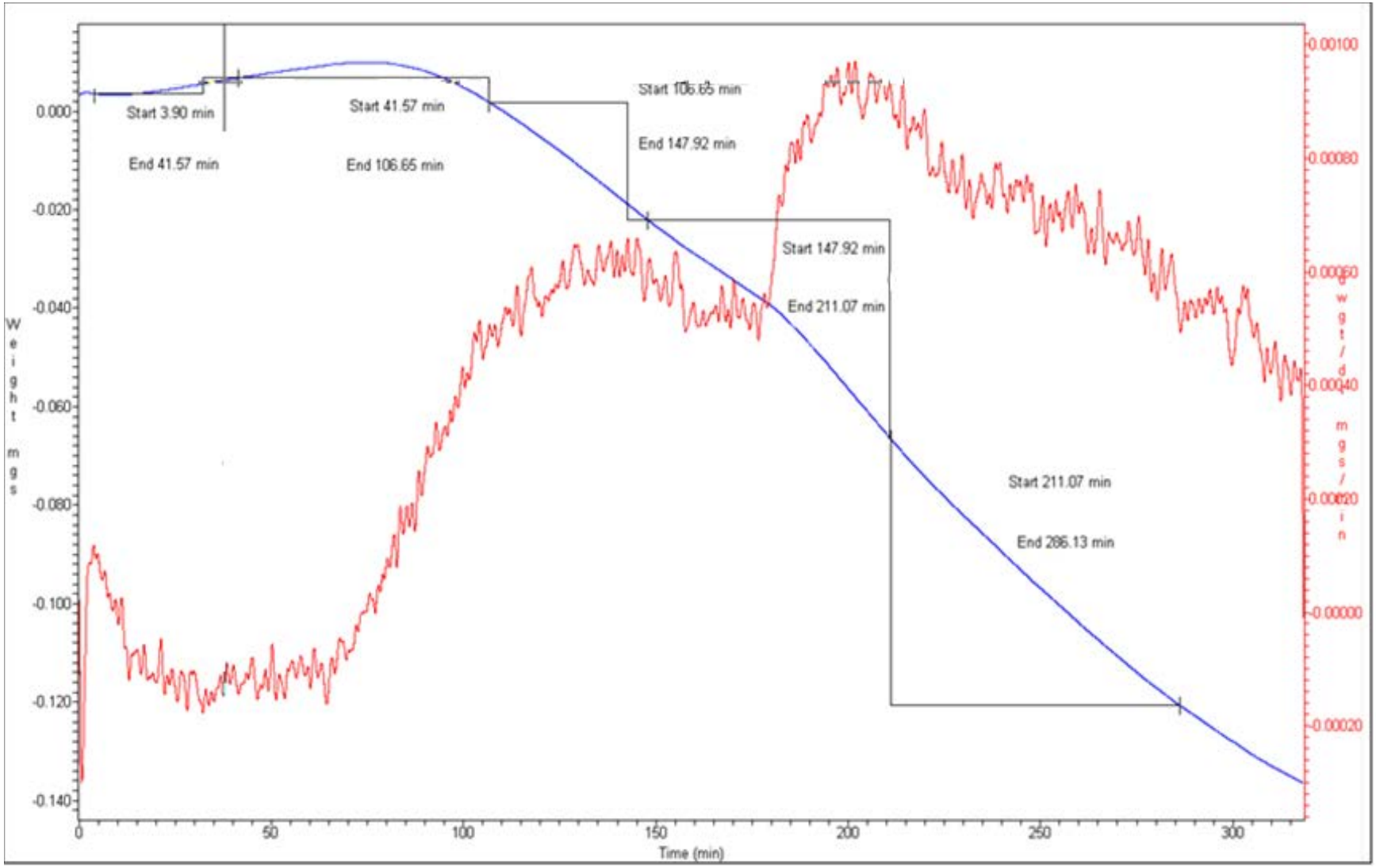

Figure 22. Copper (2) [22 Oct 14] Exposed to Malathion DTG Curve, Displays Inflection TG Curve Inflection Points

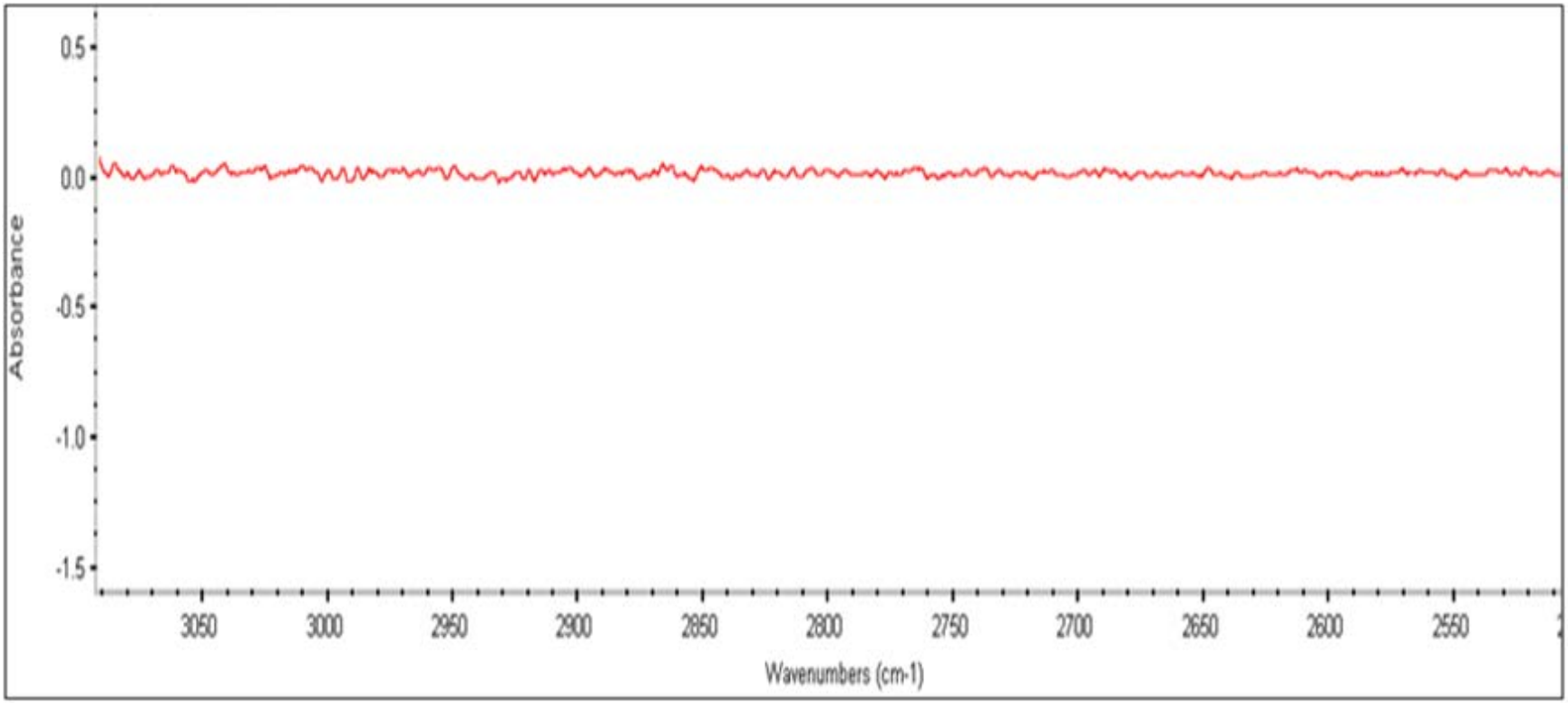

Figure 23. Copper (2) [22 Oct 14] Exposed to Malathion FT-IR Spectrum at 0.168 min, 3150 cm^{-1} to 2600 cm^{-1}, MCT Detector, Smoothing

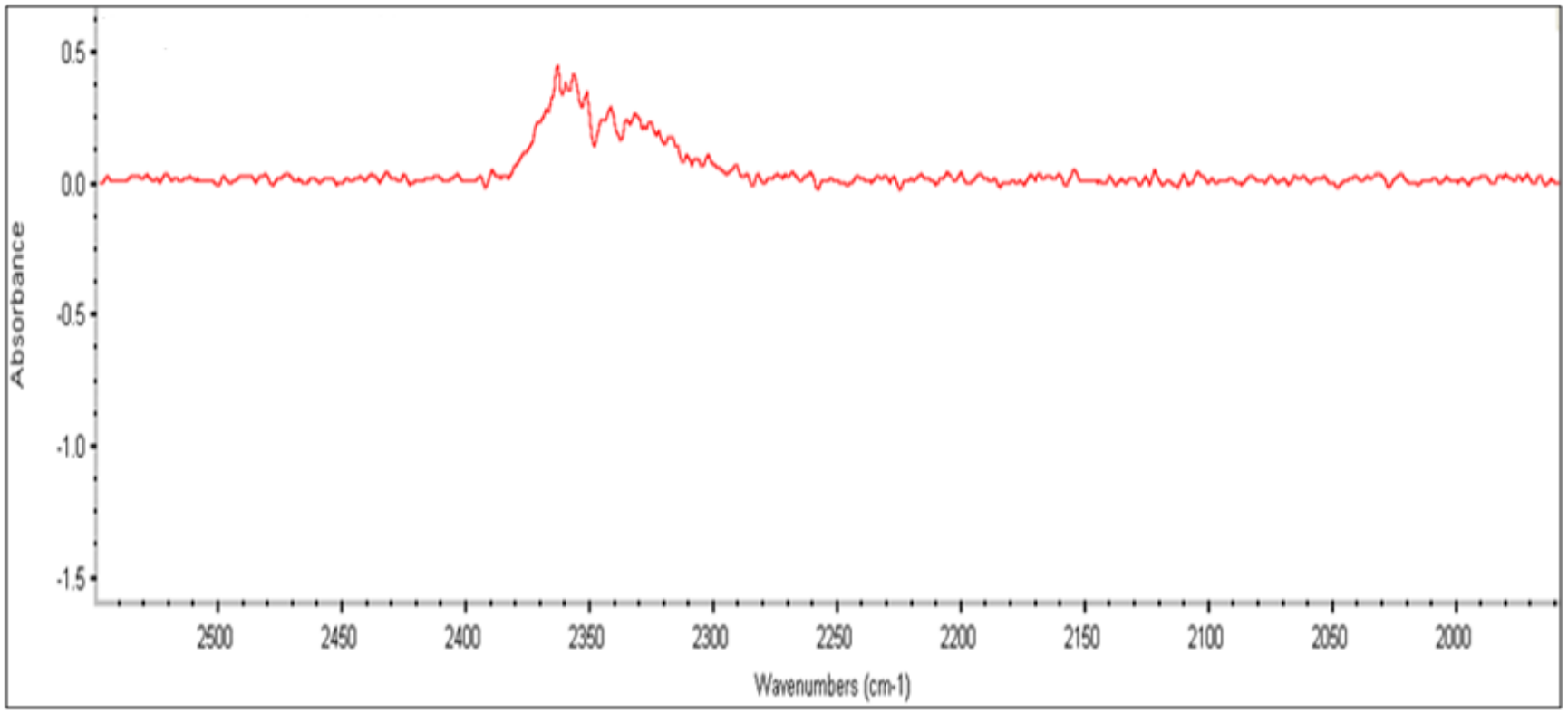

Figure 24. Copper (2) [22 Oct 14] Exposed to Malathion FT-IR Spectrum at 0.168 min, 2550 cm^{-1} to 1950 cm^{-1}, MCT Detector, Smoothing

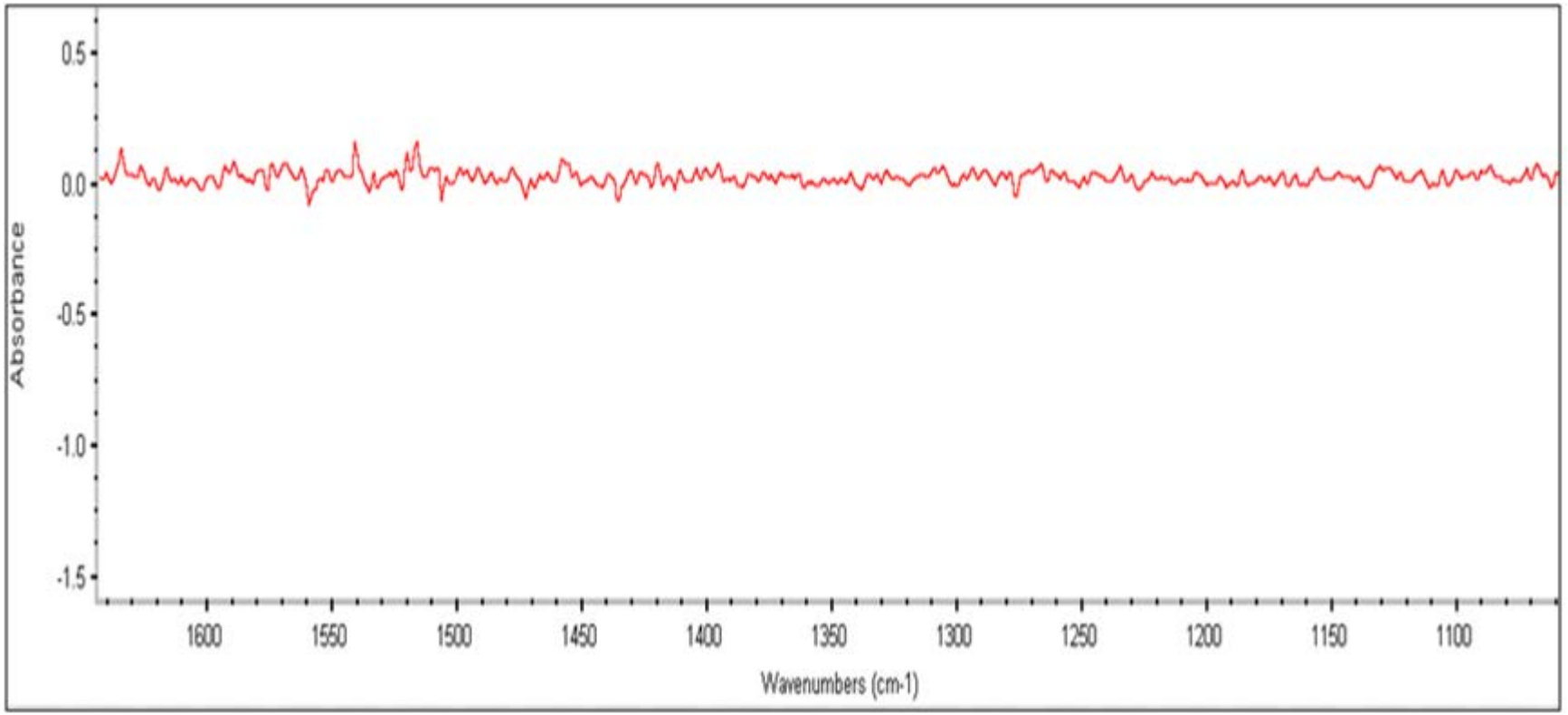

Figure 25. Copper (2) [22 Oct 14] Exposed to Malathion FT-IR Spectrum at 0.168 min, 1650 cm^{-1} to 1050 cm^{-1}, MCT Detector, Smoothing

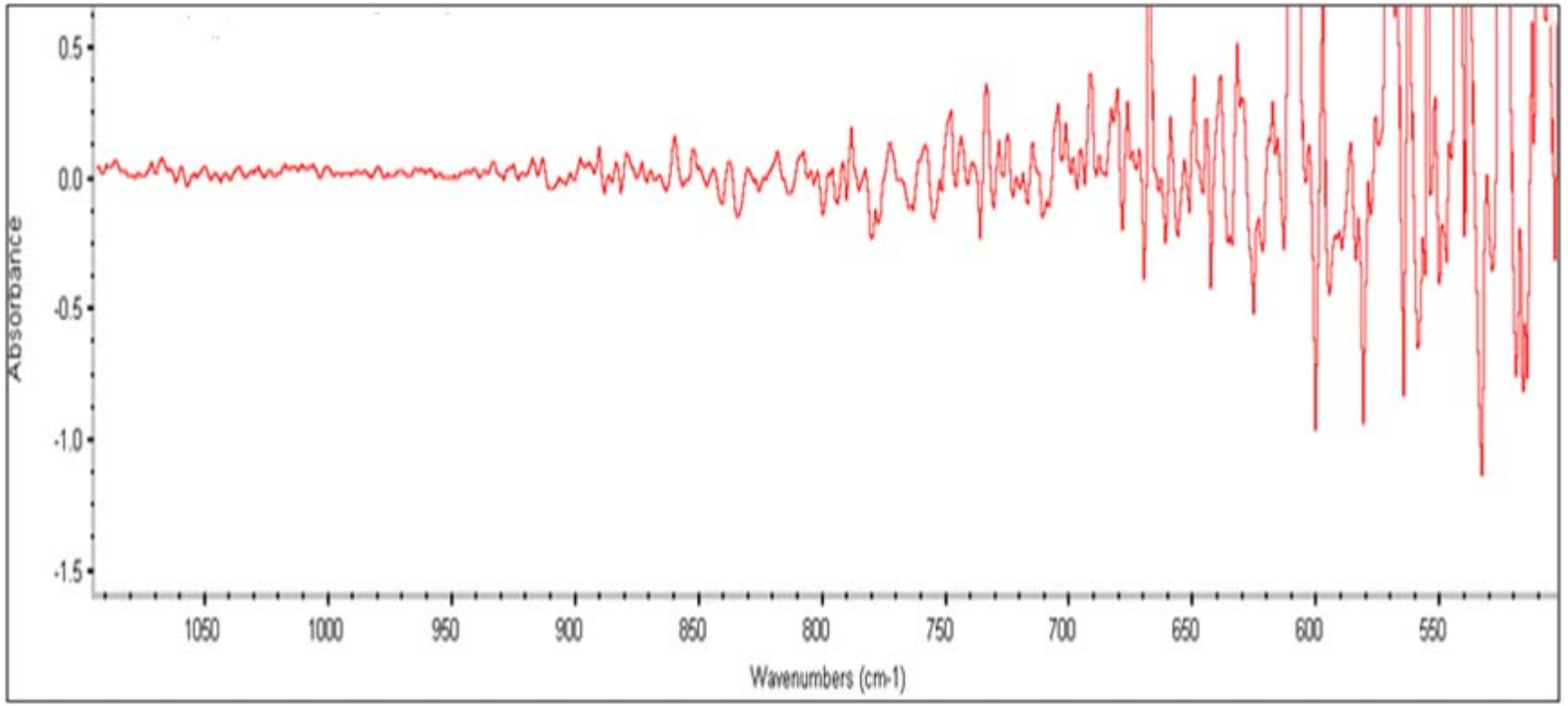

Figure 26. Copper (2) [22 Oct 14] Exposed to Malathion FT-IR Spectrum at 0.168 min, 1100 cm^{-1} to 500 cm^{-1}, MCT Detector, Smoothing

Table 6 shows FT-IR library spectral data for chemicals and the number of occurrence throughout the analysis pertaining to the analyzed spectrums. These data were taken five times between TGA time or temperature interval points (shown in Table 4). The number of occurrences is associated with the number of times the FT-IR library identified the chemical between the TGA data points. The table shows proposed chemicals associated with potential constituents of malathion. Random analysis of the copper specimen exposed to deionized water revealed water molecules present. Glycol esters and associated organic hydrocarbons were identified for copper specimens exposed to malathion. The butanediol is associative to the butenedioic acid and succinic acid indicated in the Bender (1969), and Kralj, Franko, and Tresbse (2006) studies. This association infers the chemical may be evolving from the malathion. The FT-IR identified Hydrogen sulfide, which may be the result of surface reactions between malathion and the coating on the copper specimen. As expected, the copper specimens show features similar to carbon monoxide and carbon dioxide, which are common combustion byproducts. Appendix G, shows the full list of chemicals present in the analysis corresponding to associated inflection points.

Table 6. FT-IR Chemicals of Interest Copper Exposed to Deionized Water and Malathion

TGA Point	Compound Name	Chemical Formula	Molecular Weight	Number of Occurrences between the TGA points
1	Carbon Monoxide	CO	28.01	5
2	Hydrogen Sulfide	H_2S	34.09	1
2	Carbon Dioxide	CO_2	44.01	5
2	Trans-Piperylene	C_5H_8	68.12	2
3	Cyclohexane	C_6H_{12}	84.16	2
3	Butanediol	$C_4H_{10}O_2$	90.12	2
1	4-Vinyl-1-Cyclohexene	C_8H_{14}	110.2	3
2	Alpha-Terpineol	$C_{10}H_{18}O$	154.2	2

5.3.2 FT-IR Results for Iron

Table 7 shows the inflection points taken across the DTG curve. Time and temperature information was tabulated across four inflection points. Table 8 shows the chemical identification for Iron exposed to water. The match signifies the strength of correlation of the proposed chemical with the FT-IR library. The only byproduct identified for the iron specimens was water. Iron exposed to malathion was analyzed; however, the results were inconclusive. These results are highly correlated with the failed MCT detector. Use of the DTGS-KBr detector was also unsuccessful in identifying byproducts. This was due to the detector's low sensitivity. Appendix F displays the full spectrums.

Table 7. TGA Inflection Points Coordinating with FT-IR Spectra for Iron Exposed to Deionized Water

TGA Point	Temp Interval (Kelvin)	Time Interval (minutes)	Time (a)	Time (b)
1	296.6 - 364.9	3.170 - 45.55	11.58	94.30
2	364.9 - 479.9	45.55 - 102.8	55.21	101.9
3	479.9 - 625.1	102.8 - 175.4	120.5	170.5
4	625.1 - 773.1	175.4 - 252.2	185.8	248.0

Table 8. FT-IR Chemicals of Interest Iron Exposed to Deionized Water

TGA Point	Match	Compound Name	Chemical Formula	Possibility: Yes/ No
1	53.16	Water	H_2O	Yes
2	74.82	Water	H_2O	Yes
3	74.21	Water	H_2O	Yes
4	75.16	Water	H_2O	Yes
5	75.33	Water	H_2O	Yes

5.4 Limitations of Research

5.4.1 Literature Data

Typically, TGA is used to study thermal stability in the areas of biology, ceramics, foodstuff, polymers and plastics as well as metals and alloys (Dodd & Tonge, 1987). There is limited research on the use of TGA and FT-IR to characterize metal exposure to chemicals like malathion. This datum gap produces difficulty in finding useful data for comparison.

5.4.2 Air Intrusion

Air intrusion caused mass increases during TGA analysis. This problem interfered with the determination of activation energies and the elucidation of reaction mechanisms. The Air intrusion may have been a result of improper vacuuming of the system. Also, lowered purge gas rates may have been a possible cause. Air intrusion should be controlled by necessary means to prevent oxidation and possible mass increases.

5.4.3 Equipment Malfunctions and Part Replacement

The equipment and instrumentation was unused for approximately two years prior to research experimentation. As a result, the equipment required extensive maintenance and repair. Daily, weekly, monthly maintenance was performed throughout, and repairs were performed during equipment failures. Each repair required equipment calibration and testing. This changed the condition of the equipment throughout the course of the research. Routine maintenance and checks on instrumentation should be periodically performed to prevent equipment malfunctions.

5.4.3.1 TGA Sample Loading and Weight-Balance Stabilizing

Typical TGA component maintenance and failures were those relative to sample loading and weight balancing and stabilizing. The TGA sample load area was problematic. After

approximately five to ten runs, the TGA mass loss profiles depicted high data variance as a result of electrostatic build-up between the porcelain baffle and platinum wire. Immediately following sample loading, this electrostatic build-up was visible. The platinum wire was electrostatically attached to the inside casing on the baffle. Erratic weight fluctuations were also observed (± 10 mg to 20 mg). To rectify this problem, a few procedures were performed, depending on the severity of data variance: the platinum wire was detached and straightened or the baffle and wire were shortened. Iron and copper both have relatively different atomic weights, thus each required balancing using similar or heavier weights to properly align the TGA balance fulcrum between the sample and the tare sides. Moreover, weight stabilization of the balance was necessary to prevent erratic disposition of the platinum crucible during analysis, and, if not performed, led to erratic data.

5.4.3.2 FT-IR Detectors

The mercury cadmium telluride (MCT) detector is very sensitive with wavelength resolutions around 4.8 cm^{-1} (Stuart, 1996; ThermoFisher, undated) and required cryogenic cooling prior to use. Over time the cryogenic cooling of the detector produced mechanical failure of the detector preventing it from retaining liquid nitrogen. Once the detector became inoperable, it could no longer retain enough liquid nitrogen to remain cooled. Data collection, particularly, the wavelength resolution was severely hindered. The inoperable MCT detector was replaced with a DTGS-KBr detector, which did not require cryogenic cooling. However, the sensitivity of detection was severely reduced to approximately 16 cm^{-1} wavelength resolutions. The DTGS-KBr detection range prevented collection of useful data.

The aforementioned instrumentation and experimental issues rendered portions of the data unusable. Data proportions among the sample, solutions, and experiment types are described in Table 9. Twenty-six TGA and FT-IR experiments were performed over the course of research. Approximately 42% of the TGA experiments produced useable mass loss profiles. Of the total FT-IR experiments performed, only 46% are useable, meaning they can be used to produce spectra able to be used to identify gas byproducts. Future research should focus on the use of the more sensitive MCT detector for gas byproduct identification.

Table 9. Copper and Iron TGA Coupled with FT-IR Experimentation

Sample Type	Aqueous Solution Type	TGA Experiments Total	TGA Useable Experiments Total	FT-IR Experiments Total	FT-IR Useable Experiments Total
Copper	Deionized Water	6	1	2	3
Copper	Malathion	8	6	6	2
Iron	Deionized Water	6	2	3	1
Iron	Malathion	6	3	2	0
Total		26	12	13	6

VI. Conclusion

This research explored the effect of malathion on experimental results retrieved from TGA and FT-IR analysis. The research addressed two objectives: 1) Determine the effect of malathion exposure on standard activation energy required for malathion to begin volatizing from copper and iron piping, and 2) determine the volatile chemical effect of malathion on the elemental composition of copper and iron gas evolution during thermogravimetric analysis.

Exposure to malathion solution created a visible silver coating on all copper samples and graphite flake particles on iron specimens. Thermogravimetric mass loss curves revealed linear decomposition stages associated with first order mass loss reactions. The TGA profiles also showed that the copper and iron specimens were thermally stable, as expected. Visual observations revealed metal oxide coatings on the surface of the specimens, before and after TGA analysis. Copper specimens exposed to malathion were associated with E_a values (2.28 kJ mol^{-1} to 4.40 kJ mol^{-1}) that were lower than for iron specimens that were exposed only to deionized water (10.42 kJ mol^{-1} and 12.87 kJ mol^{-1}). Iron specimens exposed to malathion were associated with E_a values (1.54 kJ mol^{-1} and 1.28 kJ mol^{-1}) than for iron specimens that were exposed only to deionized water (3.30 kJ mol^{-1} and 6.40 kJ mol^{-1}). These results satisfy research objective one suggesting that malathion may be associative to lowering activation energies; however, further experimental confirmation is required due in part to limited data. Metal-driven catalysis was a proposed mechanism, which may explain the magnitude of the E_a values. The FT-IR results suggested that there was minimal malathion adsorption to either copper or iron. Additionally, the FT-IR results appease objective two suggesting that hydrogen sulfide and possibly butenedioic acid are gas evolution byproducts produced during TGA analysis of copper specimens exposed to malathion.

Thermogravimetry coupled with the Fourier transform infrared spectroscopy technique is very useful. However there are instrumentation and sample limitations, which this research showed with use of the technique on chemical to metal adherence. The research proposed a list of chemicals (see Appendix G) that should be clarified in further research efforts with the use of liquid isotherm experiments and chromatography. At this time, further research and experimentation are required to determine if thermogravimetry is a viable method for EPA use in its chemical detection efforts. With that said, there may be usefulness of the technique in additional water contamination studies (see *Future Work*). Conclusively, this research, based on the author's knowledge and literature review, is the first to use thermogravimetry coupled with spectroscopy to test malathion adherence to metal surfaces.

VII. Future Work

The research study should focus on the following:

(1) The effect of biological films on TGA and FT-IR data.

(2) The application of corrosion engineering for water infrastructure modeling

(3) The application of TGA and GC-MS for identification of off-gas chemicals.

(4) The effect of other toxic chemicals on TGA and FT-IR results.

(5) The characterization of the silver metallic coat produced on copper specimens after TGA.

Appendix A. Experimentation Procedure and Sample Preparation Data

List of Figures

List of Tables

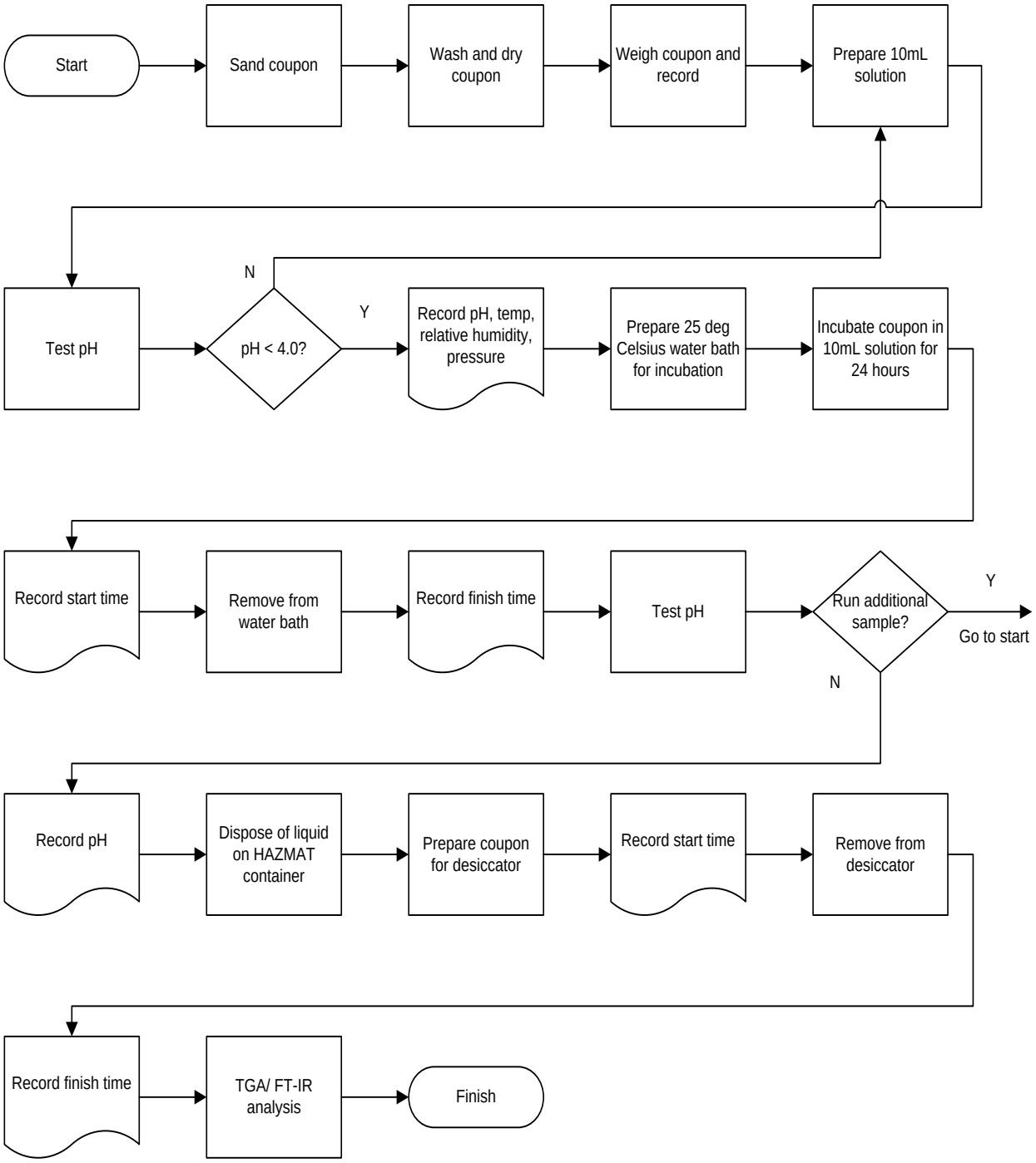

Figure A1. Experimentation Procedure

Table A1. Coupon Sample Preparation for Copper (1) Exposed to Deionized Water and Malathion for Experiment 1

Copper Sample Coupon #1			
Date	10/06/2014	Date	10/16/2014
Pressure (mmHg)	738.0	Pressure (mmHg)	741.0
Temp ambient (Celsius)	25.0	Temp ambient (Celsius)	25.0
Weight (grams)	0.7634	Weight (grams)	0.7634
Solution (type)	Deionized H_2O	Solution (type)	Malathion in H_2O
Solution volume (mL)	20.0	Solution volume (mL)	20.0
PH before	5.70	PH before	4.60
PH after	N/A	PH after	5.80
24hr Incubation:			
Start Time	1156L, 10/6/2014	Start Time	1015L, 10/16/2014
Finish Time	1030L, 10/7/2014	Finish Time	0950L, 10/17/2014
4hr Desiccation:			
Start Time	1030L, 10/7/2014	Start Time	0955L, 10/17/2014
Finish Time	1450L, 10/7/2014	Finish Time	1400L, 10/17/2014
4hr TGA/FTIR:			
Start Time	1500L, 10/7/2014	Start Time	1500L, 10/17/2014
Finish Time	2030L, 10/7/2014	Finish Time	2000L, 10/17/2014

Table A2. Coupon Sample Preparation for Copper (2) Exposed to Deionized Water and Malathion for Experiment 1

Copper Sample Coupon #2			
Date	10/08/2014	Date	10/21/2014
Pressure (mmHg)	746.0	Pressure (mmHg)	745.0
Temp ambient (Celsius)	25.0	Temp ambient (Celsius)	25.0
Weight (grams)	0.9458	Weight (grams)	0.9458
Solution (type)	Deionized H_2O	Solution (type)	Malathion in H_2O
Solution volume (mL)	20.0	Solution volume (mL)	10.0
PH before	5.50	PH before	5.80
PH after	5.80	PH after	6.04
24hr Incubation:			
Start Time	0915L, 10/08/2014	Start Time	1000L, 10/21/2014
Finish Time	0900L, 10/08/2014	Finish Time	0940L, 10/22/2014
4hr Desiccation:			
Start Time	0952L 10/09/2014	Start Time	0940L, 10/22/2014
Finish Time	1400L 10/09/2014	Finish Time	1340L, 10/22/2014
4hr TGA/FTIR:			
Start Time	1415L 10/09/2014	Start Time	1600L, 10/22/2014
Finish Time	1900L 10/09/2014	Finish Time	2200L, 10/22/2014

Table A3. Coupon Sample Preparation for Copper (3) Exposed to Deionized Water and Malathion for Experiment 1

Copper Sample Coupon #3			
Date	10/22/2014	Date	10/28/2014
Pressure (mmHg)	751.0	Pressure (mmHg)	743.0
Temp ambient (Celsius)	25.0	Temp ambient (Celsius)	25.0
Weight (grams)	0.9807	Weight (grams)	0.9807
Solution (type)	Deionized H_2O	Solution (type)	Malathion in H_2O
Solution volume (mL)	10.0	Solution volume (mL)	10.0
PH before	6.20	PH before	4.52
PH after	6.00	PH after	5.30
24hr Incubation:			
Start Time	1000L, 10/22/2014	Start Time	0950L, 10/28/2014
Finish Time	0920L, 10/23/2014	Finish Time	0940L, 10/29/2014
4hr Desiccation:			
Start Time	0930L, 10/23/2014	Start Time	0940L, 10/29/2014
Finish Time	1430L, 10/23/2014	Finish Time	1400L, 10/29/2014
4hr TGA/FTIR:			
Start Time	1500L, 10/23/2014	Start Time	1415L, 10/29/2014
Finish Time	2000L, 10/23/2014	Finish Time	1915L, 10/29/2014

Table A4. Coupon Sample Preparation for Copper (1) Exposed to Deionized Water and Malathion for Experiment 2

Copper Sample Coupon #1			
Date	11/03/2014	Date	11/09/2014
Pressure (mmHg)/Hum%	750.0/47.0	Pressure (mmHg)	745.0/51.0
Temp ambient (Celsius)	21.0/25.0	Temp ambient (Celsius)	20.0/25.0
Weight (grams)	0.7634	Weight (grams)	0.7634
Solution (type)	Deionized H_2O	Solution (type)	Malathion in H_2O
Solution volume (mL)	10.0	Solution volume (mL)	5.00
PH before	6.38	PH before	3.12
PH after	5.94	PH after	5.32
24hr Incubation:			
Start Time	0900L, 11/03/2014	Start Time	0630L, 11/09/2014
Finish Time	0900L, 11/04/2014	Finish Time	0630L, 11/09/2014
4hr Desiccation:			
Start Time	0930L, 11/04/2014	Start Time	0630L, 11/10/2014
Finish Time	1400L, 11/04/2014	Finish Time	0930L, 11/10/2014
4hr TGA/FTIR:			
Start Time	1500L, 11/04/2014	Start Time	1000L, 11/10/2014
Finish Time	2000L, 11/04/2014	Finish Time	1400L, 11/10/2014

Table A5. Coupon Sample Preparation for Copper (2) Exposed to Deionized Water and Malathion for Experiment 2

Copper Sample Coupon #2			
Date	11/05/2014	Date	12/02/2014
Pressure (mmHg)	749.0/59.0	Pressure (mmHg)	752.0/44.0
Temp ambient (Celsius)	21.0/25.0	Temp ambient (Celsius)	20.0/25.0
Weight (grams)	0.9458	Weight (grams)	0.9458
Solution (type)	Deionized H_2O	Solution (type)	Malathion in H_2O
Solution volume (mL)	10.0	Solution volume (mL)	10.0
PH before	5.24	PH before	3.57
PH after	5.23	PH after	5.12
24hr Incubation:			
Start Time	0900L, 11/05/2014	Start Time	0630L, 11/22/2014
Finish Time	0630L, 11/06/2014	Finish Time	0630L, 11/23/2014
4hr Desiccation:			
Start Time	0630L, 11/06/2014	Start Time	0830L, 12/02/2014
Finish Time	1000L, 11/06/2014	Finish Time	1100L, 12/02/2014
4hr TGA/FTIR:			
Start Time	1030L, 11/06/2014	Start Time	1130L, 12/02/2014
Finish Time	1500L, 11/06/2014	Finish Time	1400L, 12/02/2014

Table A6. Coupon Sample Preparation for Copper (3) Exposed to Deionized Water and Malathion for Experiment 2

Copper Sample Coupon #3			
Date	11/07/2014	Date	12/02/2014
Pressure (mmHg)	748.0/53.0	Pressure (mmHg)	753.0/47.0
Temp ambient (Celsius)	20.0/25.0	Temp ambient (Celsius)	20.0/25.0
Weight (grams)	0.9807	Weight (grams)	0.9807
Solution (type)	Deionized H_2O	Solution (type)	Malathion in H_2O
Solution volume (mL)	10.0	Solution volume (mL)	10.0
PH before	5.70	PH before	4.96
PH after	5.60	PH after	5.54
24hr Incubation:			
Start Time	0900L, 11/07/2014	Start Time	0830L, 12/02/2014
Finish Time	0600L, 11/08/2014	Finish Time	0630L, 12/03/2014
4hr Desiccation:			
Start Time	0600L, 11/08/2014	Start Time	0630L, 12/03/2014
Finish Time	1000L, 11/08/2014	Finish Time	0900L, 12/03/2014
4hr TGA/FTIR:			
Start Time	1100L, 11/08/2014	Start Time	0930L, 12/03/2014
Finish Time	1600L, 11/08/2014	Finish Time	1430L, 12/03/2014

Table A7. Coupon Sample Preparation for Iron (1) Exposed to Deionized Water and Malathion for Experiment 1

Iron Sample Coupon #1			
Date	10/07/2014	Date	10/20/2014
Pressure (mmHg)	741.0	Pressure (mmHg)	744.0
Temp ambient (Celsius)	25.0	Temp ambient (Celsius)	25.0
Weight (grams)	0.6361	Weight (grams)	0.6361
Solution (type)	Deionized H_2O	Solution (type)	Malathion in H_2O
Solution volume (mL)	20.0	Solution volume (mL)	10.0
PH before	4.50	PH before	5.68
PH after	6.30	PH after	5.52
24hr Incubation:			
Start Time	1156L, 10/07/2014	Start Time	1215L, 10/20/2014
Finish Time	0915L, 10/08/2014	Finish Time	1030L, 10/21/2014
4hr Desiccation:			
Start Time	0915L, 10/08/2014	Start Time	1040L, 10/21/2014
Finish Time	1315L, 10/08/2014	Finish Time	1430L, 10/21/2014
4hr TGA/FTIR:			
Start Time	1135L 10/08/2014	Start Time	1530L, 10/21/2014
Finish Time	1800L 10/08/2014	Finish Time	2030L, 10/21/2014

Table A8. Coupon Sample Preparation for Iron (2) Exposed to Deionized Water and Malathion for Experiment 1

Iron Sample Coupon #2			
Date	10/13/2014	Date	10/17/2014
Pressure (mmHg)	746.0	Pressure (mmHg)	739.0
Temp ambient (Celsius)	25.0	Temp ambient (Celsius)	25.0
Weight (grams)	0.8161	Weight (grams)	0.8161
Solution (type)	Deionized H_2O	Solution (type)	Malathion in H_2O
Solution volume (mL)	20.0	Solution volume (mL)	10.0
PH before	6.30	PH before	3.74
PH after	6.53	PH after	5.26
24hr Incubation:			
Start Time	1020L, 10/13/2014	Start Time	1030L, 10/17/2014
Finish Time	0855L, 10/16/2014	Finish Time	1015L, 10/18/2014
4hr Desiccation:			
Start Time	0855L, 10/16/2014	Start Time	1010L, 10/18/2014
Finish Time	1512L, 10/16/2014	Finish Time	1400L, 10/18/2014
4hr TGA/FTIR:			
Start Time	1600L, 10/16/2014	Start Time	1415L, 10/18/2014
Finish Time	2100L, 10/16/2014	Finish Time	2000L, 10/18/2014

Table A9. Coupon Sample Preparation for Iron (3) Exposed to Deionized Water and Malathion for Experiment 1

Iron Sample Coupon #3			
Date	10/27/2014	Date	10/29/2014
Pressure (mmHg)	745.0	Pressure (mmHg)	746.0
Temp ambient (Celsius)	25.0	Temp ambient (Celsius)	25.0
Weight (grams)	0.9065	Weight (grams)	0.9065
Solution (type)	Deionized H_2O	Solution (type)	Malathion in H_2O
Solution volume (mL)	10.0	Solution volume (mL)	10.0
PH before	6.82	PH before	5.36
PH after	6.06	PH after	5.53
24hr Incubation:			
Start Time	1000L, 10/27/2014	Start Time	0944L, 10/29/2014
Finish Time	0950L, 10/28/2014	Finish Time	0950L, 10/30/2014
4hr Desiccation:			
Start Time	0950L, 10/28/2014	Start Time	1000L, 10/30/2014
Finish Time	1400L, 10/28/2014	Finish Time	1400L, 10/30/2014
4hr TGA/FTIR:			
Start Time	1430L, 10/28/2014	Start Time	1500L, 10/30/2014
Finish Time	1930L, 10/28/2014	Finish Time	2000L, 10/30/2014

Table A10. Coupon Sample Preparation for Iron (1) Exposed to Deionized Water and Malathion for Experiment 2

Iron Sample Coupon #1			
Date	11/04/2014	Date	11/10/2014
Pressure (mmHg)	749.0/49.5	Pressure (mmHg)	744.0/50.0
Temp ambient (Celsius)	20.0/25.0	Temp ambient (Celsius)	20.0/25.0
Weight (grams)	0.6361	Weight (grams)	0.6361
Solution (type)	Deionized H_2O	Solution (type)	Malathion in H_2O
Solution volume (mL)	10.0	Solution volume (mL)	5.00
PH before	5.58	PH before	3.22
PH after	5.67	PH after	5.23
24hr Incubation:			
Start Time	1000L, 11/4/2014	Start Time	0600L, 11/10/2014
Finish Time	1000L, 11/5/2014	Finish Time	0600L, 11/11/2014
4hr Desiccation:			
Start Time	1000L, 11/5/2014	Start Time	0600L, 11/11/2014
Finish Time	1300L, 11/5/2014	Finish Time	1000L, 11/11/2014
4hr TGA/FTIR:			
Start Time	1340L, 11/5/2014	Start Time	1030L, 11/11/2014
Finish Time	1900L, 11/5/2014	Finish Time	1500L, 11/11/2014

Table A11. Coupon Sample Preparation for Iron (2) Exposed to Deionized Water and Malathion for Experiment 2

Iron Sample Coupon #2			
Date	11/06/2014	Date	12/03/2014
Pressure (mmHg)	744.0/62.0	Pressure (mmHg)	752.0/50.0
Temp ambient (Celsius)	20.0/25.0	Temp ambient (Celsius)	20.0/25.0
Weight (grams)	0.8161	Weight (grams)	0.8161
Solution (type)	Deionized H_2O	Solution (type)	Malathion in H_2O
Solution volume (mL)	10.0	Solution volume (mL)	10.0
PH before	5.15	PH before	4.60
PH after	5.15	PH after	5.50
24hr Incubation:			
Start Time	0630L, 11/06/2014	Start Time	0640L, 12/03/2014
Finish Time	0600L, 11/07/2014	Finish Time	0700L, 12/04/2014
4hr Desiccation:			
Start Time	0600L, 11/07/2014	Start Time	0730L, 12/04/2014
Finish Time	1000L, 11/07/2014	Finish Time	1030L, 12/04/2014
4hr TGA/FTIR:			
Start Time	1030L, 11/07/2014	Start Time	1100L, 12/04/2014
Finish Time	1500L, 11/07/2014	Finish Time	1500L, 12/04/2014

Table A12. Coupon Sample Preparation for Iron (3) Exposed to Deionized Water and Malathion for Experiment 2

Iron Sample Coupon #3			
Date	11/08/2014	Date	12/04/2014
Pressure (mmHg)	749.0/50.0	Pressure (mmHg)	753.0/49.0
Temp ambient (Celsius)	21.0/25.0	Temp ambient (Celsius)	20.0/25.0
Weight (grams)	0.9065	Weight (grams)	0.9065
Solution (type)	Deionized H_2O	Solution (type)	Malathion in H_2O
Solution volume (mL)	10.0	Solution volume (mL)	10.0
PH before	5.03	PH before	5.41
PH after	5.56	PH after	N/A
24hr Incubation:			
Start Time	0600L, 11/08/2014	Start Time	N/A
Finish Time	0630L, 11/09/2014	Finish Time	N/A
4hr Desiccation:			
Start Time	0630L, 11/09/2014	Start Time	N/A
Finish Time	1000L, 11/09/2014	Finish Time	N/A
4hr TGA/FTIR:			
Start Time	1030L, 11/09/2014	Start Time	N/A
Finish Time	1500L, 11/09/2014	Finish Time	N/A

Appendix B. TGA and FT-IR System of Operations

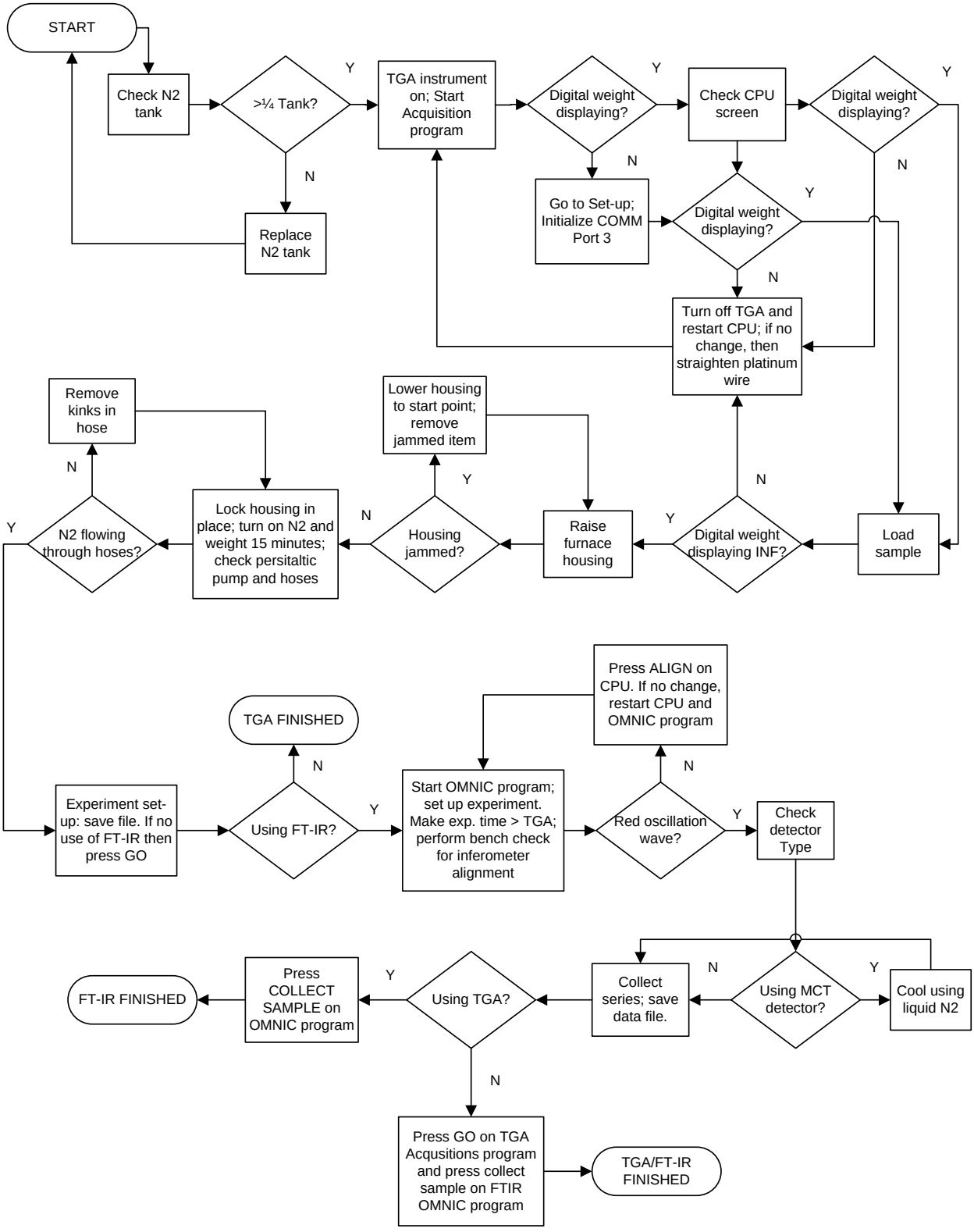

Figure B1. TGA and FT-IR System of Operations for Experimentation Procedure

Appendix C. Integration Steps of the Arrhenius-Based Reaction Model

(1) INITIAL CONDITIONS $t = 0$, $X = 0$

$$\frac{dX}{dt} = k(1-X) \quad (EQ.1) \qquad k = Ae^{\left(\frac{-E_a}{RT}\right)} \quad (EQ.3)$$

<ARRHENIUS EQ>

$$\frac{dT}{dt} = h \Rightarrow \frac{1}{h} = \frac{dt}{dT} \quad (EQ.2)$$

<h = HEATING RATE>

(2) COMBINE EQUATIONS (1) & (2)

$$\frac{dX}{dt} \cdot \frac{dt}{dT} = k(1-X) \cdot \frac{1}{h}$$

$$\frac{dX}{dT} = \frac{k}{h}(1-X)$$

(3) SUBSTITUTE EQ 3 INTO EQ. 2 FOR K-CONSTANT

$$\frac{dX}{dT} = \frac{k}{h}(1-X) = \frac{Ae^{\left(\frac{-E_a}{RT}\right)}}{h}(1-X)$$

(4) REARRANGE EQUATION

$$\frac{1}{(1-X)} \cdot \frac{dX}{dT} = \frac{A}{h} e^{\left(\frac{-E_a}{RT}\right)} (1-X) \cdot \frac{1}{(1-X)}$$

(5) INTEGRATE EQUATION

$$\int_0^X \frac{1}{(1-X)} \cdot dX = \frac{A}{h} \int_0^T e^{\left(\frac{-E_a}{RT}\right)} \cdot dT$$

WRL (1)

(6) IMPROPER, SO USE u-SUBSTITUTION FOR EXPONENT & REWRITE

LET $u = -\frac{E_a}{RT} \Rightarrow u = \frac{E_a}{RT} = \frac{E_a}{R} T^{-1}$

INTEGRATION LIMITS

$T = 0 \;,\; T = T$

$u = \infty \;,\; u = u$

$du = -\frac{E_a}{R} T^{-2} \cdot dT \Rightarrow -\frac{E_a}{RT^2} \cdot dT$

$du = -\frac{E_a}{RT^2} \cdot dT$

REARRANGE & SOLVE FOR dT

$dT = -\frac{RT^2}{E_a} \cdot du$

(7) MAKE u & du SUBSTITUTIONS & REARRANGE CONSTANTS

$$\int_0^X \frac{1}{(1-X)} \cdot \frac{dX}{dT} = \frac{A}{h} \int_0^T e^{-u}\, dT \qquad u = \frac{E_a}{RT} \;,\; \frac{1}{u} = \frac{RT}{E_a}$$

$$\int_0^X \frac{1}{(1-X)} \cdot \frac{dX}{dT} = \frac{A}{h} \int_\infty^u e^{-u} \cdot \frac{-RT^2}{E_a}\, du$$

* REVERSE LIMITS OF INTEGRATION, RHS, TO CHANGE NEG. SIGN

$$\int_0^X \frac{1}{(1-X)} \cdot \frac{dX}{dT} = \frac{A}{h} \int_u^\infty e^{-u} \cdot \frac{RT^2}{E_a}\, du$$

$$\int_0^X \frac{1}{(1-X)} \cdot \frac{dX}{dT} = \frac{A}{h} \int_u^\infty e^{-u} \cdot \frac{1}{u} \cdot T\, du$$

$$\int_0^X \frac{1}{(1-X)} \cdot \frac{dX}{dT} = \frac{AT}{h} \int_u^\infty \frac{1}{u} e^{-u}\, du$$

WRL (2)

(8) PERFORM APPROXIMATIONS FOR RHS OF EQUATION

$$\int_0^X \frac{1}{(1-X)} \cdot \frac{dX}{dT} = \int_u^\infty \frac{1}{u} e^{-u}\, du \approx e^{-u} \sum_{n=0}^{\infty} \frac{-1^n}{u^{n+1}}$$

$$= e^{-u}\left(\frac{1}{u} - \frac{1}{u^2}\right)$$

($n=0$, $n=1$)

(9) PERFORM SUBSTITUTION FOR u ON RHS & INTEGRATE LHS

$$-\ln(1-X) = \frac{AT}{h}\left[e^{\frac{-E_a}{RT}} \cdot \left(\frac{RT}{E_a} - \frac{R^2T^2}{E_a^2}\right)\right]$$

$$-\ln(1-X) = \frac{AT}{h}\left[e^{\frac{-E_a}{RT}} \cdot \frac{RT}{E_a}\left(1 - \frac{RT}{E_a}\right)\right]$$

$$-\ln(1-X) = \frac{AT}{h} \cdot \frac{RT}{E_a}\left[e^{\frac{-E_a}{RT}}\left(1 - \frac{RT}{E_a}\right)\right]$$

$$-\ln(1-X) = \frac{ART^2}{hE_a}\left[e^{\frac{-E_a}{RT}}\left(1 - \frac{RT}{E_a}\right)\right]$$

WRL (3)

(10) PERFORM NATURAL LOG OF LHS & RHS

$$\ln\left[-\ln(1-X)\right] = \ln\left(\frac{ART^2}{hE_a}\right) + \ln e^{\frac{-E_a}{RT}} + \ln\left(1-\frac{RT}{E_a}\right)$$

$$\ln\left[-\ln(1-X)\right] = \ln\left(\frac{ART^2}{hE_a}\right) - \frac{E_a}{RT} + \ln\left(1-\frac{RT}{E_a}\right)$$

$$\ln\left[-\ln(1-X)\right] = -\frac{E_a}{RT} + \ln\left[\frac{ART^2}{hE_a}\left(1-\frac{RT}{E_a}\right)\right]$$

WRL (4)

Appendix D. Raw TGA Mass Loss Profile for Copper and Iron

Graph Features and Units

Temperature Gradient = 2 K min^{-1}

Max Temperature = 773 K

Time = 0 – 270 min

Mass Fraction = unitless

List of Figures

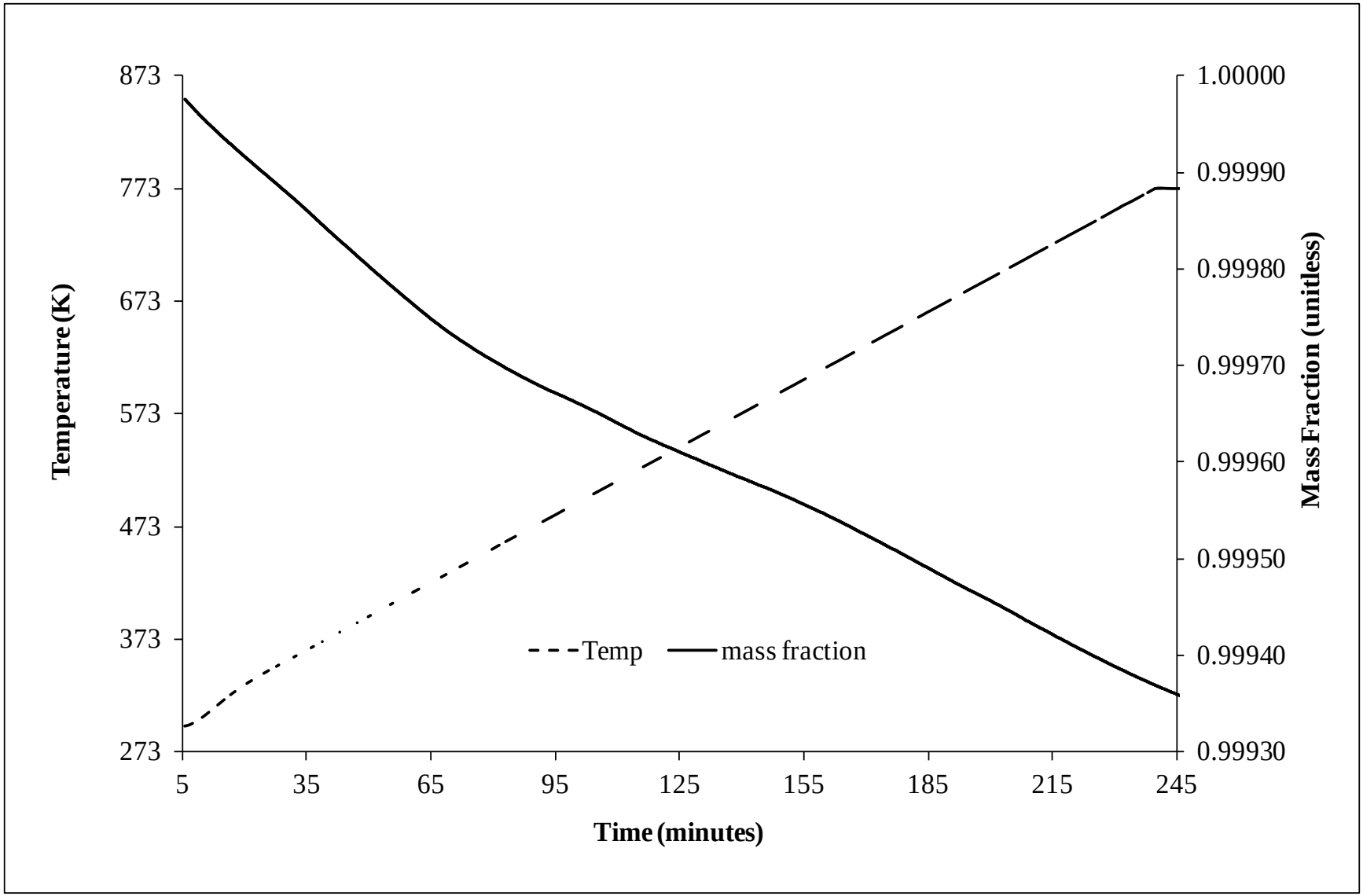

Figure D1. Copper (1) [5 Sep 14] Exposed to Malathion, Mass Loss Profile Displaying Consistent Mass Loss

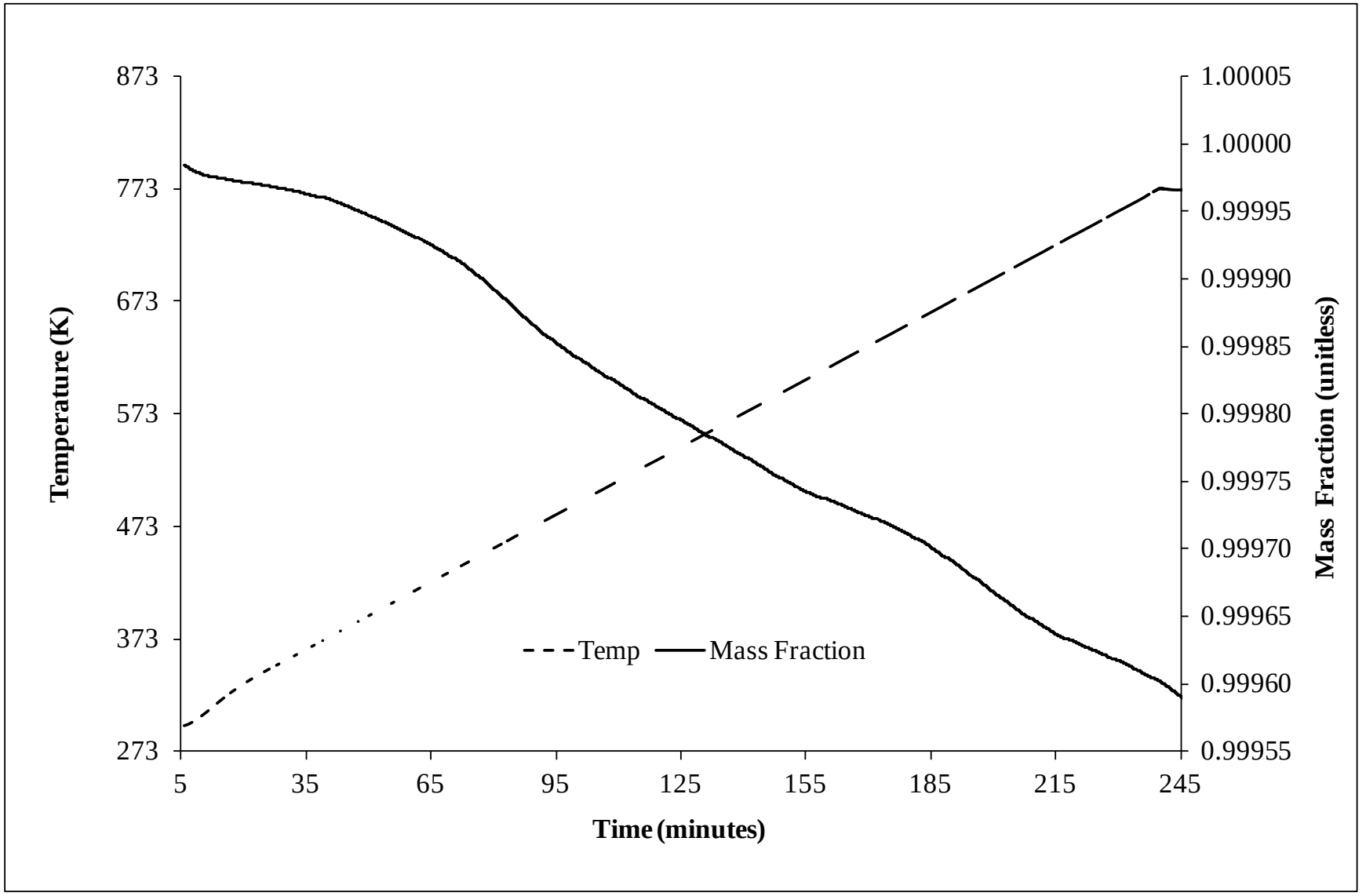

Figure D2. Copper (1) [15 Aug 14] Exposed to Malathion Mass Loss Profile Displaying Consistent Mass Loss

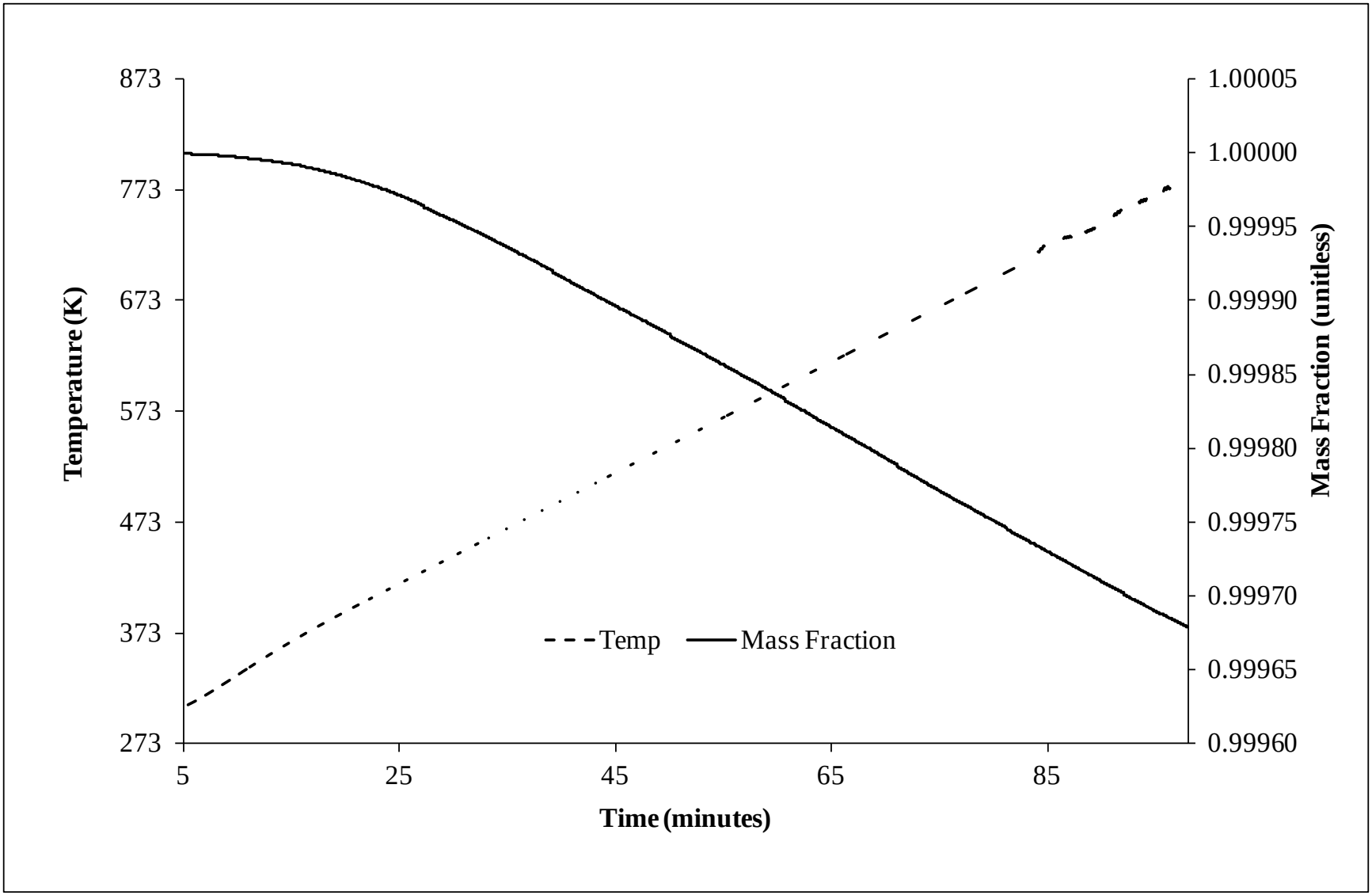

Figure D3. Copper (1) [Aug 14] Exposed to Malathion Mass Loss Profile Displaying Consistent Mass Loss

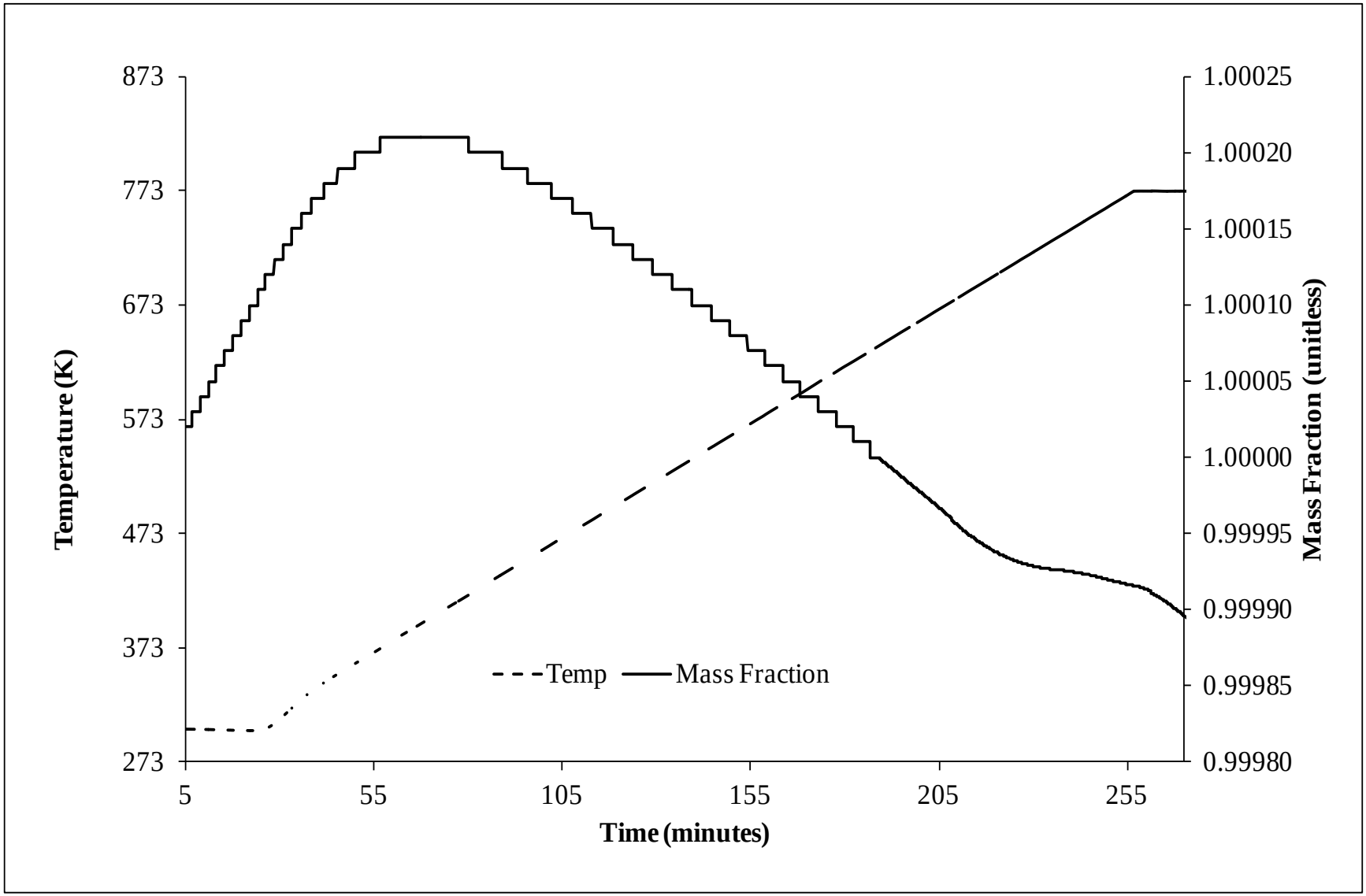

Figure D4. Copper (2) [6 Nov 14] Exposed to Deionized Water Mass Loss Profile Displaying Mass Gain and Loss

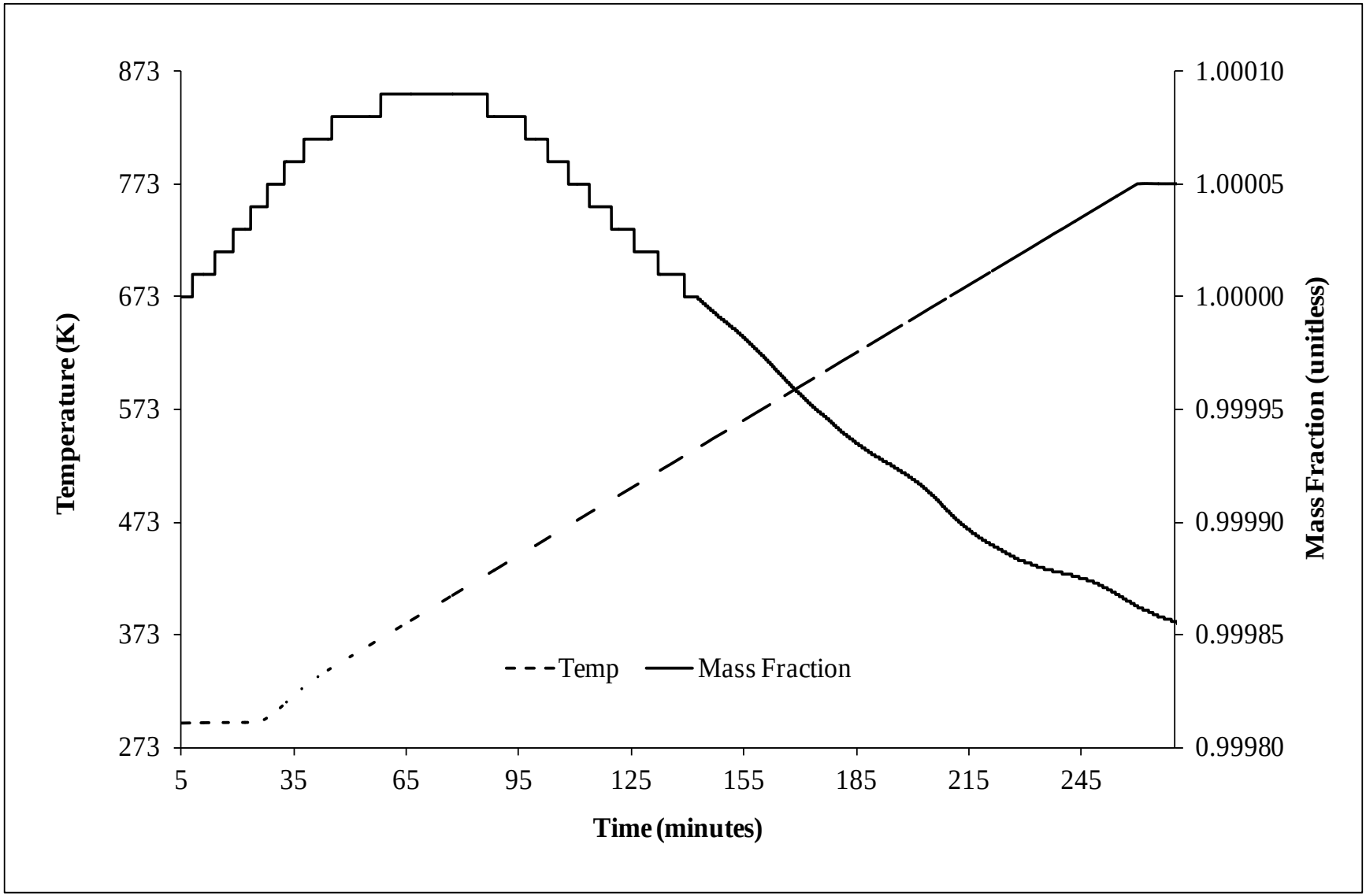

Figure D5. Copper (3) [29 Oct 14] Exposed to Malathion Mass Loss Profile Displaying Mass Gain and Loss

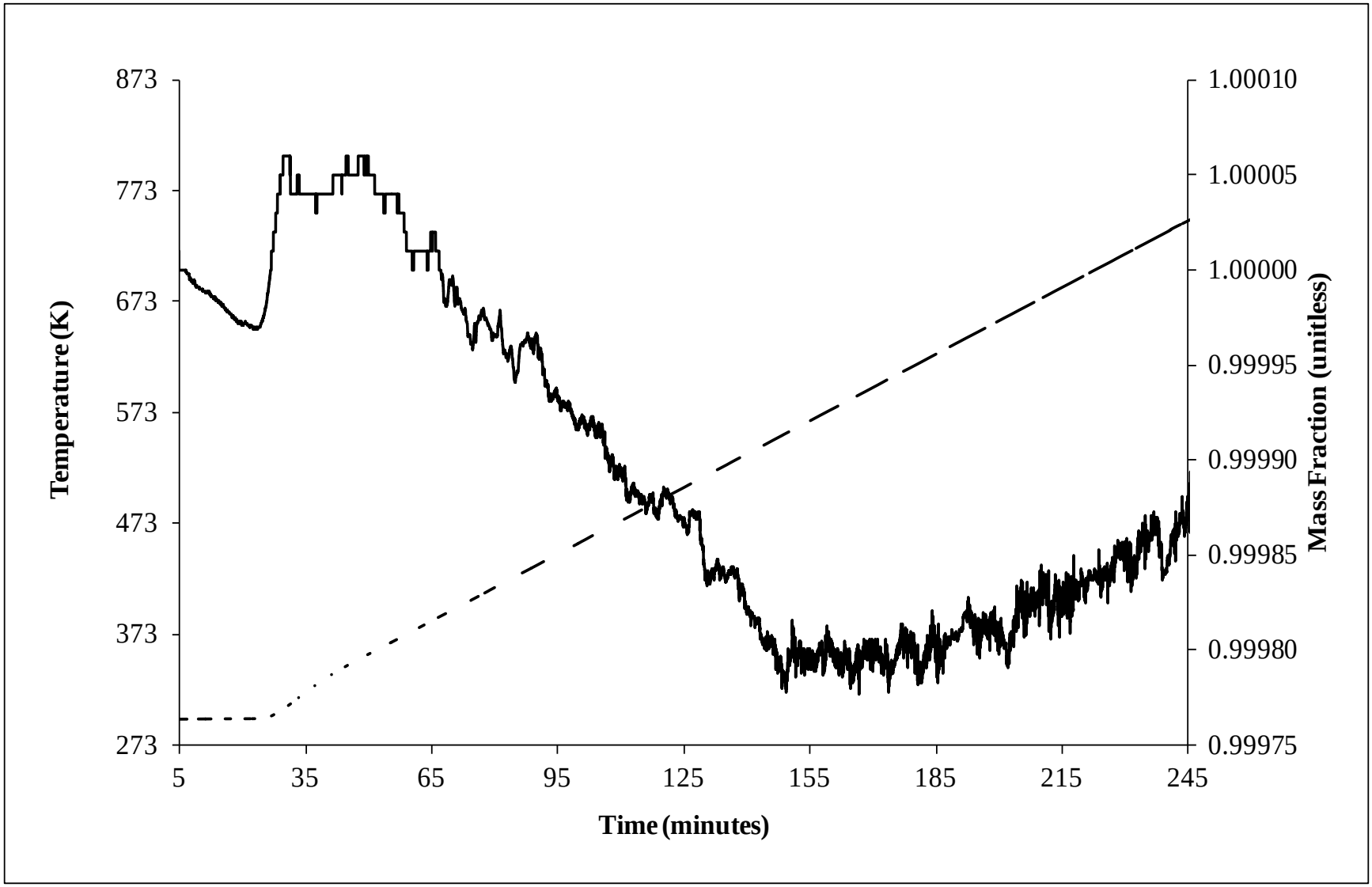

Figure D6. Iron (1) [11 Nov 14] Exposed to Malathion Mass Loss Profile Displaying Mass Gain and Loss

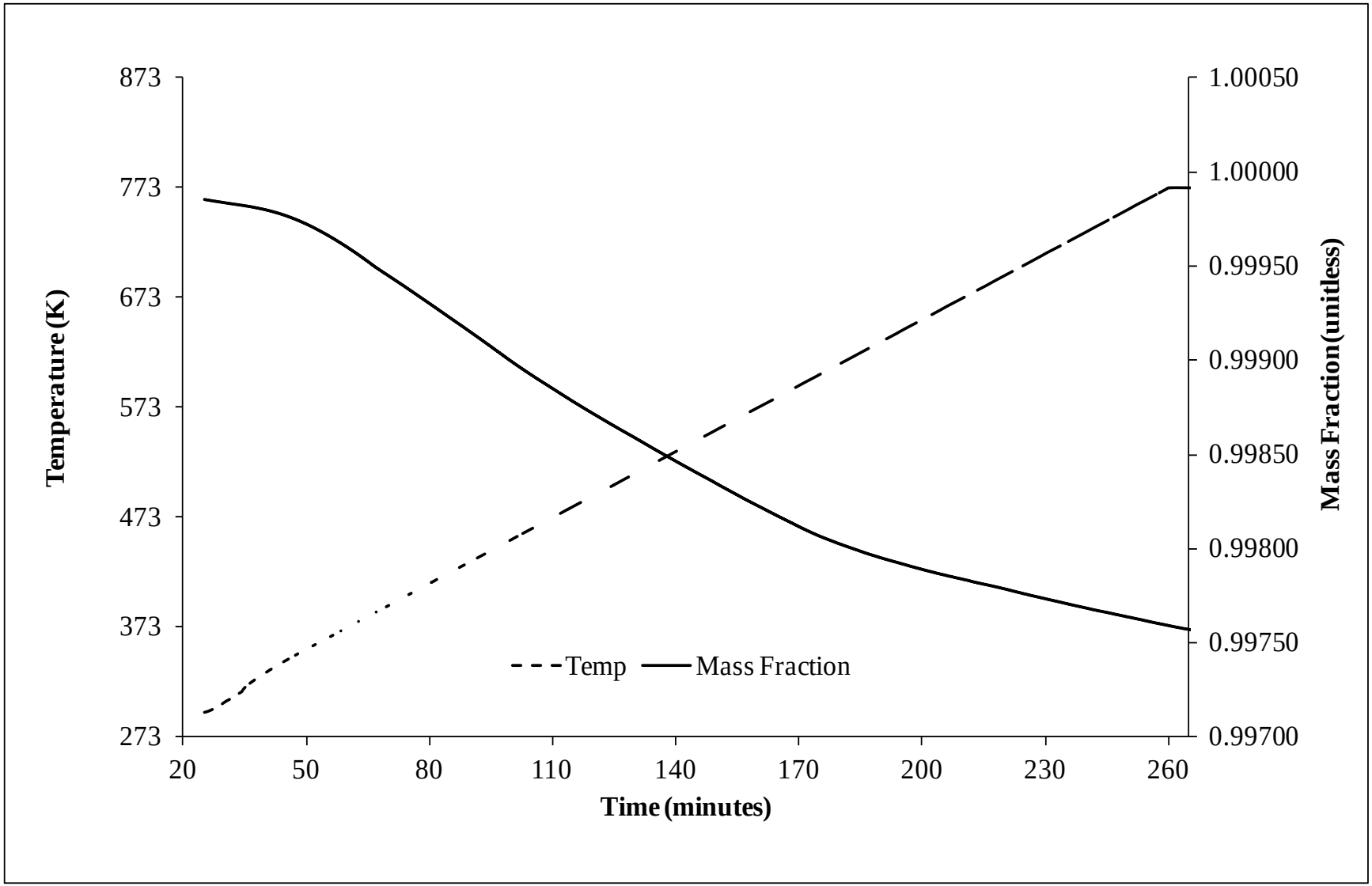

Figure D7. Iron (3) [9 Nov 14] Exposed to Deionized Water Mass Loss Profile Displaying Consistent Mass Loss

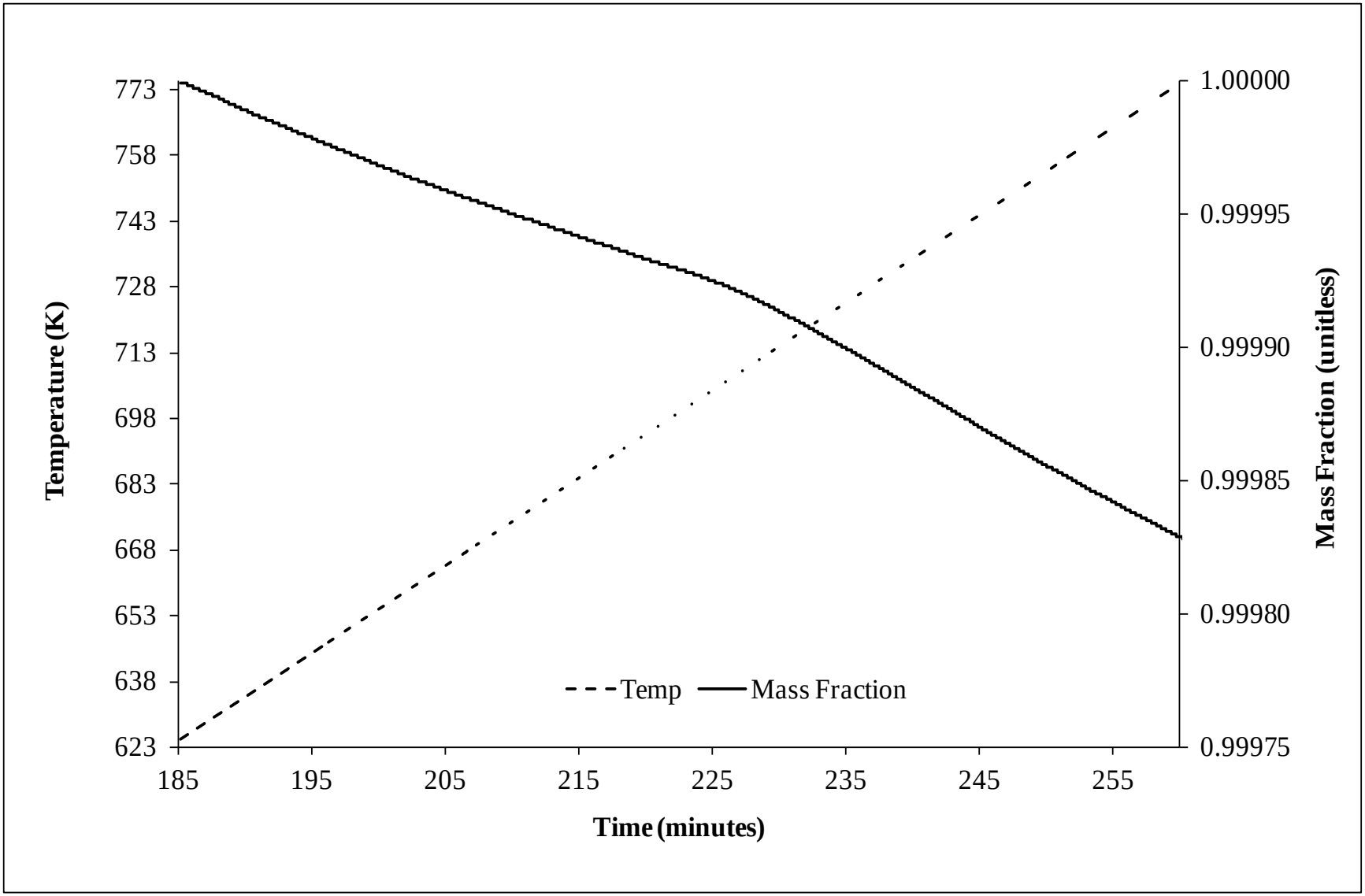

Figure D8. Iron (3) [30 Oct 14] Exposed to Malathion Mass Loss Profile Displaying Consistent Mass Loss

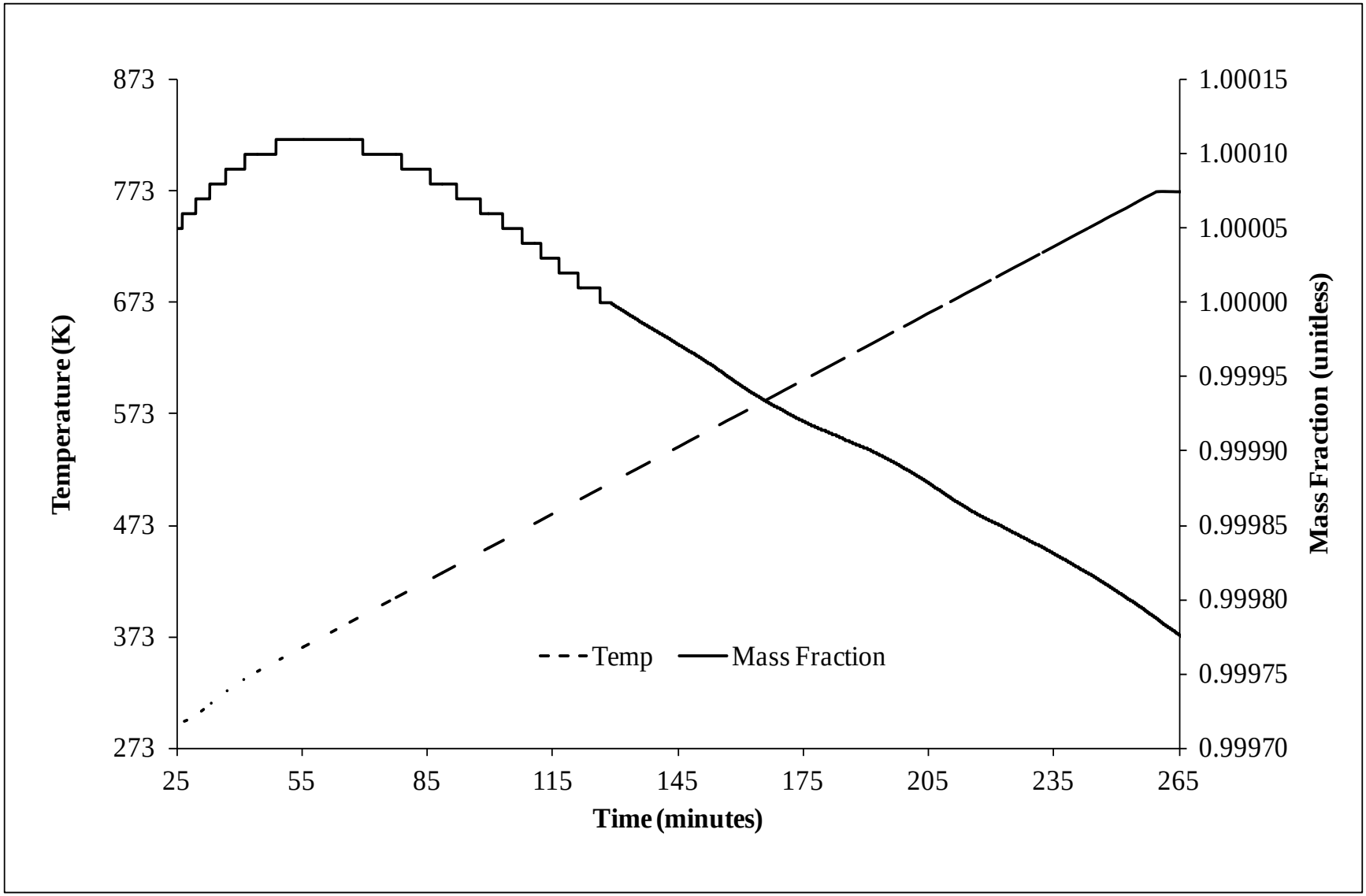

Figure D9. Iron (3) [28 Oct 14] Exposed to Deionized Water Mass Loss Profile Displaying Mass Gain and Loss

Appendix E. Arrhenius Plots for Copper and Iron

Graph Features and Units

Natural Log of Mass Loss Function (ln[-ln(1-X)]) = unitless

Inverse Temperature (1/T) = K^{-1}

Activation Energy (E_a) = kJ mol^{-1}

Coefficient of Determination (R^2) = unitless

List of Figures

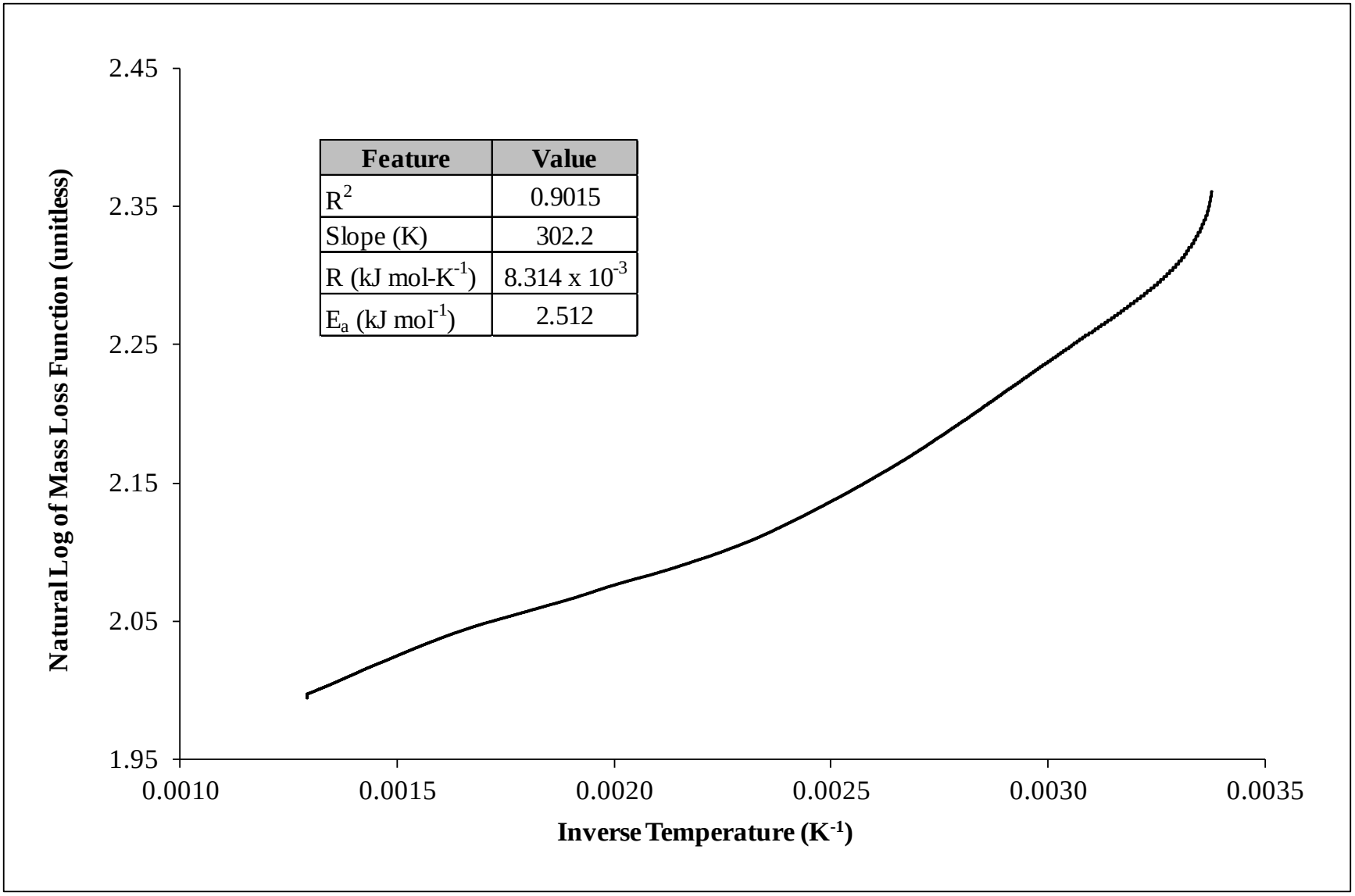

Figure E1. Copper (1) [5 Sep 14] Exposed to Malathion Arrhenius Plot, the Straight Line Indicates Mass Loss is Consistent with First-Order

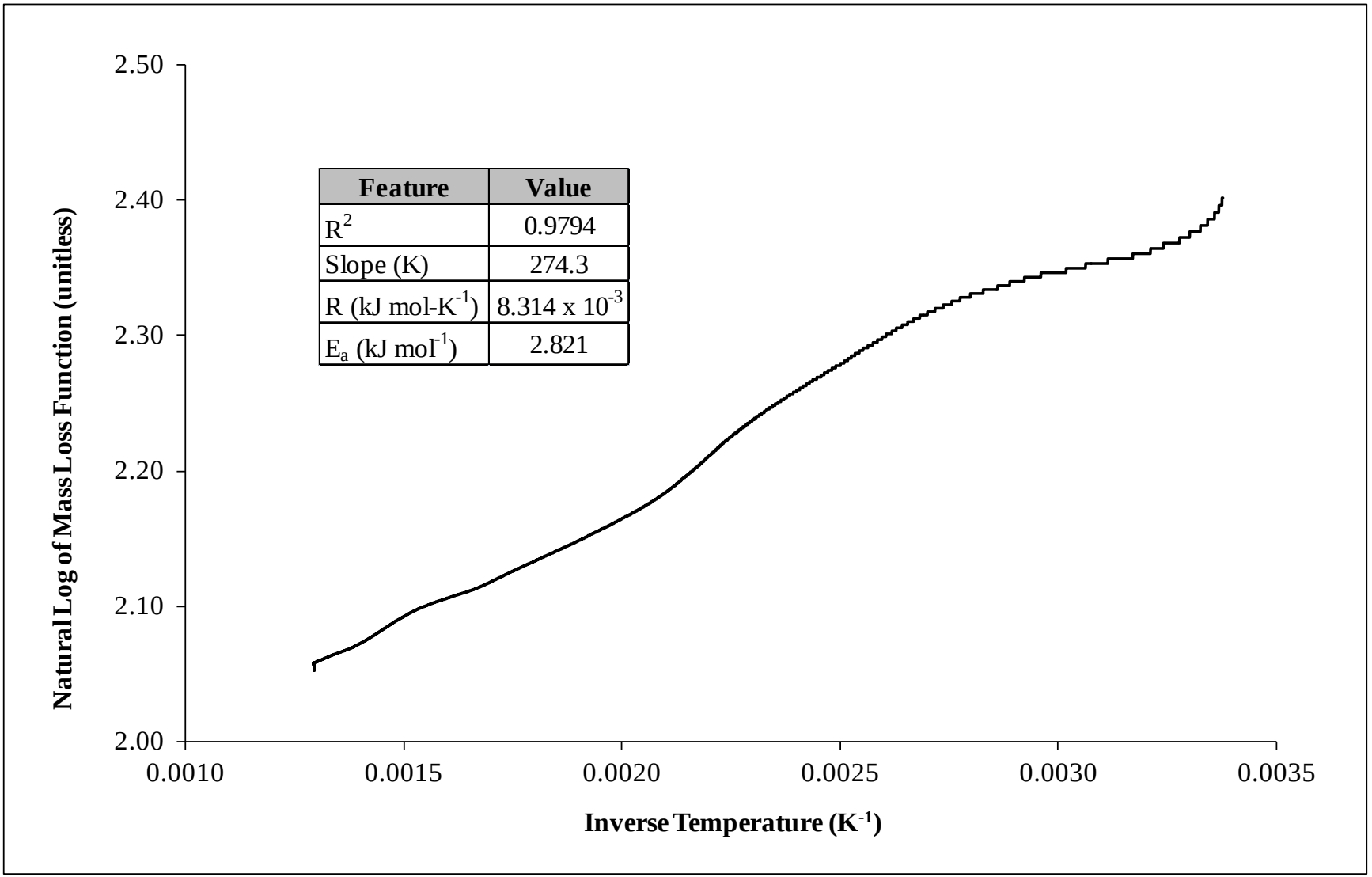

Figure E2. Copper (1) [15 Aug 14] Exposed to Malathion Arrhenius Plot, the Straight Line Indicates Mass Loss is Consistent with First-Order

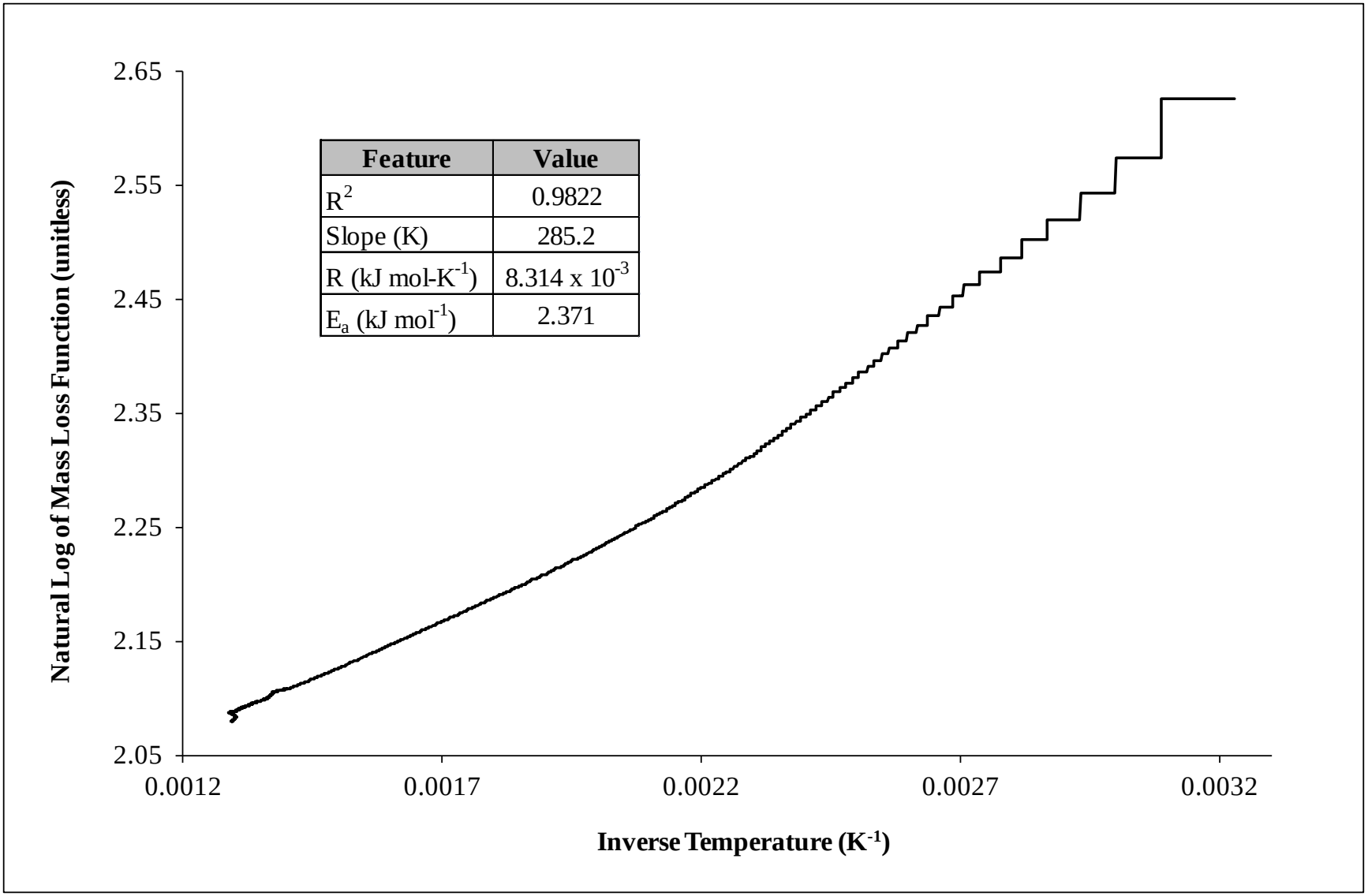

Figure E3. Copper (1) [Aug 14] Exposed to Malathion, Arrhenius Plot, the Straight Line Indicates Mass Loss is Consistent with First-Order

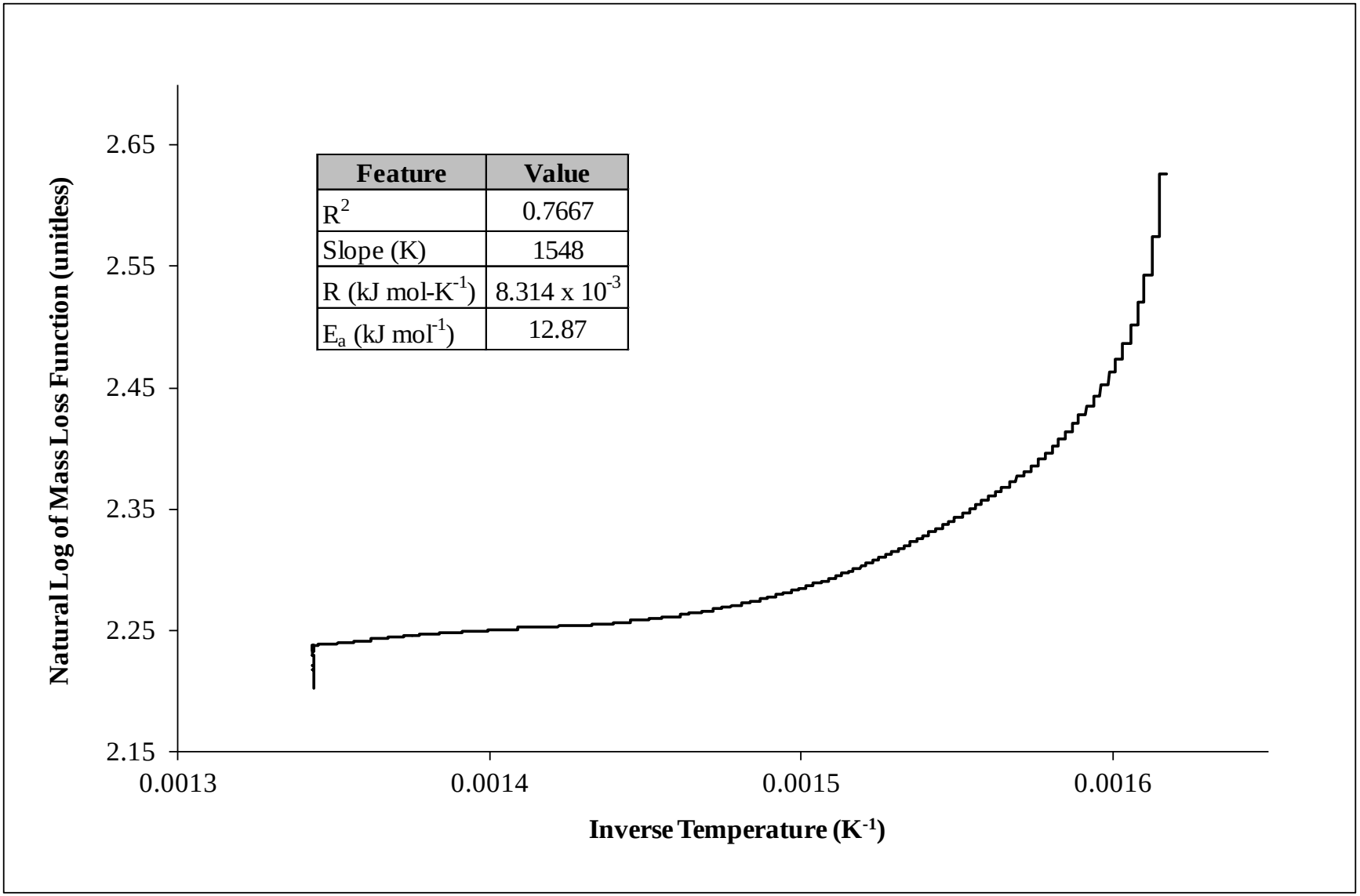

Figure E4. Copper (2) [6 Nov 14] Exposed to Deionized Water Arrhenius Plot, the Curved Line Indicates Mass Loss is Inconsistent with First-Order

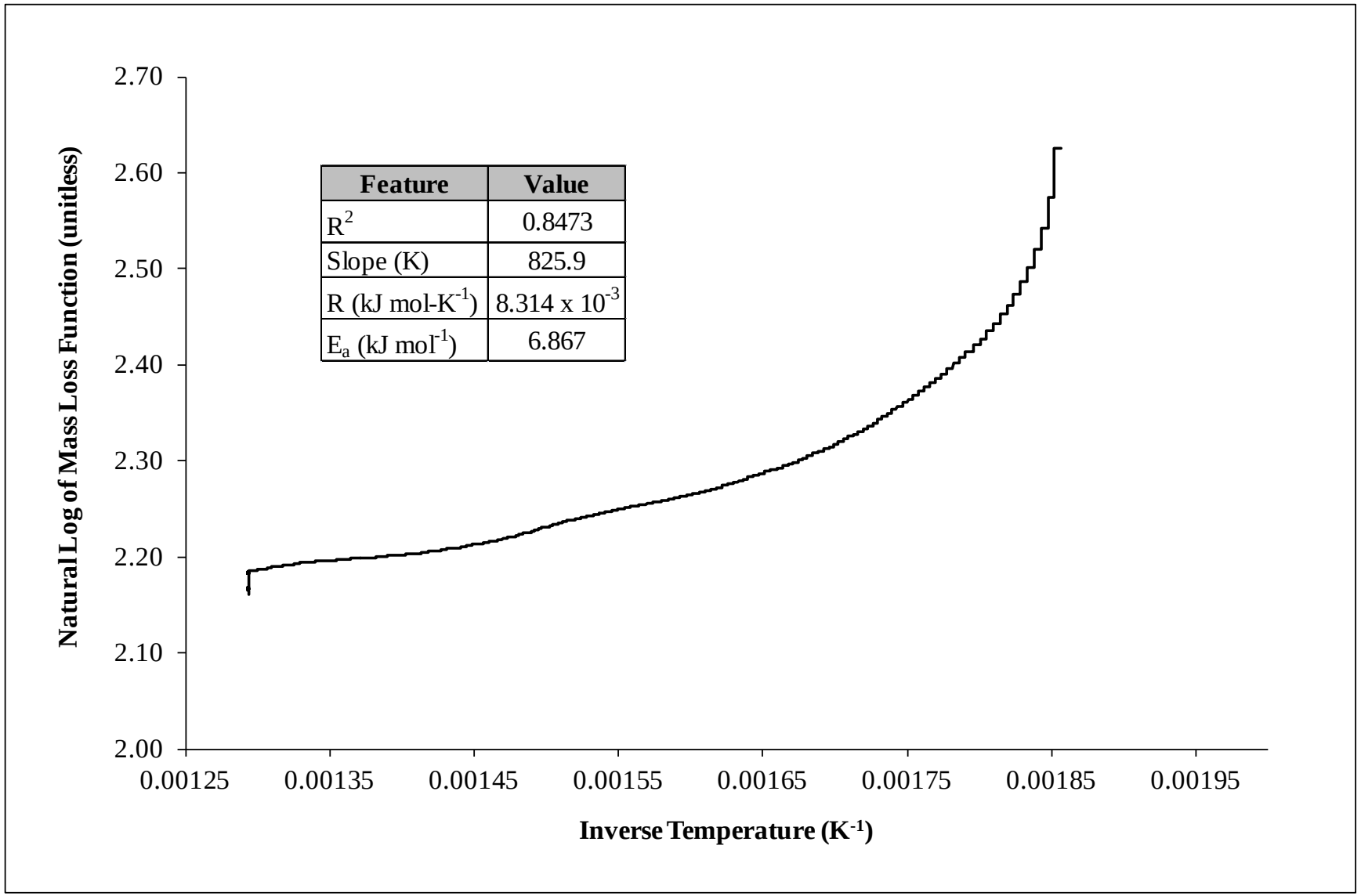

Figure E5. Copper (3) [29 Oct 14] Exposed to Malathion Arrhenius Plot, the Curved Line Indicates Mass Loss is Inconsistent with First-Order

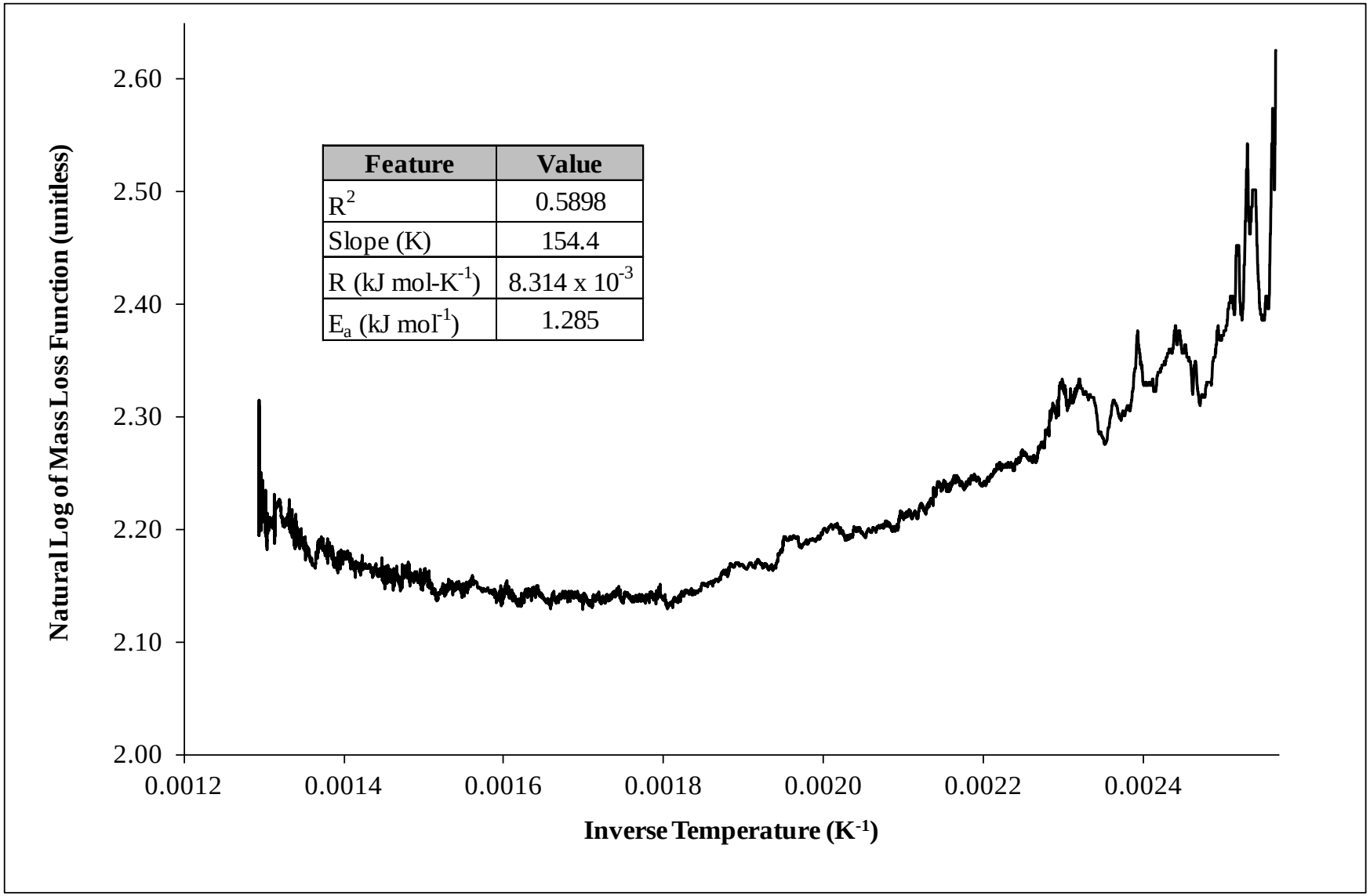

Figure E6. Fe (1) [11 Nov 14] Exposed to Malathion, Arrhenius Plot, the Curved and Erratic Line Indicates Mass Loss is Inconsistent with First-Order

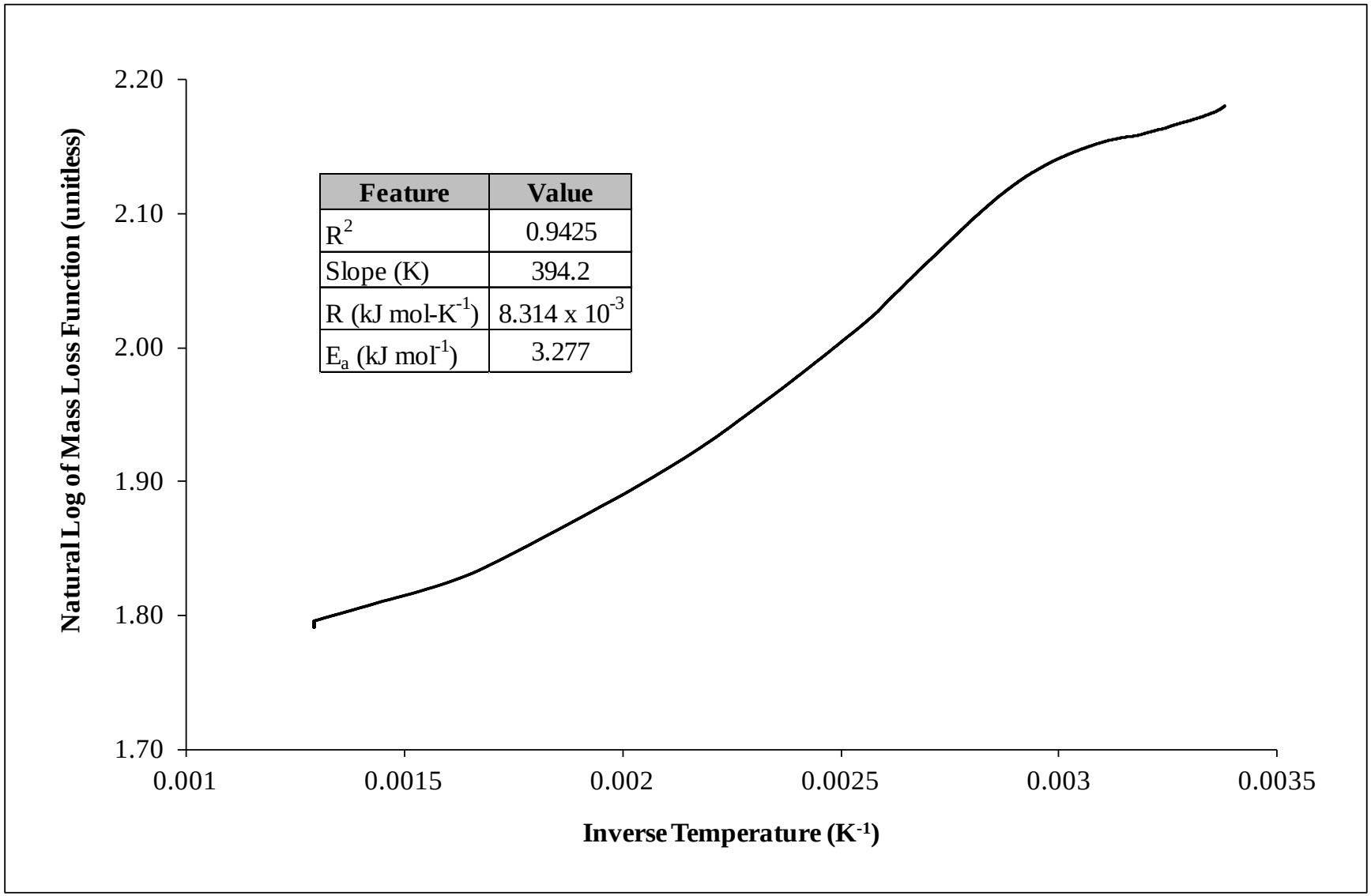

Figure E7. Iron (3) [9 Nov 14] Exposed to Water Arrhenius Plot, the Straight Line Indicates Mass Loss is Consistent with First-Order

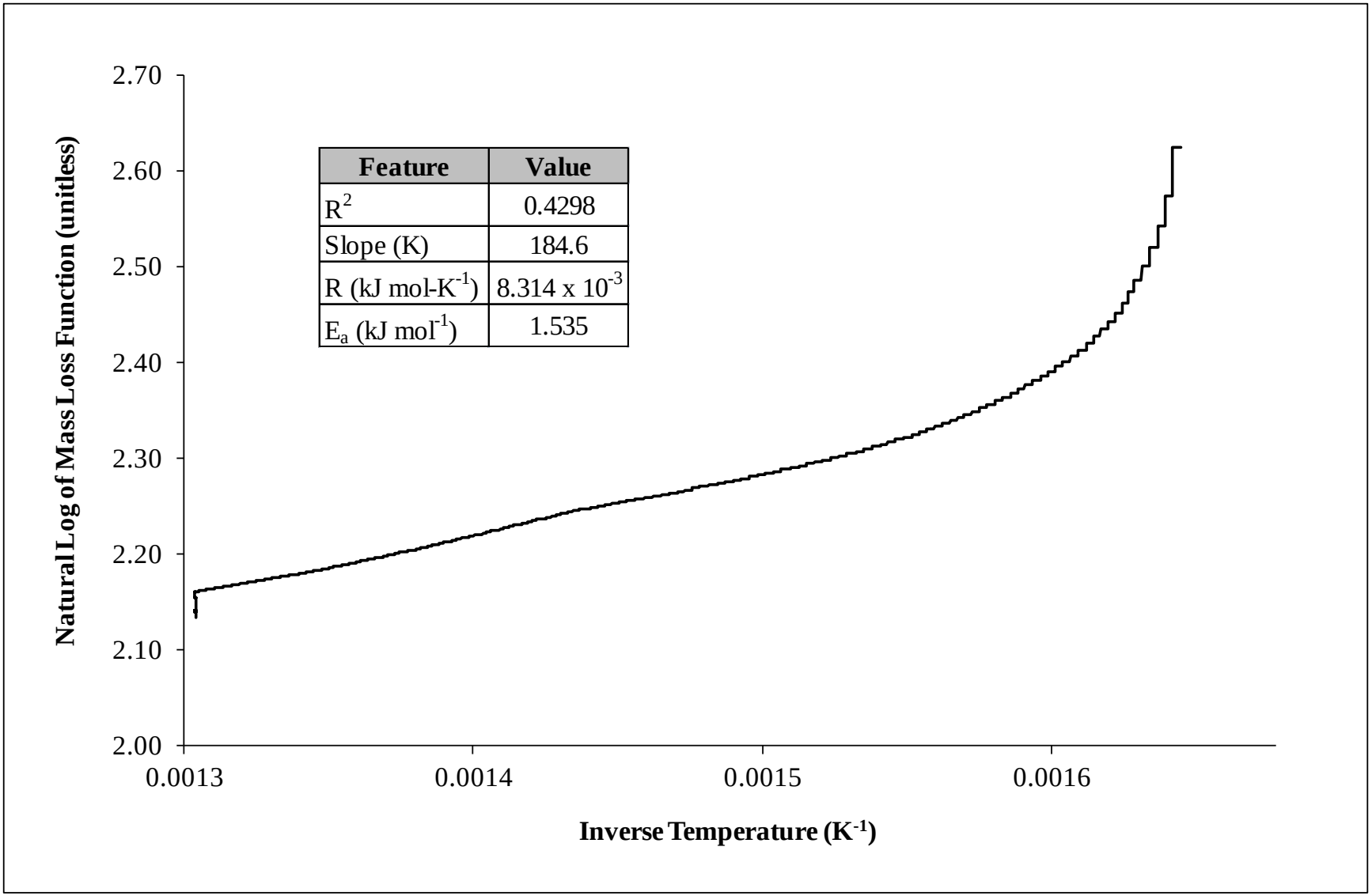

Figure E8. Iron (3) [30 Oct 14] Exposed to Malathion Arrhenius Plot, the Curved Line Indicates Mass Loss is Inconsistent with First-Order

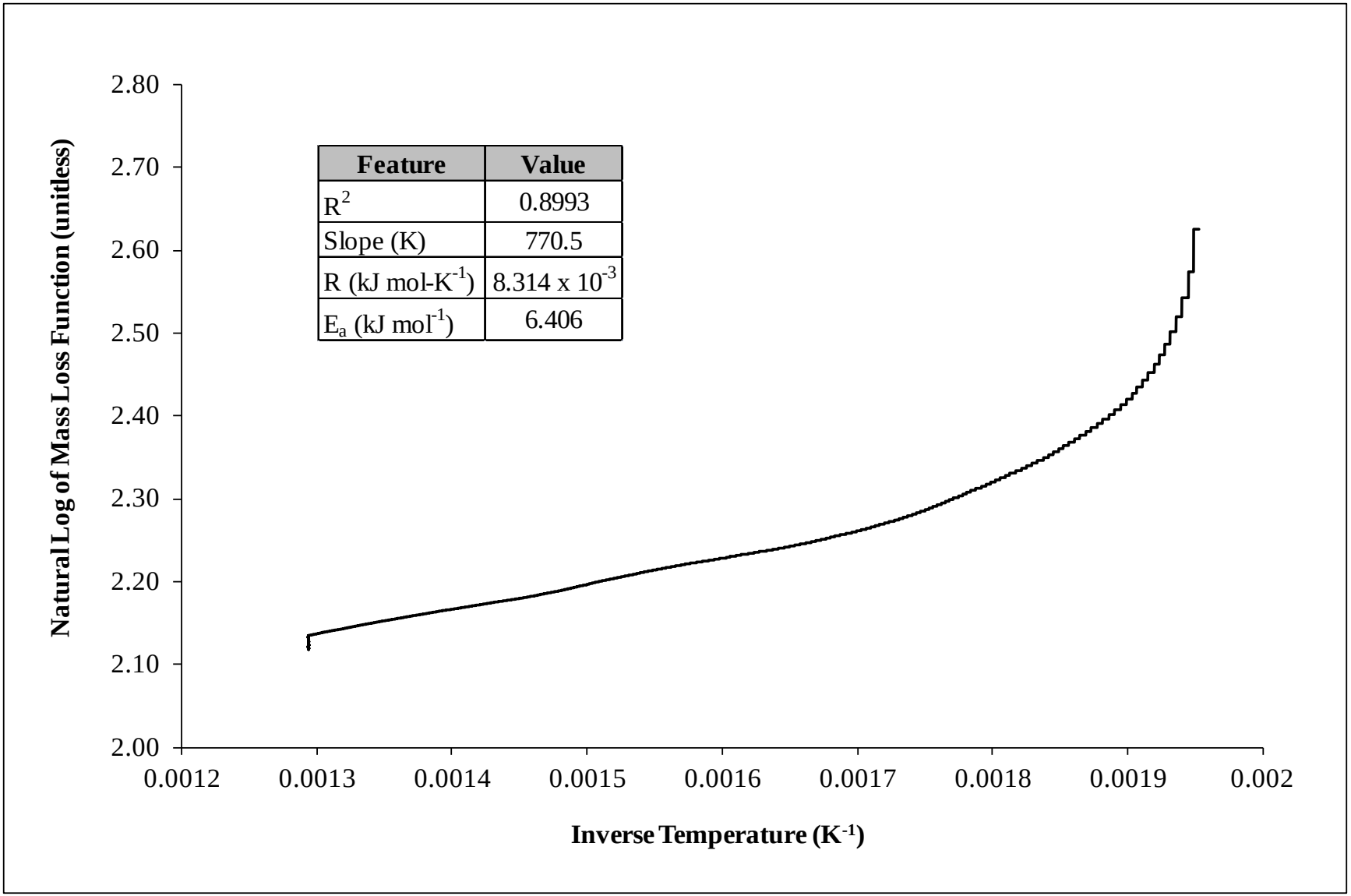

Figure E9. Iron (3) [28 Oct 14] Exposed to Deionized Water Arrhenius Plot, the Curved Line Indicates Mass Loss is Inconsistent with First-Order

Appendix F. FT-IR Spectrums for Copper and Iron

Spectral Features and Units

Absorbance = unitless

Wave numbers = cm^{-1}

List of Figures

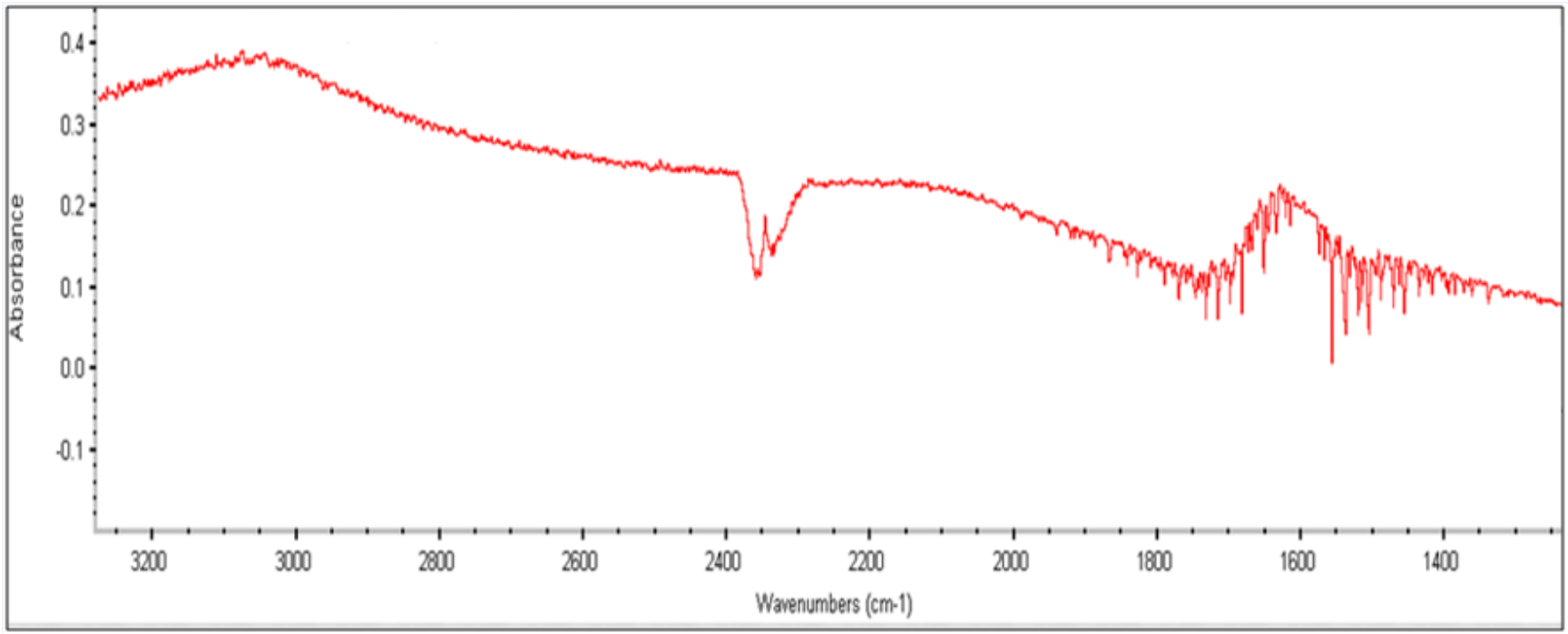

Figure F1. Copper (2) [22 Oct 14] Exposed to Malathion FT-IR Spectrum at 8.221 min, 3400 cm^{-1} to 1100 cm^{-1}, MCT Detector, Smoothing

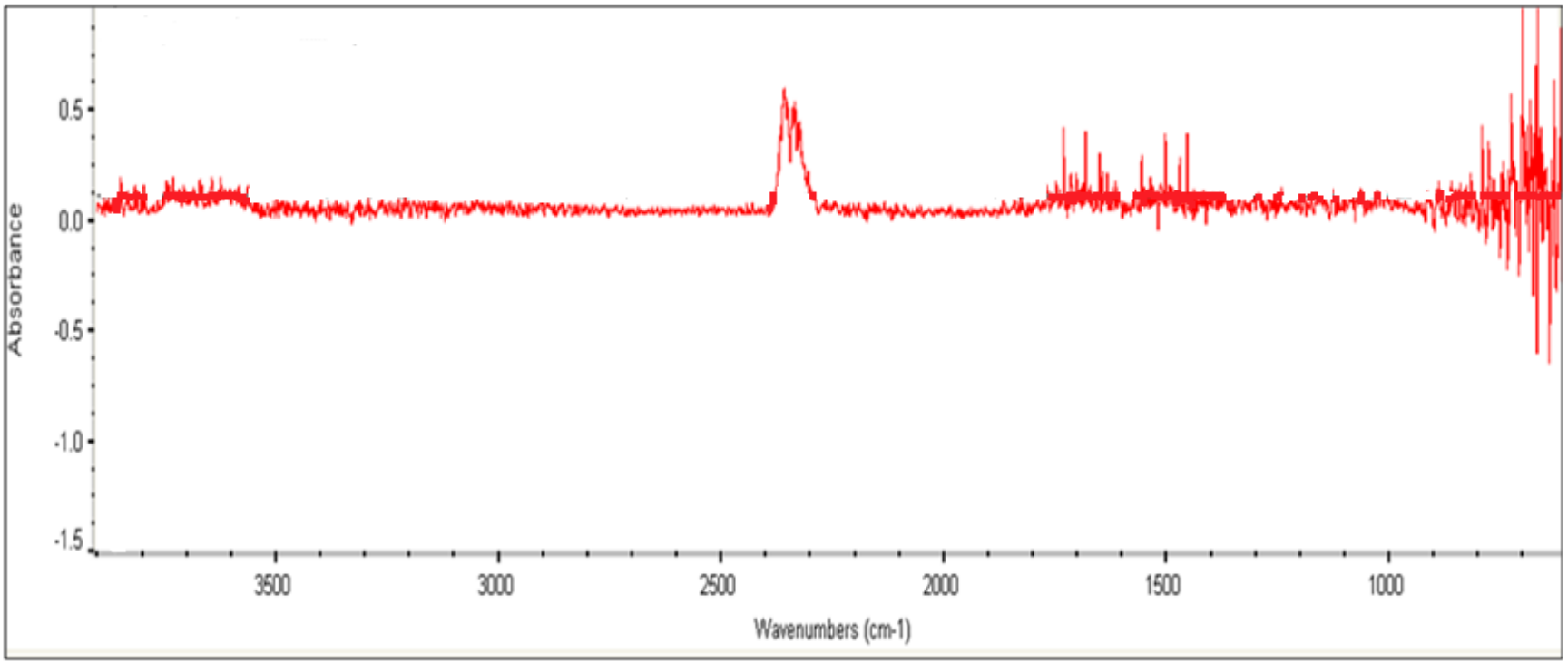

Figure F2. Copper (2) [22 Oct 14] Exposed to Malathion FT-IR Spectrum at 12.56 min, 4000 cm^{-1} to 500 cm^{-1}, MCT Detector, no Smoothing

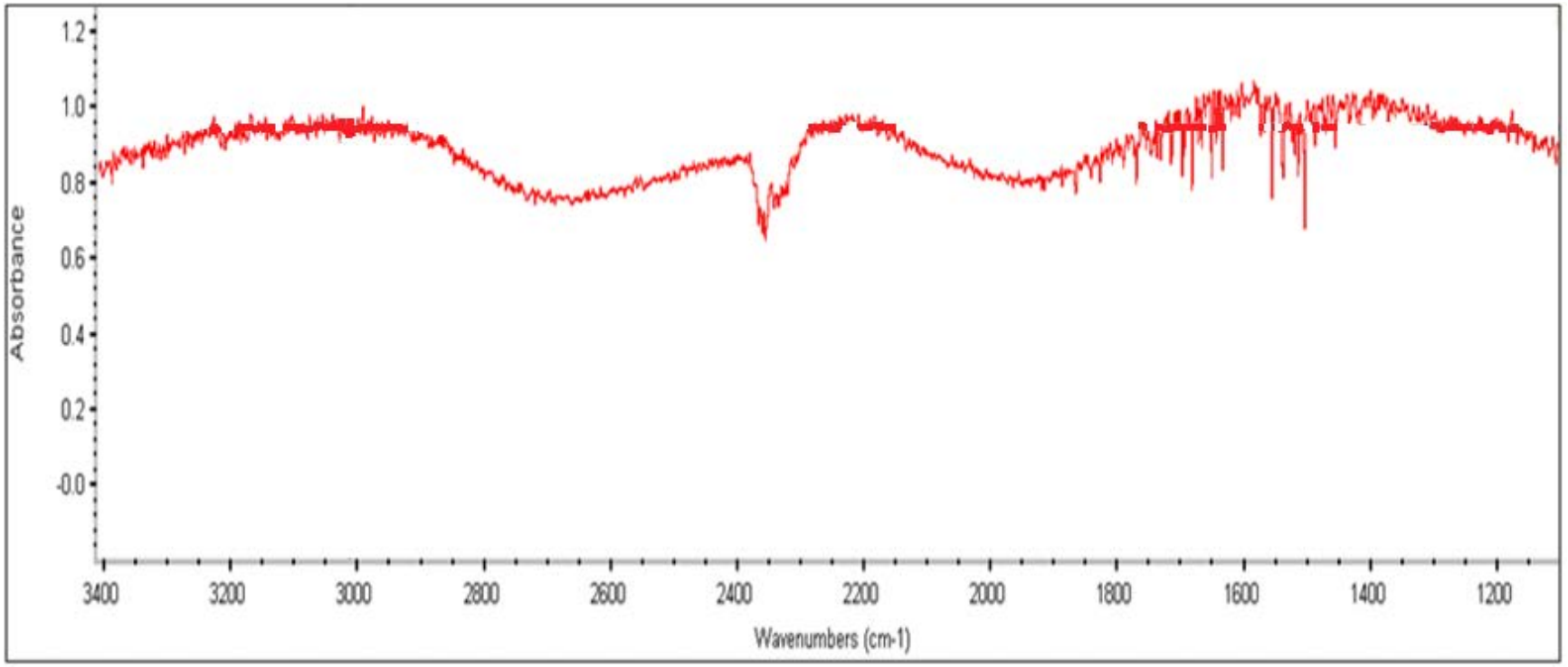

Figure F3. Copper (2) [22 Oct 14] Exposed to Malathion FT-IR Spectrum at 71.83 min, 3400 cm^{-1} to 1000 cm^{-1}, MCT Detector, Smoothing

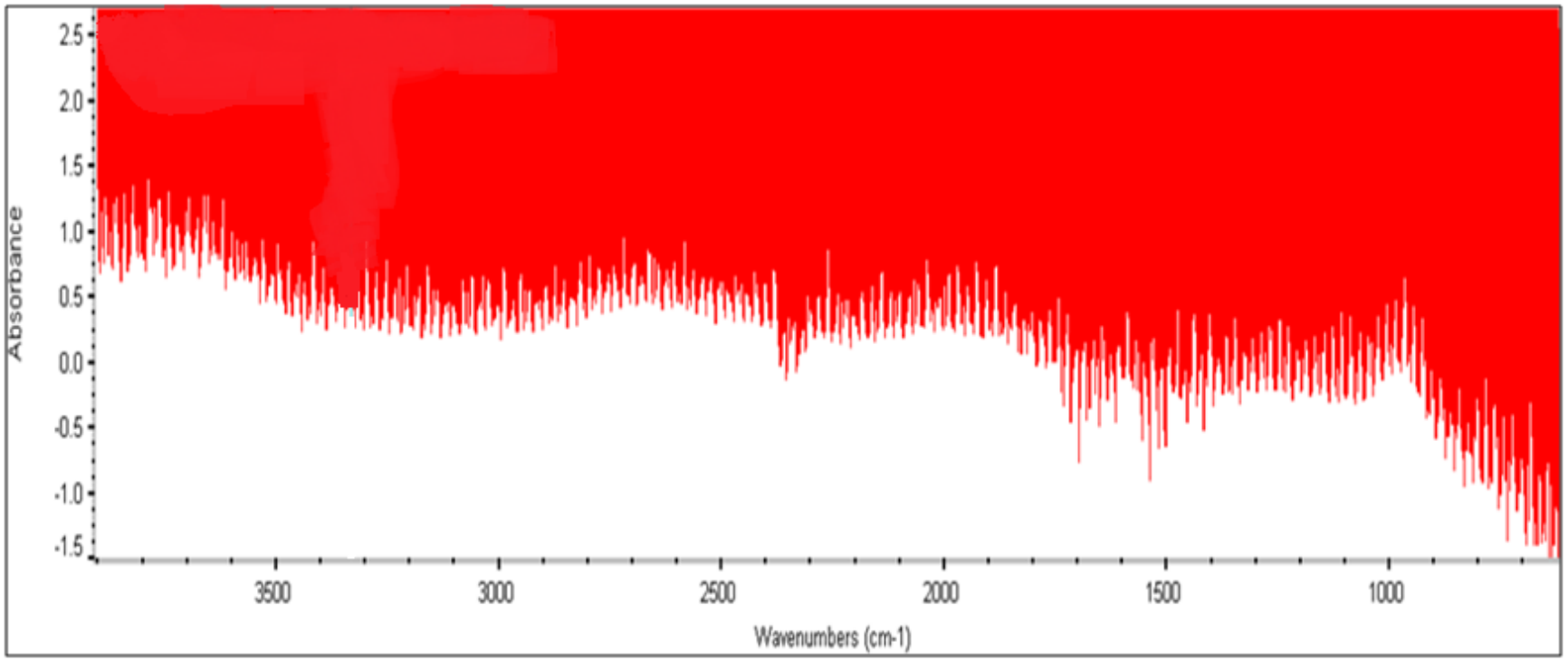

Figure F4. Copper (2) [22 Oct 14] Exposed to Malathion FT-IR Spectrum at 97.95 min, 3500 cm^{-1} to 1400 cm^{-1}, MCT Detector is Warm, no Smoothing

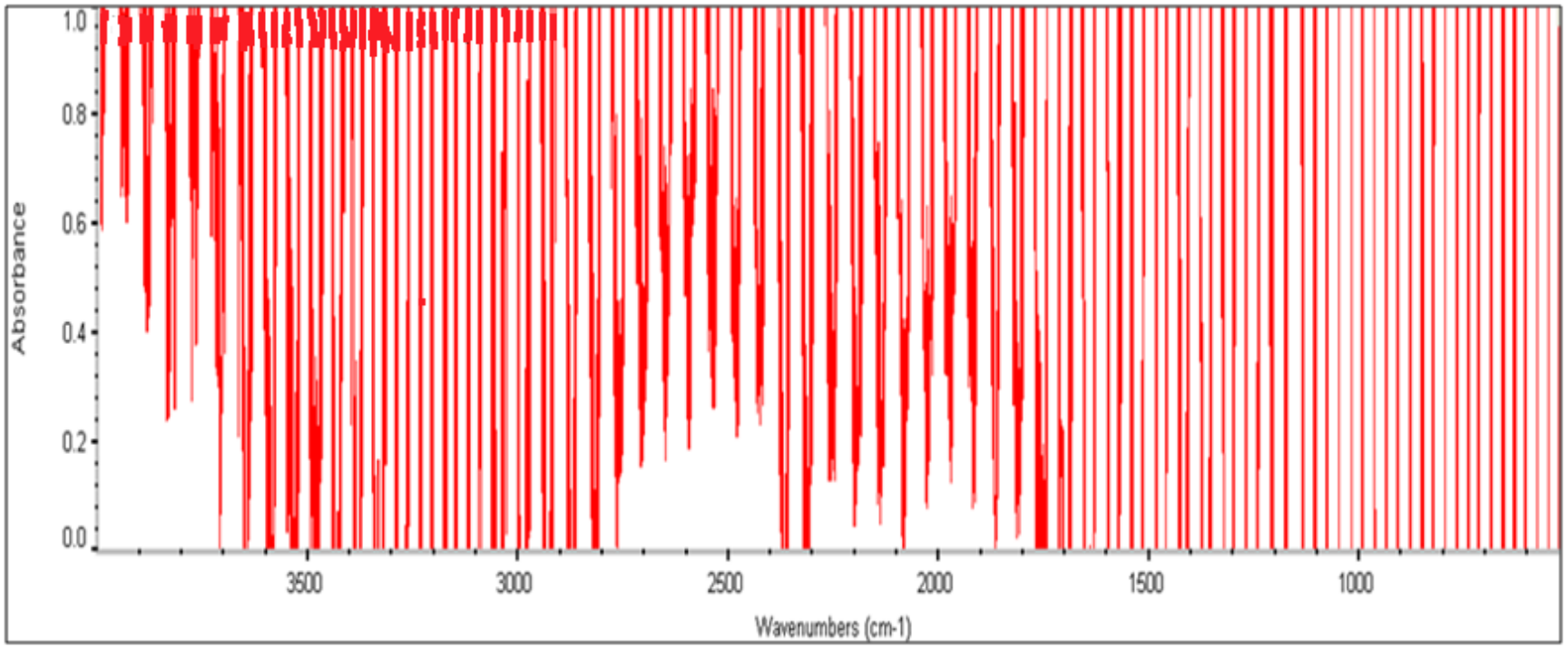

Figure F5. Iron (2) [16 Oct 14] Exposed to Deionized Water, FT-IR Spectrum at 300.2 min, 4000cm^{-1} to 500 cm^{-1}, MCT Detector Warming, no Smoothing

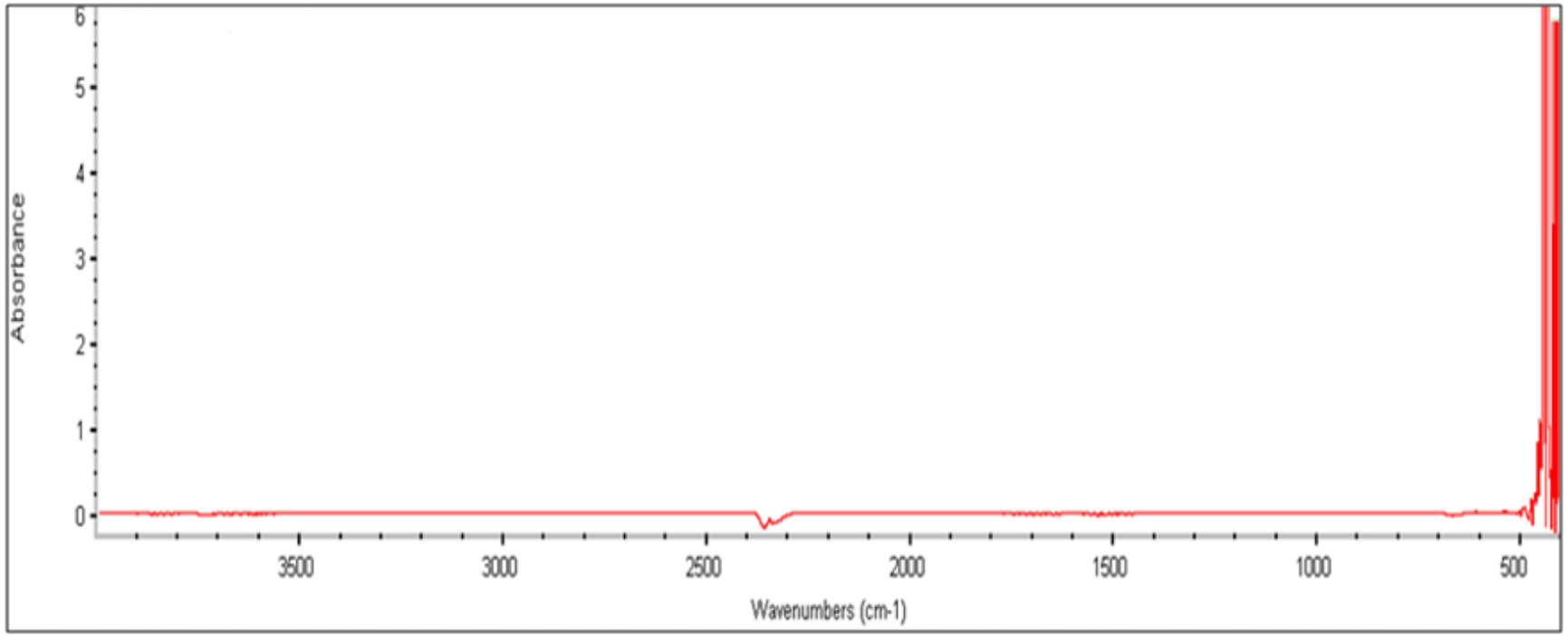

Figure F6. Iron (2) [7 Nov 14] Exposed to Deionized Water, FT-IR Spectrum at 3.286 min, 4000 cm^{-1} to 500 cm^{-1}, DTGS-KBr Detector, no Smoothing

Appendix G. FT-IR Chemicals of Interest

Table G1. Table of Chemicals of Interest for FT-IR

TGA Point	Match	Compound Name	Chemical Formula	Molecular Weight
1	77.46	Alpha-Terpineol	$C_{10}H_{18}O$	154.2
	54.77	Collidine	$C_8H_{11}N$	121.2
	77.46	Methacrylic Acid, Butyl Ester	$C_4H_6O^2$	86.09
2	50.00	4-Vinyl-1-Cyclohexene	C_8H_{14}	110.2
	40.65	Cyclododecene	$C_{12}H_{22}$	166.3
	54.86	Cyclohexane	C_6H_{12}	84.16
	42.67	Hydrogen Sulfide	H_2S	34.08
	42.97	Phenanthrene	$C_{14}H_{10}$	178.2
	50.00	Thiazolidine	C_3H_7NS	89.16
3	60.96	4-Vinyl-1-Cyclohexene	C_8H_{14}	110.2
	63.96	Benzyl Alcohol	C_7H_8O	108.1
	58.54	Quinoline	C_9H_7N	129.2
	69.63	Trans-Piperylene	C_5H_8	68.12
4	47.98	2-Propanol, Isopropyl Alcohol	C_3H_8O	60.10
	55.40	Butanediol	$C_4H_{10}O_2$	90.12
	53.11	Dioxane	$C_4H_8O_2$	88.11
5	44.68	Butanediol	$C_4H_{10}O_2$	90.12
	43.72	Cyclohexane	C_6H_{12}	84.16
	57.47	Ethylidene Cyclohexane	C_8H_{14}	110.2
6	41.28	4-Vinyl-1-Cyclohexene	C_8H_{14}	110.2
	49.59	Alpha-Terpineol	$C_{10}H_{18}O$	154.3
	58.71	Ethylene Glycol, Ethanediol	$C_2H_6O_2$	62.07
	56.83	Trans-Piperylene	C_5H_8	68.12
	44.95	Bromo Cyclohexane	$C_6H_{11}Br$	163.1

Bibliography

Arii, T., & Masudo, Y. (1999). Thermal decomposition of calcium copper acetate hexahydrate by simultaneous measurement of controlled-rate thermogravimetry and mass spectrometry (CRTG-MS). *Thermochimica Acta, 342,* 139-146. Retrieved from http://www.sciencedirect.com/science/article/pii/S0040603199002944

Ashauer, R., Hintermeister, A., O'Connor, I., Elumelu, M., Hollender, J., & Escher, B. (2012, February 9). Significance of xenobiotic metabolism for bioaccumulation kinetics of organic chemicals in gammarus pulex. *Environmental Science& Technology, 46*(6), 3498-3508. Retrieved from http://pubs.acs.org/doi/pdf/10.1021/es204611h

Bender, M. E. (1969). The toxicity of the hydroloysis and breakdown products of malathion to the fathead minnow (pimephales promelas, rafinesque). *Water Research, 3*(8), 571-582. Retrieved from http://ac.els-cdn.com/0043135469900463/1-s2.0-0043135469900463-main.pdf?_tid=3a0a8002-b3a9-11e4-8999-00000aacb360&acdnat=1423850193_fe50e02044f038e2490bf13b5752de21

Bourquin, A. W. (1977, February). Degradation of malathion by salt-marsh microorganisms. *Applied and Environmental Microbiology, 33*(2), 356-362. Retrieved from http://aem.asm.org/content/33/2/356.full.pdf

Boyd, J. W., Eckman, C. K., Romero, N. A., Ramkumar, S. S., Cox, S. B., & Cobb, G. P. (2006, December 5). The use of a thermogravimetric analyzer for the generation of primary analytical vapor standards of organophosphate pesticides. *Analytica Chimica Acta, 558,* 35-41. Retrieved from http://www.sciencedirect.com/science/article/pii/S000326700501857X

Centers for Disease Control and Prevention Office of the Director. (2013, July 26). *The National Institute of Occupational Safety and Health (NIOSH).* Retrieved December 21, 2014, from Centers for Disease Control and Prevention: http://www.cdc.gov/niosh/about.html

Centers for Disease Control and Prevention Office of the Director. (2014, June 6). *NIOSH Manual of Analytical Methods, 4th ed: Chapter A: Purpose and Scope.* (K. Ashley, & P. F. O'Connor, Eds.) Retrieved December 21, 2014, from Centers for Disease Control and Prevention: http://www.cdc.gov/niosh/docs/2003-154/chaps.html

Chen, H., & Liu, N. (2010). Application of non-arrhenius equations in interpreting calcium carbonate decomposition kinetics: revisited. *Journal of American Ceramic Society, 93*(2), 548-553.

Coats, A. W., & Redfern, J. P. (1964, January 4). Kinetic parameters from thermogravimetric data. *Nature, 201,* 68-69.

Dodd, J. W., & Tonge, K. H. (1987). *Analytical Chemistry by Open Learning: Thermal Analysis.* (B. P. Currell, Ed.) New York , NY: John Wiley & Sons.

Dollimore, D., & Lerdkanchanaporn, S. (1998, June 25). Thermal analysis. *Analytical Chemistry, 70*(12), 27R-32R.

Gallardo, V., Cole, K., Treado, S., Kedzierski, M., Watson, S., & Martys, N. (2012). *Removing biological and chemical contamination from a building's plumbing system: method development and testing.* Cincinnati, OH: National Homeland Security Research Center, US EPA.

Gervais, J. A., Luukinen, B., Buhl, K., & Stone, D. (2009). *Malathion Technical Fact Sheet.* Retrieved September 9, 2014, from National Pesticide Information Center: http://npic.orst.edu/factsheets/malatech.pdf

Graham, M. J. (1972). Transition from linear to parabolic kinetics during the oxidation of iron in CO2 at 400–500°C. *12*(8), 683-685. Retrieved from http://www.sciencedirect.com/science/article/pii/S0010938X72800702

Groenewoud, W., & de Jong, W. (1996, February 28). The thermogravimetric anlayser - coupled - Fourier transform infrared/mass spectrometry technique. *Thermochimica Acta, 286*, 341-354. Retrieved from http://www.sciencedirect.com/science/article/pii/0040603196029401

Grosvenor, A. P., Kobe, B. A., & Mclntyre. (2005, January 10). Activation energies for the oxidation of iron by oxygen gas and water vapour. *Surface Science, 574*, 317-321. Retrieved from http://www.sciencedirect.com/science/article/pii/S0039602804014116

Henson-Ramsey, H., Kennedy-Stoskopf, S., Levine, J. F., Taylor, S. K., Shea, D., & Stoskopf, M. K. (2008, January 29). Acute Toxicity and Tissue Distributions of Malathion in Ambystoma tigrinum. *Archives of Envrionmental Contamination and Toxicology, 55*(3), 481-487. Retrieved from http://link.springer.com/article/10.1007/s00244-007-9091-4#

Henson-Ramsey, H., Kennedy-Stoskopf, S., Levine, J., Shea, D., Taylor, S. K., & Stoskopf, M. K. (2007). A Comparison of Two Exposure Systems to Apply Malathionto Lumbricus terrestris L. *Bullentin Environmental Contamination Toxicology, 78*, 427-431. Retrieved from http://download.springer.com/static/pdf/667/art%253A10.1007%252Fs00128-007-9194-7.pdf?auth66=1423521968_46b38d4eb61a5301d459532e575e3213&ext=.pdf

Jaber, J., & Probert, S. (2000). Non-isothermal thermogravimetry and decomposition kinetics of two Jordanian oil shales under different processing conditions. *Fuel Processing Technology, 63*, 57-70. Retrieved from http://www.sciencedirect.com/science/article/pii/S0378382099000648

Jakic, M., Vrandecic, N. S., & Klaric, I. (2013, May 29). Thermal degradation of poly(vinyl chloride)/poly(ethylene oxide). *Polymer Degradation and Stability, 98*, 1738-1743. Retrieved from http://www.sciencedirect.com/science/article/pii/S0141391013001687

Jiao, L.-l., & Sun, J.-h. (2014). A Thermal degradation study of insulation materials extruded polystyrene. *Procedia Engineering, 71*, 622-628. Retrieved from http://ac.els-cdn.com/S1877705814005074/1-s2.0-S1877705814005074-main.pdf?_tid=01e8775e-b0ae-11e4-b93d-00000aab0f02&acdnat=1423522393_6ccacc74450beeacabb45f4acbd64f05

Kok, M. V., & Okandan, E. (1995). Kinetic analysis of in situ combustion processes with thermogravimetric and differential thermogravimetric analysis and reaction tube experiments. *Analytical Applied Pyrolysis, 31*, 63-73. Retrieved from http://www.sciencedirect.com/science/article/pii/016523709400812F

Kralj, M. B., Franko, M., & Trebse, P. (2006, November 13). Photodegradation of organophosphorus insecticides – Investigations of products and their toxicity using gas chromatography–mass spectrometry and AChE-thermal lens spectrometric bioassay. *Chemosphere, 67*, 99-107. Retrieved from http://ac.els-cdn.com/S0045653506012707/1-s2.0-S0045653506012707-main.pdf?_tid=4297b29c-b397-11e4-8d6d-00000aacb362&acdnat=1423842476_30eae2ec2d8803fbcbdb11aff4f11523

Lai, Z., Ma, X., Tang, Y., & Lin, H. (2012). Thermogravimetric analysis of the thermal decomposition of MSW in N2, CO2/N2 atmospheres. *102*, 18-23. Retrieved from http://www.sciencedirect.com/science/article/pii/S0378382012001476

Lasram, M. M., El-Golli, N., Lamine, A. J., Douib, I. B., Bouzid, K., Annabi, A., . . . Gharbi, N. (2014). Changes in glucose metabolism and reversion of genes expressionin the liver of insulin-resistant rats exposed to malathion. Theprotective effects of N-acetylcysteine. *General and Comparative Endocrinology*. Retrieved from http://www.sciencedirect.com/science/article/pii/S0016648014003967

Lazarevic-Pasti, T., Colovic, M., Savic, J., Momic, T., & Vasic, V. (2011, March 17). Oxidation of diazinon and malathion by myeloperoxidase. *Pesticide Biochemistry and Physiology, 100*, 140-144. Retrieved from http://ac.els-cdn.com/S0048357511000447/1-s2.0-S0048357511000447-main.pdf?_tid=038a6048-b39e-11e4-bc5f-00000aab0f01&acdnat=1423845377_3277813859828d1a4748edcfed0e1d1c

Magnusson, M., Heimann, K., Ridd, M., & Negri, A. P. (2013). Pesticide contamination and phytotoxicity sediment interstitial water to tropical benthic microalgae. *Water Research Journal*. Retrieved from http://www.sciencedirect.com/science/article/pii/S0043135413004946

Moore, P. D., Yedjou, C. G., & Tchounwou, P. B. (2010, June). Malathion-Induced Oxidative Stress, Cytotoxocity, and Genotoxicity in Human Liver Carcinoma (HepG(2)) Cells. *Environmental Toxicology, 25*(3), 221-226. Retrieved from http://www.ncbi.nlm.nih.gov/pmc/articles/PMC2862833/pdf/nihms190535.pdf

National Institute of Standards and Technology. (2011). *Malathion*. Retrieved November 15, 2014, from NIST Chemistry Webbook: http://webbook.nist.gov/cgi/cbook.cgi?ID=C121755&Units=SI&Mask=80#IR-Spec

National Pesticide Information Center. (n.d.). *Malathion Information Fact Sheet.* Retrieved from National Pesticide Information Center: http://npic.orst.edu/factsheets/malatech.pdf

New Jersey Precision Technologies, Inc. (2015). *What is Electrical Discharge Machining?(EDM).* Retrieved from New Jersey Precision Technologies, Inc. improving lives through manufacturing innovation: http://www.njpt.com/wire-edm.html

Niu, S., Han, K., Lu, C., & Sun, R. (2010). Thermogravimetric analysis of the relationship among calcium magnesium acetate, calcium acetate and magnesium acetate. *Applied Energy, 87*, 2237-2242. Retrieved from http://www.sciencedirect.com/science/article/pii/S0306261910000097

Park, H. Y., & Kim, T. H. (2006, February 2006). Non-isothermal pyrolysis of vacuum residue (VR) in a thermogravimetric analyzer. *Energy Conversion and Management, 47*, 2118-2127. Retrieved from http://www.sciencedirect.com/science/article/pii/S0196890405003420

Pazur, R. J. (2014). Activation energy of poly(isobutylene) under thermo-oxidative conditions from 40 to 100 degrees celsius. *Polymer Degradation and Stability, 104*, 57-61. Retrieved from http://www.sciencedirect.com/science/article/pii/S0141391014001207

Prado, J. R., & Vyazovkin, S. (2011). Activation energies of water vaporization from the bulk and from laponite, montmorillonite, and chitosan powders. *Thermochimica Acta, 524*(1-2), 197-201. Retrieved from http://www.sciencedirect.com/science/article/pii/S0040603111003261

Quintas, G., Garrigues, S., & de la Guardia, M. (2004). FT-Raman spectrometry determination of malathion in pesticide formulations. *Talanta, 63*, 345-350. Retrieved from http://www.sciencedirect.com/science/article/pii/S0039914003006581

Rychly, J., Matisova-Rychla, L., Csomorova, K., Janigova, I., Schilling, M., & Learner, T. (2011, September). Non-isothermal thermogravimetry, differential scanning calorimetry and chemiluminescence in degradation of polyethylene,polypropylene, polystyrene and poly(methyl methacrylate). *Polymer Degradation and Stability, 96*(9), 1573-1581. doi:doi:10.1016/j.polymdegradstab.2011.05.020

Schweitzer, P. A. (1987). *What every engineer should know about corrosion* (Vol. 21). New York, New York, USA: Marcel Dekker, Incorporated.

Smith, R. (2014, February 5). Assault on california power station raises alarm on potential for terrorism. *The Wall Street Journal*, p. 1. Retrieved from http://www.wsj.com/articles/SB10001424052702304851104579359141941621778

Starink, M. J. (2003). The determination of activation energy from linear heating rate experiments: a comparison of the accuracy of isoconversion methods. *Thermochimica Acta, 404*, 163-176. Retrieved from www.elsevier.com/locate/tca

Stuart, B. (1996). *Modern infrared spectroscopy: Analytical chemistry by open learning.* (D. J. Ando, Ed.) Chichester, England, New York, USA: Wiley.

ThermoFisher. (2008, November 21). Thermax 400. *ThermoFisher Scientific*.

ThermoFisher. (n.d.). OMNIC: Beginners Guide Tool Book II.

Tudorachi, N., & Chiriac, A. P. (2011, February 21). TGA/FTIR/MS study on thermal decompostion of poly(succinimide) and sodium poly(aspartate). *Polymer Testing, 30*, 397-407. Retrieved from http://www.sciencedirect.com/science/article/pii/S0142941811000250

U.S. Department of Homeland Security. (2012, June 9). *Homeland security presidential directive 7: Critical infrastructure identification, prioritization, and protection*. Retrieved from U.S. Deparment of Homeland Security: http://www.dhs.gov/homeland-security-presidential-directive-7

U.S. Environmental Protection Agency. (2012, March 12). *Water legislation and directives: Security and bioterrorism preparedness and response act of 2002.* Retrieved December 21, 2014, from Environmental Protection Agency: http://www.epa.gov/safewater/watersecurity/pubs/security_act.pdf

U.S. Environmental Protection Agency. (2014, February 11). *Water security: Basic information about water security*. Retrieved January 9, 2015, from EPA: http://water.epa.gov/infrastructure/watersecurity/basicinformation.cfm

Van Meter, R. J., Gliniski, D. A., Hong, T., Cyterski, M., Henderson, W. M., & Purucker, S. T. (2014). Estimating terrestrial amphibian pesticide body burden through dermal exposure. *Environmental Pollution, 193*, 262-268. Retrieved from http://www.sciencedirect.com/science/article/pii/S0269749114002899

Vlaev, L., Nedelchev, N., Gyurova, K., & Zagorcheva, M. (2008). A comparative study of non-isothermal kinetics of decomposition of calcium oxalate monohydrate. *Journal of Analytical and Applied Pyrolosis, 81*(2), 253-262. Retrieved from http://www.sciencedirect.com/science/article/pii/S0165237007001738

Vyazovkin, S. (2002, March 18). Some confusion concerning integral isoconversional methods that may result from the paper by budrugeac and segal "Some methodological problems concerning nonisothermal kinetic analysis of heterogeneous solid-gas reactions".

Walker, C. H. (2009). *Organic Pollutants: An ecotoxicological perspective: organphosphorus and carbamate insecticides* (2nd ed.). Bocal Raton, Florida, USA: CRC Press Taylor and Francis Group.

Wang, G.-C., Tao, S.-X., & Bu, X.-H. (2006, November 15). A systematic theoretical study of water dissociation on clean and oxygen-preadsorbed transition metals. *Journal of Catalysis, 244*(1). Retrieved from http://www.sciencedirect.com/science/article/pii/S0021951706002727

Wang, X., Xing, W., Feng, X., Yu, B., Lu, H., Song, L., & Hu, Y. (2014, March 20). The effect of metal oxide decorated graphene hybrids on the improved thermal stability and the reduced smoke toxicity in epoxy resins. *Chemical Engineering Journal, 250,* 214-221. Retrieved from http://ac.els-cdn.com/S1385894714003167/1-s2.0-S1385894714003167-main.pdf?_tid=1ac98cde-c1f4-11e4-931d-00000aab0f6c&acdnat=1425421669_528e81742b55de3102b8da3a1d09f15b

Whitten, K. W., Davis, R. E., & Peck, M. L. (2000). *General Chemistry, 6th ed.* (J. Vondeling, M. Sherman, & T. Lewis, Eds.) Orlando, Florida, USA: Saunders College Publishing.

Zhu, Y., Mimura, K., & Isshiki, M. (2002). Oxidation mechanism of copper at 623-1073K. *43*(9), pp. 2173-2176. Retrieved from https://www.jim.or.jp/journal/e/pdf3/43/09/2173.pdf

Vita

Captain Walter R. Lee Jr. graduated from Pine Forest High School in Fayetteville, North Carolina. He entered undergraduate studies at North Carolina Agricultural and Technical State University (NCATSU) in Greensboro, North Carolina where he graduated Summa Cum Laude with a Bachelor of Science degree in Architectural Engineering in May 2006. He was commissioned through the Detachment 605 AFROTC at NCATSU where he was recognized as a Distinguished Graduate and nominated for a Regular Commission.

He attended Air and Space Basic Course at Maxwell AFB, Alabama in June 2006. His first assignment was 1st Civil Engineer Squadron, Langley AFB, Virginia as a project engineer and Manager in 2006. While stationed at Langley, he deployed to Al Asad AB, Iraq in 2008 for six months with a Facility Engineer Team. In July 2009, Capt Lee was reassigned to the Air Force Center for Engineering and Environment (AFCEE), Contingency Construction Division, Lackland AFB, Texas as an Afghanistan security transition program manager. While there, he forward deployed to Kabul, Afghanistan for six months with AFCEE as contracting officer representative. Upon returning, he was reassigned to the 8th Civil Engineer Squadron, Kunsan AB, Korea where he served for 13 months as chief of construction. In 2013, Capt Lee attended Squadron Officer School at Maxwell AFB, Alabama. Upon graduation, he was assigned to Wright-Patterson AFB, Ohio, Air Force Institute of Technology (AFIT), The Civil Engineer School as an instructor. In October 2013, he entered the Graduate School of Engineering Management, AFIT. Upon graduation, Capt Lee will be involuntarily separating from the U.S. Air Force and moving into new career opportunities.

REPORT DOCUMENTATION PAGE

Form Approved
OMB No. 074-0188

1. REPORT DATE *(DD-MM-YYYY)*	2. REPORT TYPE	3. DATES COVERED *(From – To)*
26-03-2015	Master's Thesis	1 October 2013 – 26 March 2015

TITLE AND SUBTITLE

The Fate of Malathion on Copper and Iron Piping Within a Water Distribution System

5a. CONTRACT NUMBER

5b. GRANT NUMBER

5c. PROGRAM ELEMENT NUMBER

6. AUTHOR(S)

Lee Jr., Walter R., Captain, USAF

5d. PROJECT NUMBER
15V119

5e. TASK NUMBER

5f. WORK UNIT NUMBER

7. PERFORMING ORGANIZATION NAMES(S) AND ADDRESS(S)
Air Force Institute of Technology
Graduate School of Engineering and Management (AFIT/EN)
2950 Hobson Way, Building 640
WPAFB OH 45433-7765

8. PERFORMING ORGANIZATION REPORT NUMBER
AFIT-ENV-MS-15-M-164

9. SPONSORING/MONITORING AGENCY NAME(S) AND ADDRESS(ES)
Environmental Protection Agency
National Homeland Security Research Center
26 West Martin Luther King Drive
Cincinnati, OH 45268
Matthew Magnuson
513-569-7321, magnuson.matthew@epa.gov

10. SPONSOR/MONITOR'S ACRONYM(S)
EPA/NHSRC

11. SPONSOR/MONITOR'S REPORT NUMBER(S)

12. DISTRIBUTION/AVAILABILITY STATEMENT
DISTRUBTION STATEMENT A. APPROVED FOR PUBLIC RELEASE; DISTRIBUTION UNLIMITED.

13. SUPPLEMENTARY NOTES
This material is declared a work of the U.S. Government and is not subject to copyright protection in the United States.

14. ABSTRACT
Thermogravimetry, the study of mass loss as a function of temperature, has been used for oxidation, decomposition, and solid-state studies. This research used a thermogravimetric analyzer (TGA) coupled with Fourier transform infrared (FT-IR) spectroscopy in the study of copper and iron specimens exposed to malathion. Exposure to the malathion solution created a visible silver coating on copper and graphite-flake particles on iron specimens. Thermogravimetric mass loss curves revealed linear and nonlinear decomposition stages associated with mass loss reactions. Copper specimens exposed to malathion exhibited lower activation energy (Ea) values (2.28 to 4.40 kJ mol^{-1}) than for copper specimens exposed to deionized water (10.42 and 12.87 kJ mol^{-1}). Iron specimens exposed to malathion show lower Ea values (1.54 and 1.28 kJ mol^{-1}) than for iron specimens exposed to deionized water (3.30 and 6.40 kJ mol^{-1}). These results suggest association between malathion and lowered activation energies across all sample specimens. The FT-IR results indicate that specimens exposed to malathion may produce hydrogen sulfide. This research is the first to the author's knowledge to use TGA and FT-IR to test malathion adherence to metal surfaces. These results have application in water distribution piping analysis.

15. SUBJECT TERMS
Activation Energy, Copper, Iron, Malathion, Thermogravimetric Analyzer, Fourier transform infrared

16. SECURITY CLASSIFICATION OF:			17. LIMITATION OF ABSTRACT	18. NUMBER OF PAGES	19a. NAME OF RESPONSIBLE PERSON
a. REPORT	b. ABSTRACT	c. THIS PAGE			Willie F. Harper Jr., Ph.D., P.E., AFIT/ENV
U	U	U	UU	142	19b. TELEPHONE NUMBER *(Include area code)* (937) 255-3636 ext 4528 (willie.harper@afit.edu)

Standard Form 298 (Rev. 8-98)
Prescribed by ANSI Std. Z39-18